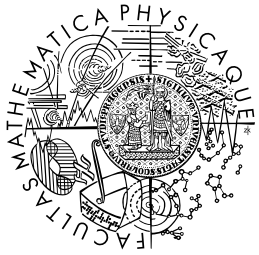

FACULTY
OF MATHEMATICS
AND PHYSICS
Charles University

DOCTORAL THESIS

Myank Singhal

Shaping the Inner Galactic Center: The Role of Stellar Dynamics around Sagittarius A*

Astronomical Institute of Charles University

Supervisor of the doctoral thesis: Ladislav Šubr

Study programme: Theoretical Physics, Astronomy and Astrophysics (P0533D110020)

Prague 2026

I declare that I carried out this doctoral thesis on my own, and only with the cited sources, literature and other professional sources. I understand that my work relates to the rights and obligations under the Act No. 121/2000 Sb., the Copyright Act, as amended, in particular the fact that the Charles University has the right to conclude a license agreement on the use of this work as a school work pursuant to Section 60 subsection 1 of the Copyright Act.

In ..... date ....

Author's signature

There are many people I would like to acknowledge who guided and supported me during this chaotic adventure of my life. Starting from my biggest supporters and my guiding stones, my parents, Sunita and Satyender Singhal. Not only did they do their best to answer my unending stream of questions, but they also pushed me to find the answers myself. I can never thank them enough for their crucial role in my life. To my brother Sanchit Singhal, who always had to be the one to wake up at ungodly hours to drive me to my classes and exams, and who waited for hours, I will always appreciate the countless sacrifices you made for my sake. I would be remiss not to acknowledge the role my sister-in-law, Shreya Singhal, has been a friend and mediator when the rest of my family would not be so friendly, just like every family. The little (who are no longer so little) bundles of joy, my nephew and niece, Yuvansh and Mishka, who bring an unending stream of laughter to my life. I would also like to remember my dog Buddy, who always slept on my sandals and brought me coziness during his life.

I cannot continue without thanking my friends, Sai, Yugantar, Sneheil, and Ritvik, who have not only been there for me at my toughest times, even while on different continents, but also always cheered me on, even when I did something stupid. The friends I have made here in Prague through my time in the dorms and also the Prague Social run club, including my colleagues, Nick and Iris, who have listened to my yapping, which resulted in many unproductive days at the office. I also want to say my gratitude to my girlfriend, Sruti, who has been here for me during the toughest part of my PhD journey and has been a support that I did not know I needed.

I would also like to thank my professors at UCLA and the University of Bristol for preparing me for this PhD journey. However, the biggest guidance and support have come from my supervisor, Dr. Ladislav Šubr, who stayed patient with me even when I pestered him with questions or asked for advice to fix the messes I made. I would like to continue expressing my gratitude to the people who have greatly guided and supported me: my collaborator, Dr. Florian Peißker, and Dr. Michal Zajaček. I also want to thank my therapist, Lukáš, whose words helped me navigate this journey.

I would like to end my dedication with the quote from my favorite show, Avatar: The Last Airbender, that kept me going through my entire journey:

> "In the darkest times, hope is something you give yourself. That is the meaning of inner strength." — Uncle Iroh

Title: Shaping the Inner Galactic Center: The Role of Stellar Dynamics around Sagittarius A*

Author: Myank Singhal

Department: Astronomical Institute of Charles University

Supervisor: Ladislav Šubr, Astronomical Institute of Charles University

Abstract: This Thesis examines how stellar dynamics shape the stellar population near a supermassive black hole (SMBH), using our galaxy's center as a case study. Focusing on binary disruptions, captures, collisions, and interactions with perturbers, we use numerical simulations to study systems with the SMBH as the central body. We investigate the VHS mechanism observed in hierarchical four-body systems on circular orbits, extend it to relativistic and eccentric cases, and explore its effects on S-stars and disk evolution in the Galactic Center. Our results show that the VHS mechanism is compatible with non-zero eccentricity and demonstrate that disk-like structures can persist or split within the S-cluster. We also investigate the evolution of a disk of binary stars using full N-body simulations, showing that the Hills mechanism can explain hypervelocity stars such as S5-HVS1 originating from the young stellar disk in our Galactic Center. Our results also show that stellar mergers in these disks occur in two separate populations: one closer to the SMBH and below the inner edge of the initial disk, potentially corresponding to the observed dust-embedded objects, and the other farther out. The simulations also naturally reproduce the observed radial trends in binary fractions in our Galactic Center.

Keywords: Galactic centre, Binary stars, Celestial mechanics, Hypervelocity stars, N-body simulations

Contents

Introduction

The center of the Milky Way provides a unique environment for studying gravitational dynamics in the vicinity of a supermassive black hole. Hosting the closest known SMBH, Sagittarius A* (Sgr A*), the Galactic Center allows direct observational access to stellar, binary, and gaseous systems evolving under extreme tidal forces of the SMBH and high stellar densities. As a result, it serves as a natural laboratory for testing dynamical theories that cannot be explored in terrestrial experiments or even in most extragalactic systems.

The primary goal of this Thesis is to investigate the role of stellar dynamics, especially binaries, in shaping stellar populations observed near Sgr A* , with a focus on binary disruption, capture, collisions, and mergers in a dense galactic nucleus. By combining direct N-body simulations with high-precision few-body integrations, this work aims to explore how stars interact with the SMBH and the surrounding stellar environment, and how these interactions contribute to extreme stellar populations and drive unique dynamical phenomena in a galactic center.

This Thesis is based on a series of papers that address different aspects of these problems. Each paper explores a specific dynamical channel or numerical approach, while together they form a coherent framework for understanding stellar dynamics in galactic centers, focusing on observational results provided by the stellar population in our Galactic Center. In Chapter 1, we first provide an overview of the Galactic Center from an observational perspective. We begin by summarizing the key components observed in the region and highlighting the dynamical puzzles they pose. We then describe the gravitational environment surrounding Sgr A* and review the principal dynamical mechanisms relevant to this work, with particular emphasis on relaxation processes, secular dynamics, and binary-mediated interactions in Chapter 2. Finally, in Chapter 3, we outline the numerical tools and methods used to model these processes.

Subsequent chapters present the core findings of this research. Chapter 4 extends a previously established hierarchical four-body framework into the relativistic regime, demonstrating its direct applicability to the extreme environment of our Galactic Center. Following this, Chapter 5 investigates the dynamics of a stellar binary disk, specifically analyzing the kinematic distributions and trajectories of stars ejected during close binary encounters with the SMBH. Building upon a similar setup, Chapter 6 explores the long-term evolution, survival rates, and collision/merger pathways of these binary systems. Finally, the conclusion section presents the overarching conclusions and future outlook of this work.

1 The Galactic Center

Physics relies on a collaborative nature between theory and experiments, theory provides ideas for experiments to test while experiments allow theories to be tested in the real world, and provide baselines for future theories to prove. A lot of theories however tend to work at scales which cannot be tested in the laboratories here on Earth, for example physics of objects around compact massive objects like supermassive black holes (SMBHs).

These SMBHs are typically on the mass scales of $10^6 - 10^8 M_\odot$ and are typically found at the centers of galaxies. The growth and formation of the earliest SMBHs remains one of astrophysics' puzzles. Observations of high-redshift quasars reveal that massive billion solar mass black holes alreay existed in galaxies as soon as a billion years after the big bang. This raises questions about the nature of galactic evolution, weather these massive black holes trigger formation of host galaxies or did primordial galactic structures collapse rapidly to form these early SMBHs. So these galactic centers act as a natural laboratory for us to study physics around these massive compact objects.

While the broader evolutionary history of galactic nuclei involves micro-scale stellar processes—such as accretion dynamics occurring on scales of a few stellar radii, or the disruptive tidal interactions of binary stars—this work explicitly focuses on the larger-scale gravitational dynamics of galactic centers and their components. The closest galactic center with an SMBH for us to study is within our own Galaxy, at a distance of about 8 Kpc from Earth, and is a complex region hosting old and young stars along with dense molecular clouds. All these objects orbit Saggitarius A* (Sgr A*), a SMBH of mass $M \approx 4.3 \times 10^6 M_\odot$.

1.1 Saggitarius A*

There are various studies that predicted the presence of a large concentration of mass in the Galacitc Center using gas clouds. However, these could have had uncertainties due to other effects on the gas dynamics which therefore limits its use. On the other hand, stellar objects in the Galactic Center are better object for testing gravity around Sgr A* . Eckart and Genzel (1996) and Ghez et al. (1998) tracked the motion of stars near Sgr A* . Using the motion of these stars they could identify the mass of the unseen mass at the center and found an estimate of $2.6 \times 10^6 M_\odot$ within 0.1 arcsec of the center (~ 4 mpc). With one of these stars, S0-02 (or S2), using the orbit measured over 16 years the mass of the central body could be determined more accurately. Using both proper motion and radial motion with spectroscopic measurements, updated measurements found the mass of the central dark body to be approximately $4.1 \times 10^6 M_\odot$ (Ghez et al., 2008; Gillessen et al., 2009). Recent measurements have a more accurate measurements of the mass of Sgr A* as approximately $4.3 \times 10^6 M_\odot$. Figure 1.1 illustrates key observational evidence supporting the identification of Sgr A* as a supermassive black hole. The left and central panels show the astrometric and spectroscopic measurements of the S2 orbit, demonstrating near Keplerian motion around a compact central mass. The left panel also shows that the orbit is does not close form a closed loop due to effects of relativistic precession. The right panel in

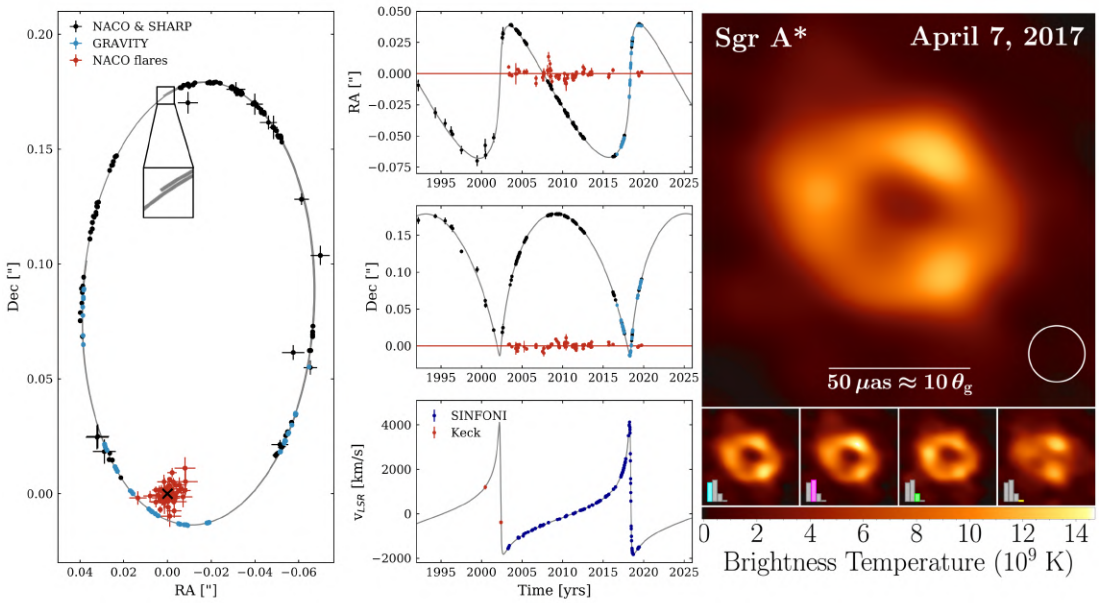

Figure 1.1 Observational evidence for the supermassive black hole at the Galactic Centre. *Left:* Astrometric measurements of the orbit of the star S2 (S0-02) around Sgr A* , obtained using NACO, SHARP, and GRAVITY, showing a Keplerian fit that does not form a closed loop around the compact central mass (taken from GRAVITY Collaboration (2020); modified with zoomed panel). *Center:* Time evolution of the right ascension, declination, and line-of-sight velocity of S2, demonstrating consistency between proper motion and spectroscopic measurements(taken from GRAVITY Collaboration (2020)). *Right:* Representative image of Sgr A* produced by the Event Horizon Telescope on April 7, 2017, showing emission from the accretion flow on angular scales of order 50 μas, corresponding to approximately ten gravitational radii(taken from Event Horizon Telescope Collaboration (2022)). Together, these observations provide compelling dynamical and horizon-scale evidence that Sgr A* is a supermassive black hole with mass $\sim 4.3 \times 10^6\, M_\odot$.

Figure 1.1 presents a representative horizon-scale image of Sgr A* obtained by the Event Horizon Telescope (EHT) using Very-Long Baseline Interferometry (VLBI) to observe Sgr A* with high angular resolution. Event Horizon Telescope Collaboration (2022) used approximations and algorithms to analyze the data and created a representative image showing the accretion flow onto Sgr A* . This image matches the expected accretion flow and provides additional independent evidence for Sgr A*'s nature as an SMBH.

The mass of Sgr A* calculated by dynamical means and the representative image produced using the EHT make Sgr A* extremely likely to be an SMBH. Astronomers have discussed other possible systems that could mimic such high densities instead of an SMBH. One of these possibilities is a compact cluster of neutron stars and white dwarfs. Even if this compact cluster could be dynamically stable, it would impact the orbits of the S-stars, which are only compatible with mass concentration at a single point (Maoz, 1998). Along with all the other hypothesis for the mass concetration at the location of Sgr A* , the SMBH is the most plausible one.

1.2 S-cluster

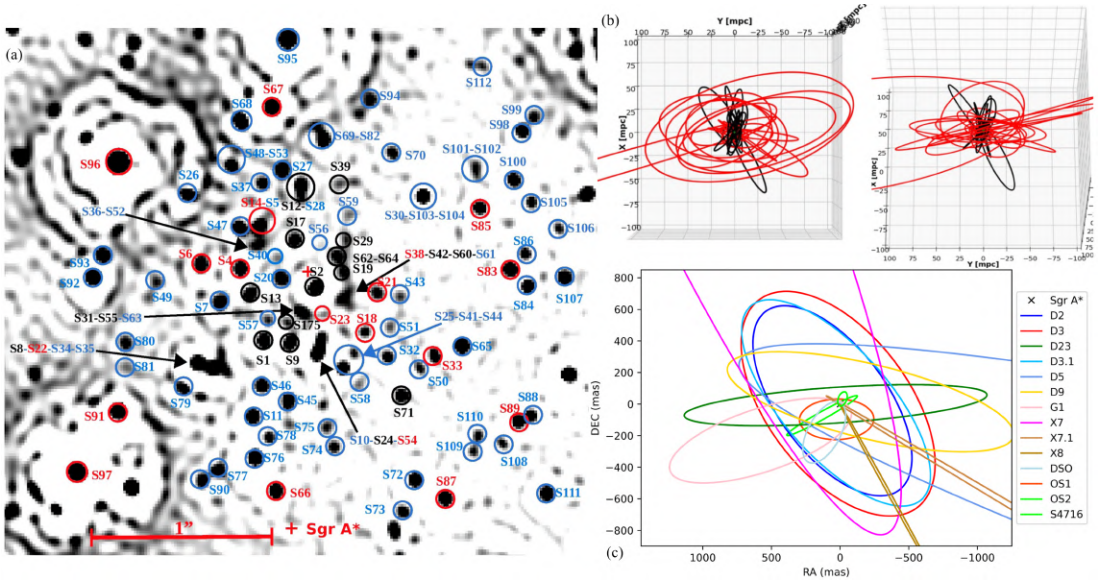

Figure 1.2 Observational overview of the S-cluster and compact objects orbiting Sgr A* . *Left:* Adaptive-optics infrared image of the central arcsecond, showing the projected positions of S-stars relative to Sgr A* (taken from Ali et al. (2020)). Individual stars are labeled, and the location of Sgr A* is marked. *Top right:* Three-dimensional orbital solutions for selected S-stars, illustrating the high eccentricities and orientations of their orbits (taken from Ali et al. (2020)). *Bottom right:* Projected orbital fits for a sample of dust-enshrouded sources, highlighting their close periapse passages and diverse orbital properties (taken from Peißker et al. (2024b)). This population of young stars and dusty objects within ~ 40 mpc of Sgr A* presents strong constraints on formation and dynamical evolution scenarios in the Galactic Centre.

As mentioned earlier, in the near vicinity of Sgr A* there is an overabundance of young, predominantly B type stars. These stars typically have highly elliptical orbits within ≈40 mpc of Sgr A* . The spatial distribution of the S-stars and representative orbital solutions are shown in Figure 1.2. The presence of these young stars in close vicinity of Sgr A* along with a collection of young stars in the young nuclear cluster (YNC) slightly farther away form the basis of the “paradox of youth” (Sanders, 1992). The formation of these young stars in the close vicinity of an SMBH would require high density protostellar clouds to overcome the tidal forces of Sgr A* , especially for the S-stars. Several hypotheses have been suggested for the formation of S-stars including the tidal disruption of incoming binary star systems via the Hills mechanism (Hills, 1988; Gould and Quillen, 2003; Perets et al., 2009), and the structural rejuvenation of older stars through collisional stellar mergers (Antonini et al., 2011). In this work, I focus on exploring some possible dynamical origin of S-stars originating within the YNC and migrating close to Sgr A* later in Chapter 3.

Along with the S-stars in the S cluster, there is another population of objects that orbit Sgr A* on relatively similar orbits. The nature of these objects is still debated. These are referred to as dust enshrouded objects, or ”dusty objects”. The representative orbital solutions for some of these dusty objects are shown in Figure 1.2. The two main hypotheses on the nature of these objects – that they

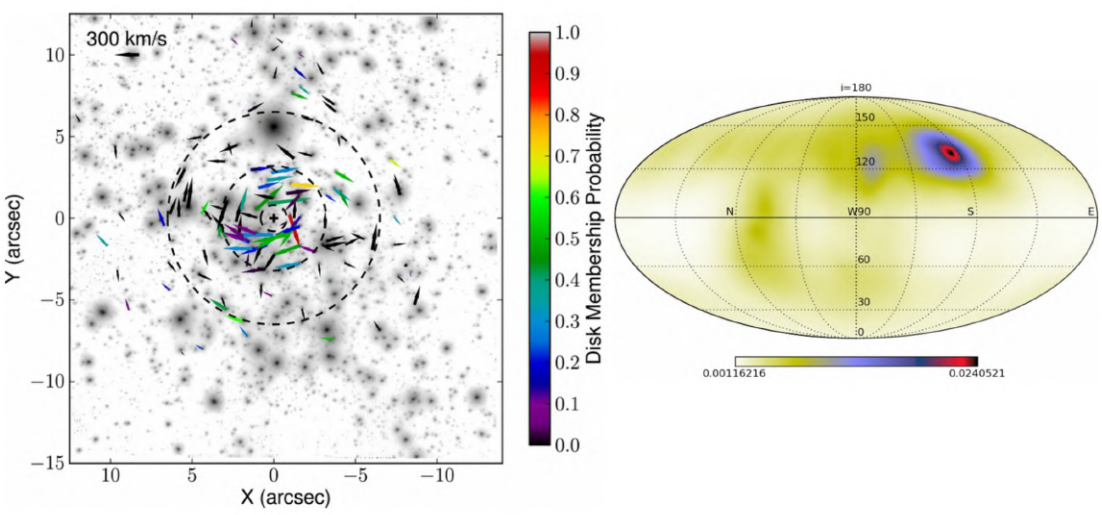

Figure 1.3 Observational properties of the young nuclear cluster (YNC) (taken from Yelda et al. (2014)). *Left:* Proper motion vectors of young stars in the central $\sim 15''$, overlaid on a near-infrared image. Arrows indicate projected velocities, with colors representing the probability of membership in the clockwise stellar disk. The dashed circles mark projected radii from Sgr A* . *Right:* Probability density map of orbital angular momentum directions, highlighting the coherent orientation of the clockwise disk relative to the background stellar population. This figure illustrates the presence of dynamically coherent disk-like structures within the YNC.

are clouds of dust orbiting Sgr A* or that they are dust clouds with a stellar core inside – are not fully mutually exclusive.

One of these dusty objects observed, G2, provides an example of the debated nature of these objects. When initially detected in 2011, it was labeled as a cold dust cloud with a mass of approximately 3 earth masses. The orbit of G2 also predicted a close approach to Sgr A* in 2014, which based on simulations, would result in large amounts of gas being spiralled into Sgr A* with an excess of X-ray emmission, while destroying G2. However, after a close passage of ≈150 AU, G2 was not destroyed from the tidal forces. This provided more evidence for the hypothesis of G2 having a stellar core.

While, this case study has not completely solved the debate on the nature of the dusty objects, it has provided more credence towards the theory of a dust enshrouded stellar core. The follow-up question to answer is, what is the nature of the stellar core. The two most likely possibilities are a binary merger product or a young stellar object (YSO). The possibility of YSOs in such close vicinity of Sgr A* is unexpected due to the large tidal forces of Sgr A* preventing star formation. In Chapter 6 I present my results showing that binary mergers are a viable channel to produce dusty objects in the Galactic center.

1.3 Young Nuclear Cluster

The presence of a young nuclear cluster (YNC) with approximately 100 young stars orbiting within 0.5 pc of Sgr A* was initially considered as evidence against

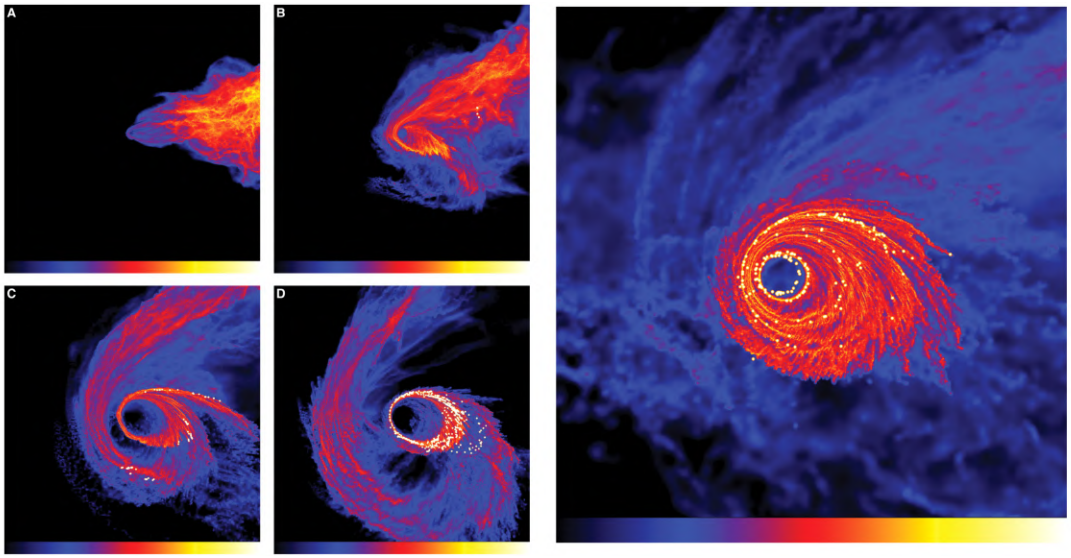

Figure 1.4 Numerical simulation of a massive gas cloud infalling toward Sgr A* and forming a dense, eccentric disk (taken from Bonnell and Rice (2008)). The cloud undergoes tidal compression and fragmentation, leading to in-situ star formation within a disk-like structure. Such simulations demonstrate that coherent stellar disks similar to the observed clockwise disk can form under favorable initial conditions, though they require fine-tuned angular momentum properties.

Sgr A* being an SMBH, since the tidal forces would be so high to prevent star formation unless the gas density was extremely high. The presence of Wolf-Rayet stars and OB stars has set some constraints on the age of the YNC to around 5 Myr (Krabbe et al., 1995; Lu et al., 2013).

Many stars within the YNC are arranged in various disk like structures. The most prominent of which is the clockwise disk (CWS) or the young stellar disk which predominantly spans within 0.04-0.4 pc from Sgr A* (Levin and Beloborodov, 2003; Paumard et al., 2006; von Fellenberg et al., 2022). Farther away, there is the counterclockwise disk and other structures (von Fellenberg et al., 2022). The projected stellar velocities, disk membership probabilities, and the orientation of the dominant disk structure of the YNC are illustrated in Figure 1.3.

While disk structures are better-established in the YNC, wide scale structures within the inner S-stars remains a subject of debate. Although the S-stars were expected to be randomly oriented due to the relaxational effects, there are studies that find correlated disk like structures within the S-cluster including the dusty objects, distinct from the structures observed within the YNC (Ali et al., 2020; Peißker et al., 2024b).

The formation of CWS and YNC is still a mystery, but there are various hypotheses. The one which is currently considered the most viable assumes an in-fall of a massive cloud toward Sgr A* . This has been explored in various studies (Bonnell and Rice, 2008; Mapelli et al., 2012). The infall forms a dense disk like structure, where star formation is possible. Figure 1.4 shows an example output from a simulation that studies the fall of a molecular clump towards Sgr A* (Bonnell and Rice, 2008). This model results in a disk like structure where the stars form in nested ellipses, with increasing eccentricity as the orbits get farther away. However, there are some arguments against this formation scenario,

as according to Dinh et al. (2021) the probability for a gas cloud to fall towards the Galactic Center with near zero angular momentum is low. Although this low-probability constraint exists, the infalling cloud scenario provides the most viable baseline for the simulations in this study.

1.4 Other Observables

In addition to the previously discussed features, the Galactic Center hosts several other components that play significant roles in its dynamics and structure. Notably, there are various clusters of stars and dust, including one that may harbor an intermediate-mass black hole (IMBH) with a mass of approximately $10^4 M_\odot$, located about 0.1 pc from Sgr A* (Peißker et al., 2024a, IRS13E).

The YNC described above is enclosed by a gaseous torus, the circumnuclear disk (CND), located between 1.5 and 2 pc of Sgr A* (Martins et al., 2006; Liu et al., 2012; Hsieh et al., 2017; Tsuboi et al., 2018; Goicoechea et al., 2018; Hsieh et al., 2021). The CND has a highly uncertain mass, estimated to be between 10^4 and $10^6 M_\odot$ (Christopher et al., 2005; Requena-Torres et al., 2012). This massive gaseous structure not only provides the environment for star formation but can also act as a distant perturber to objects within the inner parsec. In addition to these features, the Galactic Center contains various gas streams, further contributing to its complex environment. Figure 1.5 shows a representative multi-scale view of the central parsec of the Milky Way.

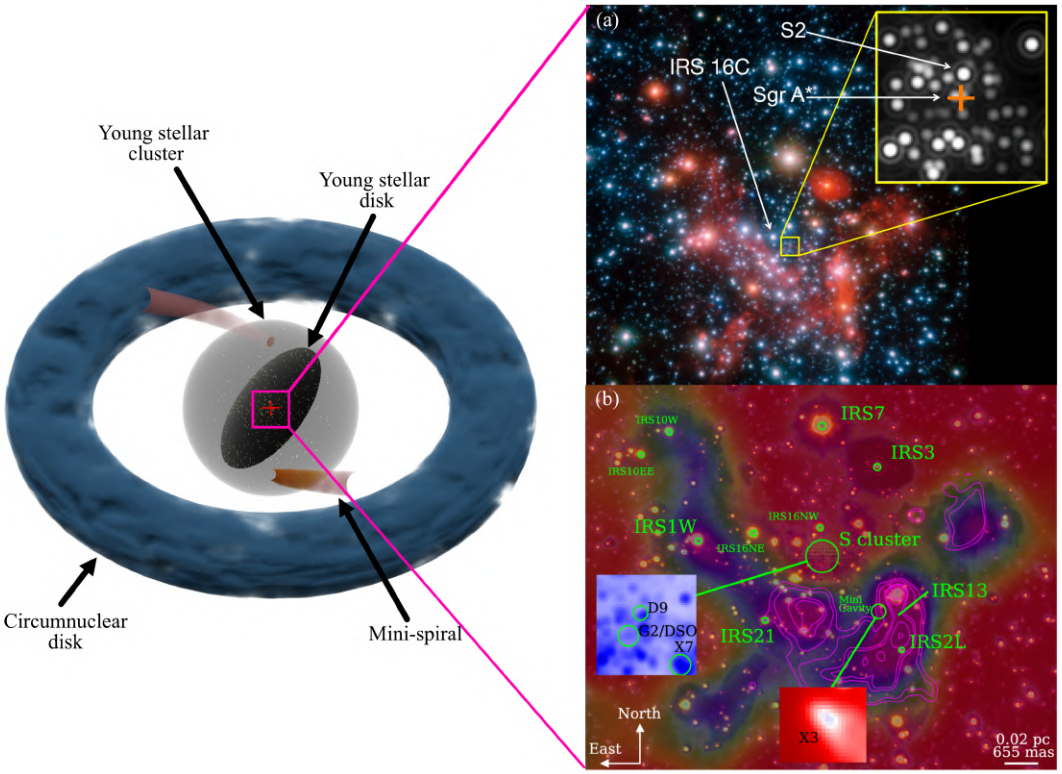

Figure 1.5 A multi-scale view of the central parsec of the Milky Way. A wide-field view illustrating the nested structures of the Galactic Center, including the young stellar cluster and the clockwise stellar disk, surrounded by the circumnuclear disk (CND) and the mini-spiral gas streams. (a) A zoomed-in view of the innermost region surrounding Sagittarius A* (marked with a red cross), highlighting the S-cluster stars (credit ESO/MPE/S. Gillessen et al.). (b) Another zoomed in view of the inner-most region highlighting known dusty objects such as G2/DSO, D9, and X7 (taken from Peißker et al. (2025).

2 Dynamical Processes near a Supermassive Black Hole

The Galactic Center is a complex and dynamic environment shaped by the interplay of multiple gravitational influences. While Sgr A* serves as the dominant central mass, the surrounding nuclear star cluster and additional structures—such as gaseous torus, stellar disks, and potential intermediate-mass black holes—each contribute to the overall gravitational potential. These overlapping influences give rise to a variety of dynamical phenomena that play crucial roles in the evolution of objects within the region. Understanding these collective gravitational effects is essential for exploring the mechanisms that govern orbital dynamics and the long-term evolution of stellar and compact object populations near Sgr A* .

2.1 Relaxation Processes

The long-term evolution of stellar orbits in the Galactic Center is governed by relaxation processes arising from gravitational interactions among stars and compact objects. These processes lead to diffusion in orbital energy and angular momentum and play a central role in shaping the phase-space distribution of objects orbiting Sgr A* . Unlike isolated hierarchical systems, relaxation in the Galactic Center operates continuously and provides the background against which other dynamical mechanisms are considered.

2.1.1 Two-body (Non-resonant) Relaxation

The most fundamental relaxation process is two-body, or non-resonant, relaxation, which arises from cumulative weak gravitational encounters between stars. These encounters lead to a random walk in both energy and angular momentum, gradually altering orbital parameters over long timescales. The characteristic relaxation timescale can be estimated using classical Chandrasekhar theory and depends on the local stellar density, velocity dispersion, and stellar mass function (Binney and Tremaine, 2008; Merritt, 2013).

In the Galactic Center, two-body relaxation governs the slow diffusion of stars into the loss cone, enabling tidal disruptions and direct plunges into the SMBH. It also drives mass segregation, causing heavier objects such as stellar-mass black holes and neutron stars to sink toward the center, potentially forming a dense dark cusp. Although two-body relaxation is generally inefficient within $\lesssim 0.01$ pc where the relaxation time exceeds the Hubble time, reducing to $\sim 10^{10}$ years at a distance of 1 pc from Sgr A* , it provides a baseline evolutionary timescale for the nuclear star cluster as a whole (Merritt, 2013). However, within a thin stellar disc, two-body relaxation is significantly accelerated due to the reduced vertical velocity dispersion, which increases the effectiveness of mutual gravitational encounters, leading to rapid heating of the disc over time (Binney and Tremaine, 2008; Šubr and Haas, 2014).

2.1.2 Resonant Relaxation

In near-Keplerian potentials dominated by a central mass, such as the region surrounding Sgr A* , relaxation can proceed much more rapidly through a process known as resonant relaxation (RR) (Rauch and Tremaine, 1996). In this regime, stellar orbits behave as nearly fixed Keplerian ellipses that exert long-lived torques on each other, leading to coherent changes in angular momentum.

Resonant relaxation can be divided into two components. Vector resonant relaxation changes the direction of the angular momentum vector, efficiently randomizing orbital orientations, while scalar resonant relaxation alters the magnitude of the angular momentum, driving changes in eccentricity. RR is particularly effective in the inner parsec and is often invoked to explain the near-isotropic distribution and high eccentricities of the S-stars. Specifically, within $\lesssim 0.01$ pc, vector resonant relaxation operates on a timescale of $\sim 10^6$ years, which results in rapid reorientation of orbital planes within the lifetime of the young S-stars (Hopman and Alexander, 2006). Meanwhile, scalar resonant relaxation is much slower and drives eccentricity evolution on a timescale of $\sim 10^7$–10^8 years, significantly outpacing classical two-body relaxation (Bar-Or and Fouvry, 2018).

2.2 Kozai–Lidov mechanism

The study of orbital mechanics in a Keplerian potential is a cornerstone of celestial mechanics. A classic study case is the secular evolution of a light (test) particle in a dominant central potential with a distant perturber also in orbit around the central body, commonly referred to as the "inner restricted problem" Merritt (2013). This kind of setup can be observed in many astrophysical systems ranging from planetary systems around stars to stars orbiting SMBHs. The dynamics of these systems were studied by von Zeipel (1910) but were later independently rediscovered by Kozai (1962) and Lidov (1962). The orbital solution developed in this hierarichal three body setup is often called Kozai–Lidov (KL) dynamics, which we will also use to stay consistent with literature. However, for various reasons, it is also known as the Lidov–Kozai mechanism or the von Zeipel–Lidov–Kozai mechanism.

The classical/quadrupole KL mechanism provides a solution to the inner restricted problem where the a test particle of mass m orbits around a dominant central body of mass $M_\bullet$ with a semi-major axis a and eccentricity e. We also have a distant perturber of mass M_p orbiting the central body on a circular orbit of radius R_p. The plane of orbit around the central body is also defining the reference plane, and we can select any arbitrary line within this plane to define the reference axis we use to calculate the longitude of ascending node, Ω. The angle of the orbital plane of the test particle with the reference plane defines the inclination, i. The setup is shown in Figure 2.1.

To analyze the long-term behavior of the test particle, we employ a secular approximation by averaging the gravitational potential over the orbital periods of both the particle and the perturber. In this averaged regime, the semi-major axes of both orbits are constants. Furthermore, because the time-averaged Hamiltonian is explicitly time-independent, the averaged perturbing potential $\overline{\mathcal{R}}_\mathrm{p}$ itself is a strict integral of motion. Expanding this secular disturbing function to the lowest

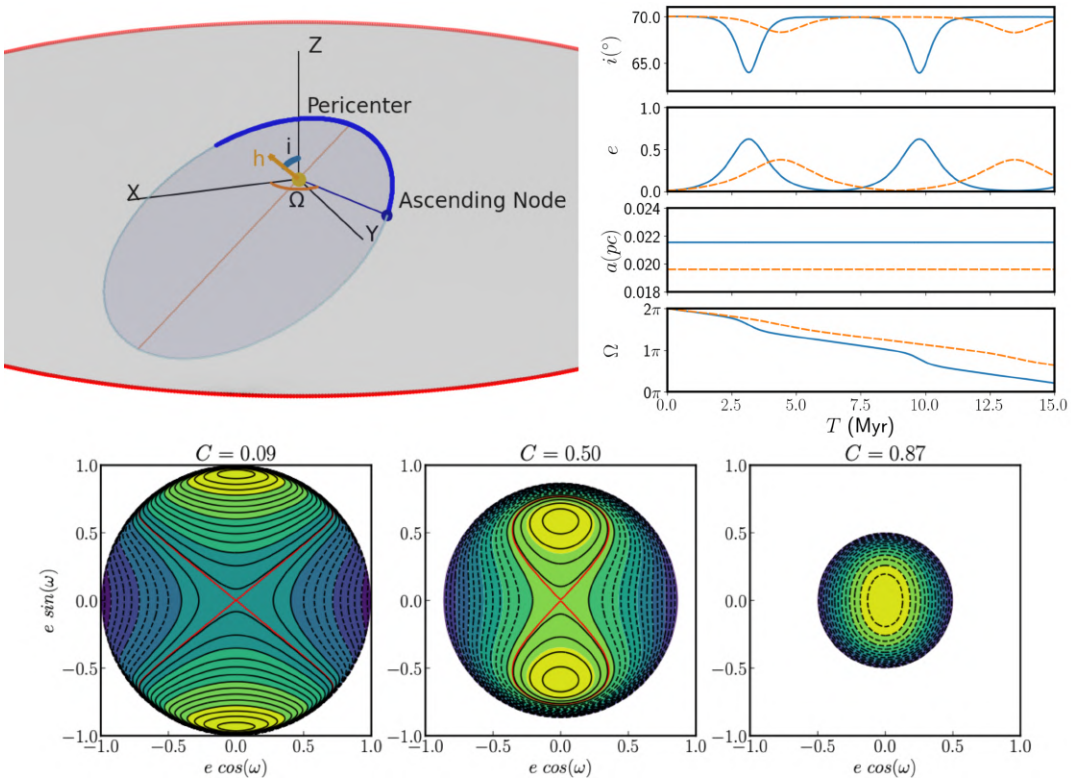

Figure 2.1 The fundamental geometry and secular evolution of the Kozai-Lidov (KL) mechanism. *Top left*: Definition of the orbital elements and reference planes for a test particle orbiting a central mass $M_\bullet$ under the influence of a distant perturber. *Top right*: Representative time evolution of the test particle's eccentricity (e) and inclination (i), demonstrating the characteristic coupled oscillations that preserve the Kozai constant, $C = \sqrt{1-e^2}\cos i$ (taken from Singhal et al. (2024)). *Bottom panels*: Phase-space trajectories in the $(e\cos\omega, e\sin\omega)$ plane for different values of the Kozai constant (C).(taken from Singhal et al. (2024))

non-vanishing order (the quadrupole order) yields the potential originally derived by Kozai (1962):

$$\overline{\mathcal{R}}_{\rm p} = -\frac{GmM_{\rm p}}{16R_{\rm p}}\left(\frac{a}{R_{\rm p}}\right)^2 \left[(2+3e^2)(3\cos^2 i - 1) + 15e^2 \sin^2 i \cos 2\omega\right] \tag{2.1}$$

where ω represents the argument of periapsis of the test particle's orbit. When this potential is evaluated, depending on the initial conditions, the orbit of the test particle may undergo large periodic oscillations in i and e, which are mutually coupled. This is an observable effect of the quadrupole KL mechanism (von Zeipel, 1910; Kozai, 1962; Lidov, 1962). Variations in i and e are coupled to preserve the Kozai integral, $C \equiv \sqrt{1-e^2}\cos i$, as a constant (that is, the component of the test particle's angular momentum vector parallel to the angular momentum vector of the perturber). While the Kozai integral maps out the permissible phase space of these variations, it is fundamentally the conservation of the energy potential $\overline{\mathcal{R}}_{\rm p}$ that determines the boundaries of the motion. The fixed value of $\overline{\mathcal{R}}_{\rm p}$ dictates the topological structure of the phase space for the corresponding value of C. The phase-space trajectories for different values of C in the $(e\cos\omega, e\sin\omega)$ space are

shown in the bottom pannel of Figure 2.1. For $C \leq \sqrt{3/5}$, a separatrix forms in $e - \omega$ space at $e = 0$, as shown in the bottom left pannels of Figure 2.1. This configuration triggers large-amplitude excursions in eccentricity over time, which drive corresponding, coupled variations in inclination, whereas for $C > \sqrt{3/5}$, the eccentricity oscillates minimally (and not at all for circular orbits) as shown in the bottom right pannel of Figure 2.1. These oscillations happen over a characteristic timescale, often referred to as the Kozai timescale, and its given by (Kozai, 1962; Lidov, 1962):

$$T_{\rm K} \equiv \frac{M_\bullet}{M_{\rm p}} \frac{R_{\rm p}^3}{a\sqrt{GM_\bullet a}}. \tag{2.2}$$

When we remove the assumption of circular orbit of the perturber, the higher-order terms in the expansion of the secular potential become important. The additional octupole-order term gives rise to the eccentric Kozai-Lidov mechanism (EKL) (Naoz, 2016). The strength of the octupole effects is commonly quantified by the dimensionless octupole parameter:

$$\epsilon_{\rm oct} = \frac{a}{a_{\rm p}} \frac{e_{\rm p}}{1 - e_{\rm p}^2}, \tag{2.3}$$

where $a_{\rm p}$ and $e_{\rm p}$ are the semi-major axis and eccentricity of the perturber. As the eccentricity of the outer orbit goes to 0, the $\epsilon_{\rm oct}$ also goes to 0, and the dynamics reduce to the quadrupole KL oscillations. With the EKL mechanism, the eccentricity of the inner orbit can reach higher eccentricity values, and in cases the inclination can cross 90°, causing the orbit to switch between prograde and retrograde configurations (Naoz, 2016).

However, KL oscillations are most effective in environments with no other torques that lead to a change of ω as otherwise the applied torque by the perturber gets averaged out. This change in ω can happen due to various reasons, for example due to effects of relativity or if the system is embedded within an extended mass. Since the orbits around Sgr A* have to deal with effects of relativistic precession for close orbits to Sgr A* but also the damping of KL oscillations by the nuclear star cluster, KL oscillations are usually damped to certain degree and need to be considered carefully in the Galactic Center.

2.3 VHS mechanism

Although the KL mechanism has been studied and has many applications in astrophysical systems, an additional fourth body brings new degrees of freedom leading to larger variety of evolutionary pattern. Variants of four body systems, such as the restricted four body problem, has been studied with interesting dynamical effects (Huang, 1960; Simó, 1978; Scheeres, 1998; Baltagiannis and Papadakis, 2011). Yet, another variant, with a very similar setup as for the KL dynamics, was considered by Haas et al. (2011b) where they study two mutually interacting light bodies in orbit around a central massive body and a distant perturber. In this study, the system was supposed to be embedded in an external non-Keplerian spherically symmetric potential to dampen the KL oscillations. This results in the two light bodies having a non-evolving eccentricity. The two

light bodies are on circular orbits with their semi major axis being close to each other. The two bodies are also initially co-planar but are inclined with respect to the reference plane set up by the orbit of outer the perturber.

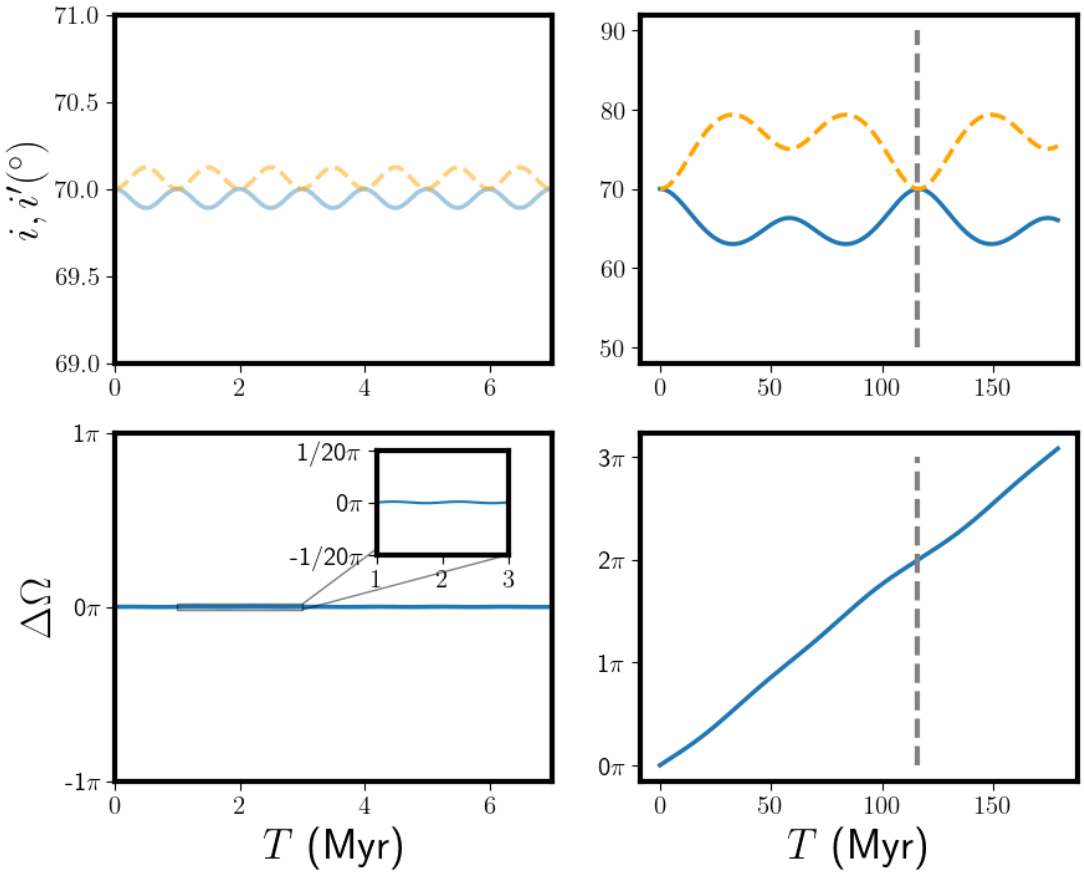

Figure 2.2 Orbital evolution of two mutually interacting light bodies orbiting a central massive object under the influence of a distant perturber, as described by the VHS mechanism. The left panels illustrates the synchronized precession of the longitude of ascending nodes (Ω) in the 'strong mode,' with small scale oscillations in mutual inclination which preserves the initial co-planar structure of the bodies. The right panels demonstrates the 'weak mode,' where independent precession leads to large-scale oscillations in mutual inclination.

In this setup, Haas et al. (2011b) using secular theory showed that the two light bodies exchange their angular momentum periodically, resulting in oscillations in their mutual inclination. We refer to the dynamics introduced by this setup as the *VHS mechanism*[1]. If the two light bodies have strong mutual interaction due to higher masses or small separation in semi-major axis, then the precession of Ω of the two bodies gets synchronized and their initial co-planar structure is nearly preserved as shown in the left column of Figure 2.2. This is referred to as the *strong mode* of the VHS mechanism. However, in the case they have weak mutual interaction, the precession of Ω is independent, and large scale oscillations in inclinations are observed, and can be seen in the right column of Figure 2.2. This is aptly referred to as the *weak mode* of the VHS mechanism.

[1]The name is based on the authors of the Haas et al. (2011b)

Haas et al. (2011a,b) used the VHS mechanism to study the evolution and formation of the CWS from a single parent disk with the perturber being the CND and the system embedded in the nuclear stellar cluster. The results suggest that the VHS mechanism in such a setup can explain the mutual near perpendicular orientation of the CWS and CND. The application of the secular theory was however limited due to requirements of a spherically symmetric extended potential, especially in the vicinity of an SMBH or other compact bodies. In the vicinity of massive bodies, we have to consider relativistic effects, which can also dampen the KL oscillations. This was explored in my published work, Singhal et al. (2024), along with studying the VHS mechanism in systems with non-zero eccentricity and disk like structures. We discuss the results later in Chapter 4.

2.4 Relativistic Effects

For stars and compact objects orbiting sufficiently close to Sgr A* , general relativistic corrections to Newtonian gravity become dynamically important. These relativistic effects introduce additional sources of orbital precession that can significantly alter secular evolution and suppress long-term coherent torques. As a result, relativistic dynamics play a crucial role in determining which mechanisms are effective in the innermost regions of the Galactic Center.

The dominant relativistic correction for most stellar orbits is Schwarzschild (apsidal) precession, which causes the argument of periapsis to advance on each orbit. The relativistic precession rate increases rapidly with decreasing semi-major axis and increasing eccentricity, and for sufficiently tight orbits, it can exceed the precession induced by the extended mass of the nuclear star cluster (Weinberg, 1972; Merritt, 2013). This rapid precession effectively averages out secular torques from distant perturbers, suppressing mechanisms such as the Kozai–Lidov oscillations and scalar resonant relaxation.

At even smaller radii, frame-dragging effects due to the spin of the SMBH (Lense-Thirring precession) can become relevant. Although typically subdominant for most observed stars, this effect is expected to play an important role in the dynamics of compact objects on very tight orbits and is particularly relevant for extreme mass ratio inspirals (EMRIs).

The combined influence of relativistic precession and resonant relaxation leads to the emergence of the Schwarzschild barrier, a region in phase space where relativistic precession suppresses further angular momentum evolution toward extreme eccentricities. This barrier has important implications for the rates of tidal disruption events, EMRIs, and direct plunges, and it needs to be considered when modeling the innermost 10^{-5} pc of the Galactic Center.

2.5 Binary Dynamics in the Galactic Center

A large fraction of stars are born in pairs, which may play an important role in the dynamical evolution of their host star cluster. In the dense Galactic Center, these binary systems significantly influence cluster dynamics due to their large effective cross-sections and their ability to efficiently exchange energy and angular momentum during gravitational encounters. Surrounded by the extreme

environment of Sgr A* , binaries undergo frequent interactions with the central supermassive black hole, background stars, and other binary systems, resulting in a rich variety of dynamical outcomes unavailable to single stars.

2.5.1 Tidal Disruption of Binaries by the SMBH

One of the most dramatic binary interactions in the Galactic Center is the tidal breakup of a binary during a close passage to Sgr A* . If a binary approaches the SMBH within its tidal radius, the differential gravitational force exerted by the SMBH can overcome the self-gravity of the binary, resulting in the disruption of the system. In this process, one component of the binary may become tightly bound to the SMBH, while the other is ejected at high velocity. This mechanism was first proposed by Hills (1988) and provides a natural explanation for the origin of hypervelocity stars, which are stars with velocities greater than the escape velocity of the galactic potential.

The captured component is expected to remain on a highly eccentric orbit around Sgr A* , because of which the Hills mechanism is considered as the major formation channel for the S-stars. This process effectively constitutes a binary loss cone, which is significantly larger than that for single stars, enhancing the efficiency of stellar capture and ejection in the Galactic Center.

2.5.2 Binary Evolution and Encounters

Beyond tidal disruption by the SMBH, binaries in the Galactic Center undergo frequent encounters with surrounding stars. Depending on their binding energy, binaries may be classified as hard or soft relative to the local velocity dispersion. Soft binaries tend to be rapidly disrupted through encounters, while hard binaries can harden further via repeated interactions, increasing their binding energy.

Binary-single and binary-binary encounters can lead to a variety of outcomes, including exchanges of companions, eccentricity excitation, and orbital reorientation. These interactions contribute to the gradual depletion of primordial binaries in the inner parsec and can significantly modify the properties of surviving systems.

2.5.3 Binary Collisions and Mergers

In the high-density environment near Sgr A* , dynamical interactions can drive binaries to extreme eccentricities, increasing the likelihood of stellar collisions and mergers. Collisions may occur during resonant three-body encounters, during tidal breakup events, or as a result of secular eccentricity excitation from KL oscillations. Binary mergers can produce rejuvenated stars that appear anomalously young, offering a possible explanation for some members of the S-cluster and for the stellar cores hypothesized to reside within dust-enshrouded objects.

Such merger products may be surrounded by residual gas and dust, naturally linking binary dynamics to the population of dusty objects observed near Sgr A* . These processes provide a compelling dynamical pathway for producing exotic stellar populations in an environment where in-situ star formation is supposed to be strongly suppressed.

Overall, binary dynamics constitute a crucial channel for redistributing energy, angular momentum, and stellar populations in the Galactic Center, complementing

relaxation-driven processes and shaping the observed demographics of stars orbiting Sgr A* . The results of numerical simulations showing how binary dynamics shapes our Galactic Center are presented later in Chapter 5 and Chapter 6.

3 Numerical Tools and Methods

The dynamical processes operating in the Galactic Center span a wide range of spatial and temporal scales, from long-term relaxation driven by the nuclear star cluster to short-timescale few-body interactions involving binaries and close encounters with the SMBH. Accurately modeling this environment therefore requires a combination of numerical approaches tailored to different dynamical regimes. In this work, a hybrid methodology is adopted, combining direct N-body simulations for the global stellar environment with specialized few-body integrations for tightly interacting subsystems.

3.1 Direct N-body Simulations with `NBODY6`

To model the collective dynamics of stars in the vicinity of Sgr A* , we employ the direct N-body code `NBODY6` (Aarseth, 2003). `NBODY6` integrates the equations of motion using a high-order Hermite scheme and incorporates adaptive individual timesteps, making it well suited for dense stellar systems with a wide dynamical range. Close encounters and bound subsystems are treated using regularization techniques, allowing accurate integration without excessive timestep reduction.

In the simulations presented in this work, `NBODY6` is used without post-Newtonian (PN) corrections. As a result, relativistic effects such as Schwarzschild precession and gravitational-wave energy loss are not included explicitly in the equations of motion. This choice is appropriate for capturing the Newtonian dynamics governing relaxation, binary encounters, and tidal breakup processes at distances where relativistic effects are subdominant, while avoiding additional computational complexity. The implications of neglecting relativistic corrections are discussed where relevant.

3.1.1 Modified Neighbor Selection Criterion

A key modification to the standard `NBODY6` implementation concerns the identification of neighboring particles for force calculations and regularization. In the default scheme, neighbors are selected primarily based on spatial proximity. However, in the Galactic Center, massive objects such as the SMBH or stellar-mass black holes can exert a dominant dynamical influence even at comparatively larger distances.

To account for this, the neighbor selection criterion was modified to incorporate both distance and mass, prioritizing particles that exert the strongest gravitational influence rather than those that are merely closest in space. This mass-weighted neighbor identification improves the treatment of interactions involving massive perturbers and enhances the accuracy of force calculations and subsystem detection in a highly mass-segregated environment.

3.2 Few-body Integrations with `ARWV`

While direct N-body simulations efficiently capture the global evolution of the system, tightly bound binaries and close encounters with the SMBH require

higher precision than is computationally feasible within a full N-body framework. For this reason, selected few-body interactions are integrated using the `ARWV` code, a specialized few-body integrator based on the algorithmic chain regularization (ARCHAIN) method (Mikkola and Merritt, 2006; Chassonnery et al., 2019).

ARCHAIN reformulates the equations of motion in a chain coordinate system and employs time transformations to handle close encounters with machine precision accuracy. This approach is particularly effective for hierarchical systems, resonant interactions, and encounters involving extreme mass ratios, such as binaries interacting with Sgr A* . `ARWV` allows for robust integration of few-body systems over many orbital times without numerical divergence, making it well suited for studying binary disruption, exchanges, collisions, and mergers.

3.3 Hybrid Approach and Applicability

The use of `NBODY6` and `ARWV` enables a flexible and efficient exploration of dynamics in the Galactic Center across multiple regimes. Global simulations with `NBODY6` provide the background stellar environment and capture long-term processes such as relaxation and binary evolution, while `ARWV` is used to study individual few-body interactions with high precision. This allows the strengths of each method to be leveraged while mitigating their respective limitations.

4 Relativistic Corrections to the Hierarchical Four-Body VHS Mechanism

In Singhal et al. (2024), we discuss the secular theory and approximations used to expand the VHS mechanism by removing constraints of the previous works. We explored the imapct of relativistic effects on the VHS mechanism, as relativistic precession has the ability to dampen KL oscillation. We find that using an approximation by Rubincam (1977), we can mimic the precession of the argument of pericenter caused due to relativistic effects with an additional potential. We use the potential to formulate equations of secular evolution of orbits of two light bodies within this setup where KL oscillations were damped due to relativity. We also compared them with few body integrations to validate the results of the secular theory, and we find the secular theory to be compatible with few body integrations for circular orbits.

However, as the secular theory requires the two nearby orbits to be circular, and currently no analytical theory is formulated for non-zero eccentricity. This is expected to be non-trivial as the nearby eccentric orbits can undergo close encounters and result in chaotic behavior. So we use numerical integrations with relativistic corrections to study evolution of the 4 body setup described earlier with different parameters for the two light bodies. We find small inclination oscillation and co-evolution of Ω for two strongly mutually interacting bodies just like the *strong mode*, and similarly we see the large inclination oscillations with independently evolving Ω for weakly mutually interacting bodies for *weak mode*. However, they are slightly modified for both the *strong mode* and *weak mode*. In *strong mode*, the small scale oscillations in inclination are mirrored, but unlike the zero eccentricity case where the sign of $\Delta i \equiv i_1 - i_2$ did not change, we see periodic changes in the sign of Δi (i_1 and i_2 are the inclination of the first and second test particle respectively). We also observe the magnitude of the oscillations of inclinations of the two bodies are larger in comparison to the zero eccentricity case. Finally in the *strong mode*, the differential precession of Ω is not as well suppressed as in the zero eccentricity case. In the case of *weak mode*, non-zero eccentricity of the orbits results in decrease in the characteristic time period of the *weak mode* of VHS mechanism. Due to close interactions, the orbits can change and the mode of the VHS mechanism can change as well. We also found that the VHS mechanism can co-exist with KL oscillations. It also affected $T_{\rm K}$ of the two bodies such that the $T_{\rm K}$ of the KL oscillations with VHS mechanism was in between the value of $T_{\rm K}$ when the bodies evolved without mutual interaction.

We follow up with an exploration of the VHS mechanism in a disk of stars, which produces a coherent structure that is nearly perpendicular to the perturbing body and an outer structure that is more spread out but with a lower value of inclination than the initial setup. The integrated system was scaled to that of the S-stars in the Galactic center. Thus, it is capable of being compatible with observations that suggest coherent disk like structures within the S-cluster (Ali et al., 2020; Peißker et al., 2024b).

In the following paper (Singhal et al., 2024), I did all the analytical calculations, numerical simulations, production of the figures and writing. The text went through iterative improvements with the co-authors inputs through comments or direct rewrites.

Monthly Notices of the ROYAL ASTRONOMICAL SOCIETY

MNRAS **531,** 2028–2039 (2024) https://doi.org/10.1093/mnras/stae1276
Advance Access publication 2024 May 17

Dynamical coupling of Keplerian orbits in a hierarchical four-body system: from the Galactic Centre to compact planetary systems

M. Singhal ,★ L. Šubr and J. Haas
Astronomical Institute, Faculty of Mathematics and Physics, Charles University, V Holešovičkách 2/747, 18000 Praha, Czech Republic

Accepted 2024 May 14. Received 2024 April 16; in original form 2023 November 6

ABSTRACT

This study focuses on the long-term evolution of two bodies in nearby initially coplanar orbits around a central dominant body perturbed by a fourth body on a distant Keplerian orbit. Our previous works that considered this setup enforced circular orbits by adding a spherical potential of extended mass, which dampens Kozai–Lidov oscillations; it led to two qualitatively different modes of the evolution of the nearby orbits. In one scenario, their mutual interaction exceeds the effect of differential precession caused by a perturbing body. This results in a long-term coherent evolution, with nearly coplanar orbits experiencing only small oscillations of inclination. We extend the previous work by (i) considering post-Newtonian corrections to the gravity of the central body, either instead of or in addition to the potential of extended mass, (ii) relaxing the requirement of strictly circular orbits, and (iii) removing the strict requirement of complete Kozai–Lidov damping. Thus, we identify the modes of interorbital interaction described for the zero eccentricity case in the more general situation, which allows for its applicability to a much broader range of astrophysical systems than considered initially. In this work, we scale the systems to the orbits of S-stars; we consider the clockwise disc to represent the perturbing body, with post-Newtonian corrections to the gravity of Sagittarius A$*$ playing the role of damping potential. Considering post-Newtonian corrections, even stellar-mass central bodies in compact planetary systems can allow for the coupled evolution of Keplerian orbits.

Key words: black hole physics – celestial mechanics – stars: kinematics and dynamics – Galaxy: centre.

1 INTRODUCTION

The study of dynamics in Keplerian potentials is an old yet very progressive area of research. The secular orbital evolution of light (test) particles in the dominating central potential accompanied by a distant perturber is one of the classical problems in celestial mechanics. According to the pioneering works of Kozai (1962) and Lidov (1962), the orbital solution within this hierarchical three-body setup is often called Kozai–Lidov (K-L) dynamics. Various works have extended its original formulation, which supposed a non-evolving circular orbit of the perturber, for example, eccentric perturber (Naoz et al. 2011; Lithwick & Naoz 2011), relativistic effects (Naoz et al. 2013; Lim & Rodriguez 2020), mass loss, and transfer (Michaely & Perets 2014).

Considering the four-body setup brings new degrees of freedom and also more variants of the general setup (Huang 1960; Simó 1978; Scheeres 1998; Baltagiannis & Papadakis 2011). A possible configuration has recently been investigated by Haas, Subr & Vokrouhlicky (2011b). Similarly to K-L dynamics, their setup consists of a dominating central body and a massive perturber on a circular orbit. Contrary to K-L dynamics, they considered the orbital evolution of two light, mutually gravitationally interacting bodies inner to the orbit of the massive perturber. In their work, Haas et al. (2011b) focused on the case when the two inner orbits are close to each other in terms of semimajor axes and are initially coplanar (with arbitrary inclination with respect to the orbit of the perturber). An additional assumption, primarily imposed due to limitations of the used calculus, was the non-evolving zero eccentricity of the two inner orbits. Haas et al. (2011b) argue that this assumption is relevant if another non-Keplerian spherically symmetric potential is present within the system, being strong enough to damp the K-L oscillations of the inner bodies enforced by the massive perturber. Within this setup, Haas et al. (2011b) developed a secular theory showing that the two inner orbits periodically exchange their angular momentum such that their inclinations oscillate. If their mutual interaction is strong enough (which depends on their mass and separation), the precession of their orbits is synchronized, that is, the initial coplanar structure is nearly preserved. In the other case, orbital planes of the inner bodies precess differentially due to the perturbing force of the outer body, which leads to disruption of the coplanar configuration. We refer to the temporal evolution of the specific four-body setup introduced by Haas et al. (2011b) as the VHS mechanism (based on the authors of the Haas et al. (2011b) paper, D. **V**okrouhlicky´, J. **H**aas and L. **Š**ubr) throughout this paper.

A shortcoming of the secular theory of VHS dynamics is the requirement of the spherically symmetric external potential needed to dampen the K-L oscillations, which reduces its applicability in observed astrophysical systems. However, Haas, Šubr & Kroupa (2011a), Haas et al. (2011b) introduced a physically realistic setup in which the VHS mechanism is applicable. They studied a system

★ E-mail: singhal.myank@matfyz.cuni.cz

in which the supermassive black hole (SMBH) in the Galaxy's centre, Saggitarius A∗ (SgrA*, Ghez et al. 2003; Eisenhauer et al. 2005; Gillessen et al. 2009a, b; Yelda et al. 2010), represents the dominant body, and the additional spherical potential is due to the surrounding nuclear star cluster. They considered the perturbing body to be the circumnuclear gaseous disc (Martín et al. 2012; Liu et al. 2012; Hsieh et al. 2017; Tsuboi et al. 2018; Goicoechea et al. 2018; Hsieh et al. 2021) and the bodies on inner nearby coplanar orbits to be the observed stars from the young stellar disc that is within the distances of 0.04–0.4 pc from the central SMBH (Levin & Beloborodov 2003; Paumard et al. 2006; Bartko et al. 2009, 2010). Haas et al. (2011a, b) suggested that the four-body dynamics in the spherically symmetric external potential can explain the specific, near-perpendicular orientation of the stellar disc with respect to the distant perturber.

Our study aims to expand the scope of the VHS dynamics described in Haas et al. (2011b) and to explore its applicability in a broader range of astrophysical systems by relaxing some of the assumptions of the underlying secular theory. First, we develop the idea, suggested in the original work, that the non-Keplerian spherical potential can be omitted if we consider post-Newtonian terms in the gravity of the central body while still working within the secular approach. Secondly, we investigate the evolution of systems with a non-zero eccentricity of the two inner orbits by directly integrating the equations of motion. Finally, we consider a scenario in which the eccentricity of the inner orbits evolves over time, that is, when the K-L oscillations are not entirely damped.

The paper is structured as follows: in Section 2, we provide a detailed description of the four-body setup we are studying. Section 3 provides a summary of the secular theory developed in Haas et al. (2011b), along with a discussion of the damping of K-L oscillations due to the effects of general relativity. Section 4 describes several examples of systems with non-zero eccentricity that were integrated. Finally, we present our conclusions on the generalized VHS dynamics in Section 5.

2 SETUP

We study a hierarchical four-body system with a dominant central body, characterized only by its mass, $M_\bullet$. The system further consists of a distant perturber of mass M_p on a circular orbit with radius R_p around the central body. The orbit of the perturber defines the reference plane. We can choose any line within this plane to define our reference axis to calculate the longitude of the ascending node, Ω. Finally, we consider two light particles of masses m and m' where $m, m' \ll M_\mathrm{p}$ on orbits around the central body with a semimajor axes a and a', which are much smaller than R_p and $a' < a$. These light bodies are in inclined orbits, having inclinations i and i' with respect to the reference plane. The last important parameters we consider are the longitudes of the ascending nodes of the two bodies, Ω and Ω'. Initial conditions are set up such that $i = i'$ and $\Omega = \Omega'$.

As an example, in this work we use the objects observed in the Galactic Centre as an astrophysical system to provide us realistic values for $M_\bullet$, M_p, and R_p. We set the system that may correspond to the situation in the vicinity of the SgrA* black hole, that is, $M_\bullet = 4 \times 10^6\,\mathrm{M}_\odot$ (Ghez et al. 2003; Eisenhauer et al. 2005; Gillessen et al. 2009a, b; Yelda et al. 2010). We consider the distant perturber of mass of $M_\mathrm{p} = 10^4\,\mathrm{M}_\odot$ and a semimajor axis of $R_\mathrm{p} = 0.1$ pc, aiming to mimic the overall gravitational influence of the observed clockwise young stellar disc (CWD, Lu et al. 2013; von Fellenberg et al. 2022). The two light particles could be representatives of the S-stars that are observed in the Galactic Centre.

3 SECULAR THEORY

In this section, we follow the mathematical approach used in Haas et al. (2011b) and briefly sketch the main ideas. In particular, we consider a secular approach to describe the long-term evolution of the system described in Section 2. For this, the mean interaction potential of the system, $\overline{\mathcal{R}}$, averaged over fast changing variables needs to be specified. As it can be given as a direct sum of the individual terms describing different components of the system, we discuss these separately in the following sections.

3.1 Potential of the distant/outer perturber

The averaged interaction potential between a perturbing body on a circular orbit with radius R_p and a particle on an orbit with semimajor axis a, eccentricity e, and inclination i with respect to the orbital plane of the perturber reads (Kozai 1962):

$$\overline{\mathcal{R}}_\mathrm{p} = -\frac{GmM_\mathrm{p}}{16R_\mathrm{p}}\left(\frac{a}{R_\mathrm{p}}\right)^2 [(2+3e^2)(3\cos^2 i - 1) + 15e^2 \sin^2 i \cos 2\omega], \quad (1)$$

where ω is the argument of periapses of the orbit. Suppose $\overline{\mathcal{R}}_\mathrm{p}$ is the only component of the total perturbing potential (i.e. the system is reduced to a three-body setup). In that case, the body on the inner orbit is subject to quadrupole K-L dynamics (Kozai 1962; Lidov 1962). Depending on the initial conditions, its eccentricity and inclination may undergo large periodic variations that are mutually coupled through the so-called Kozai integral, $C \equiv \sqrt{1-e^2}\cos i$, which, together with the semimajor axis (a) and $\overline{\mathcal{R}}_\mathrm{p}$, is a conserved quantity along the orbit evolution.

The number of known integrals of motion allows for an effective insight into the K-L dynamics through plots of isocontours of $\overline{\mathcal{R}}$ in the e–ω space, which for fixed values of a and C give sets of possible evolutionary tracks (see Fig. 1). These sets form two qualitatively different topologies: for $C > \sqrt{3/5}$, they consist of concentric ovals, which means that the eccentricity oscillates slightly along the evolutionary path and ω rotates within the whole range $(0, \pi)$ (see right panel of Fig. 1). If $C \leq \sqrt{3/5}$, the topology qualitatively changes: a separatrix crosses the central point; It divides the diagram into zones with ω librating around the value of $\pi/2$ or $3\pi/2$ and the outer rotation zone (left and middle panels of Fig. 1). The lower the value of C, the larger the eccentricity oscillations. The characteristic time scale for these oscillations is given by (Kozai 1962; Lidov 1962):

$$T_\mathrm{K} \equiv \frac{M_\bullet}{M_\mathrm{p}}\frac{R_\mathrm{p}^3}{a\sqrt{GM_\bullet a}}. \quad (2)$$

An important result from the isocontour plots is that the zero eccentric orbit is stable for $C > \sqrt{3/5}$, while it undergoes periodic variations when C below the limiting value.

Finally, let us note that the longitude of the ascending node, Ω, rotates monotonically in the full range of $(0, 2\pi)$ for arbitrary initial conditions. The rate of precession depends on the other orbital elements, as well as on the mass and semimajor axis of the perturber. However, the value of Ω does not affect the evolution of the other orbital elements, which is a natural consequence of the axial symmetry of the problem.

3.2 Spherical potential

In our study of four-body systems, we examine two distinct sources of an external spherical potential. The first source is the presence of an extended mass around the central body, while the second source is an approximation of the first-order post-Newtonian corrections

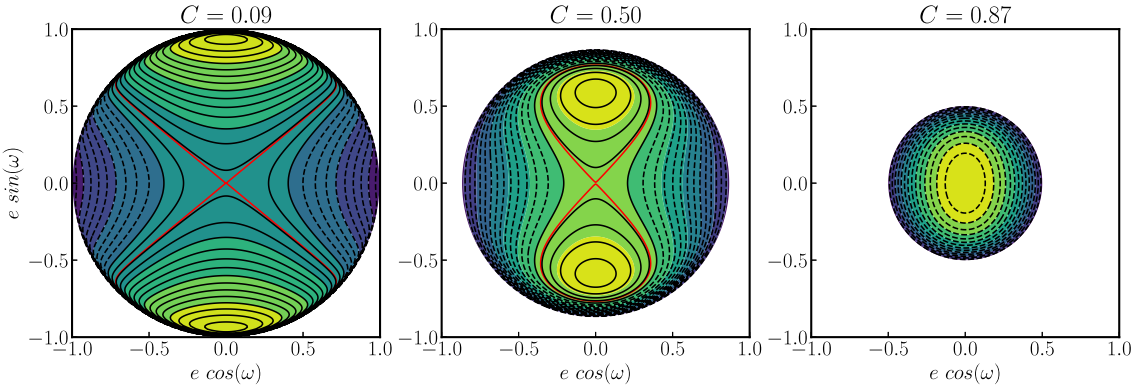

Figure 1. Isocontours of $\overline{\mathcal{R}}$ for different fixed values of the Kozai integral (C, indicated above individual panels) in a three-body system showing pure K-L dynamics. The shape of these isocontours is independent on a. The leftmost panel shows isocontours in $e - \omega$ space for $C < \sqrt{3/5}$, which shows large changes in eccentricity over the orbit. The middle panel is for C still smaller than $\sqrt{3/5}$ but with separatrix (displayed with red line) reaching smaller values of eccentricity. In the rightmost panel, we have $C > \sqrt{3/5}$ and we see oval evolutionary tracks, meaning small changes in eccentricity.

to the gravity of $M_\bullet$. Although these sources differ, they have very similar effects and impact the evolution of the two bodies in a similar manner.

3.2.1 *Extended mass*

Haas et al. (2011a, b) considered such an astrophysical context involving an extended mass around the central body, influencing the secular dynamics of the inner orbit(s). In particular, the authors provide an analytic form for the mean potential corresponding to the mass density distribution with power-law profile, $\rho_c \propto r^{\beta-2}$,

$$\overline{\mathcal{R}}_\mathrm{c} = -\frac{GmM_c}{\beta R_\mathrm{p}} \left(\frac{a}{R_\mathrm{p}}\right)^\beta \mathcal{J}(e,\beta), \tag{3}$$

where M_c stands for the integral of the extended mass density within the orbit of the perturber (R_p) and

$$\mathcal{J}(e,\beta) = \frac{1}{\pi}\int_0^\pi (1-e\cos u)^{1+\beta}\,\mathrm{d}u = 1 + \sum_{n\geq 1} a_n e^{2n}. \tag{4}$$

The coefficients a_n are given by

$$\frac{a_{n+1}}{a_n} = \left[1 - \frac{3+\beta}{2(n+1)}\right]\left[1 - \frac{2+\beta}{2(n+1)}\right], \tag{5}$$

with $a_1 = \beta(1+\beta)/4$.

From the spherical symmetry of this perturbing potential we get that its only manifestation on the orbit evolution is a monotonous (retrograde) rotation of the argument of pericentre, ω. When combined with the potential of the distant perturber $\overline{\mathcal{R}}_\mathrm{p}$, the potential of the extended mass generally leads to damping of the K-L oscillations (see Haas & Šubr 2021, for a detailed discussion). This damping stabilizes the zero eccentricity orbit for arbitrary inclination for a suitable choice of system parameters. Note also that in such a situation, monotonous rotation of the longitude of the ascending node remains the primary manifestation of the influence of the distant perturber. Šubr, Schovancová & Kroupa (2009) showed that for damped K-L oscillations, the rate of change in longitude of the ascending node is given by

$$\frac{\mathrm{d}\Omega}{\mathrm{d}t} \approx -\frac{3}{4}\frac{\cos i}{T_\mathrm{K}}\frac{1+\frac{3}{2}e^2}{\sqrt{1-e^2}} \approx \text{constant}. \tag{6}$$

This equation shows that when the K-L oscillations are damped, $\frac{\mathrm{d}\Omega}{\mathrm{d}t}$ depends on the semimajor axis through T_K (see equation 2) and will result in differential precession for different orbits.

3.3 Post-Newtonian corrections

It has already been discussed in the literature that relativistic corrections to the gravity of the central body can play a role similar to the spherical potential of the extended mass in secular dynamics (Holman, Touma & Tremaine 1997; Blaes, Lee & Socrates 2002; Karas & Šubr 2007), enforcing a (prograde) rotation of the argument of the pericentre, ω. A straightforward way to implement this relativistic effect within the framework presented above is to use the approximation given by Rubincam (1977). This approximation mimics the rotation of the argument of pericentre due to the relativistic effect of the central body using an additional spherically symmetric potential,

$$V_\mathrm{GR} = -\frac{GM_\bullet h^2}{c^2 r^3}, \tag{7}$$

where $h \equiv \sqrt{GM_\bullet a(1-e^2)}$ is the specific angular momentum of the test particle and c stands for the speed of light. Formally, this potential is equivalent to spherical mass distribution with density profile $\rho \propto r^{-5}$, that is, the form of the averaged potential given by equation (3) with $\beta = -3$ may be directly used, giving us the mean potential of the first-order post-Newtonian correction,

$$\overline{\mathcal{R}}_\mathrm{GR} = -\frac{GM_\bullet m h^2}{c^2 a^3}\mathcal{J}(e,-3). \tag{8}$$

Note that, in comparison to the general mean potential for extended mass distribution, equation (8) contains additional dependence on eccentricity through h, and it has one less parameter ($M_\bullet$ versus M_c and a_P). Also note that equation (8) diverges as e approaches unity.

We visualize the damping effect of the post-Newtonian corrections using the isocontours of the perturbing potential in the e–ω space in Fig. 2. In particular, we show three examples of $\overline{\mathcal{R}}(e,\omega)$ with $\overline{\mathcal{R}} = \overline{\mathcal{R}}_\mathrm{p} + \overline{\mathcal{R}}_\mathrm{GR}$ for a randomly selected value of $C = 0.34$ and the properties of the central body and perturber are same as SgrA*($M_\bullet = 4\times10^6\,\mathrm{M}_\odot$) and the CWD ($M_\mathrm{p} = 10^4\,\mathrm{M}_\odot$ and $R_\mathrm{p} = 0.1\,\mathrm{pc}$) as described in Section 2. We change the value of the semimajor axis of the inner body, that is, with variable strength of $\overline{\mathcal{R}}_\mathrm{GR}$ with respect to $\overline{\mathcal{R}}_\mathrm{p}$.

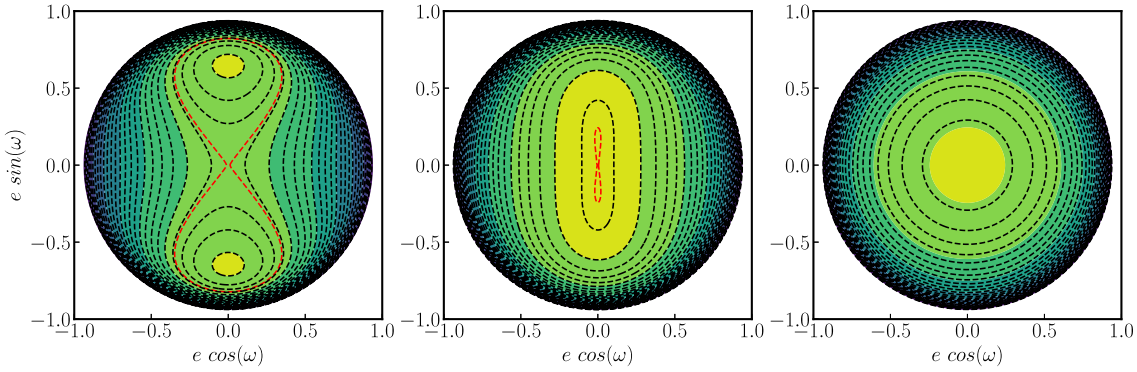

Figure 2. The potential isolines when the potential due to post-Newtonian approximation is added to the perturbing potential are displayed in three panels, representing two cases with identical parameters except for the semimajor axis of the test particle. In these examples, the value of $C = 0.34$ which is smaller than the limiting value for K-L dynamics, and the separatrix is shown in red. The panel on the left depicts the instability at $e = 0$ when $a = 0.2R_p$, while the panel on the right illustrates the stability at $e = 0$ when $a = 0.03R_p$. The central panel shows the boundary area when $a = 0.145R_p$ and the K-L oscillations are damped.

In the left panel of Fig. 2, the topology is very similar to that of the middle panel of Fig. 1, which means that $\overline{\mathcal{R}}_{\rm p}$ dominates over $\overline{\mathcal{R}}_{\rm GR}$ in absolute value for most of the parameter space. The middle panel of Fig. 2 shows a setup with a smaller value of semimajor axis, leading to a decrease in the absolute value of $\overline{\mathcal{R}}_{\rm p}$ while, at the same time, it leads to a growth in the absolute value of $\overline{\mathcal{R}}_{\rm GR}$, which means that it contributes considerably to $\overline{\mathcal{R}}$. The topology of the isocontours of $\overline{\mathcal{R}}$ remains the same as in the previous case, but the overall structure changes so that the separatrix does not reach smaller eccentricity values. Further reduction of the semimajor axis, as shown in the right panel of Fig. 2, leads to $\overline{\mathcal{R}}_{\rm GR}$ fully dominating over $\overline{\mathcal{R}}_{\rm p}$, and hence the isocontours of $\overline{\mathcal{R}}$ form nearly circular shapes as a consequence of the independence of $\overline{\mathcal{R}}_{\rm GR}$ on ω. In this case, the K-L oscillations are strongly damped, and the zero eccentricity orbit becomes stable and does not evolve.

For the sake of the analytic treatment of the four-body dynamics described in the following sections, the system configuration must be such that the zero eccentricity orbit is stable. However, due to the non-trivial dependence of $\overline{\mathcal{R}}_{\rm GR}$ and $\overline{\mathcal{R}}_{\rm p}$ on system parameters, this condition must be evaluated from case to case.

In Fig. 3, we evaluate it for parameters of the system that may correspond to the situation in the vicinity of the SgrA* black hole and the semimajor axis of the inner body is sampled within the range 0.01–0.5$R_{\rm p}$, which falls into the region of the S-stars for the example setup described in Section 2. We quantify the damping of K-L oscillations by evaluating the maximum value of eccentricity $e_{\rm max}$ reached by the system during its evolution when starting from near-zero eccentricity. The K-L oscillations are successfully damped when we obtain smaller values of $e_{\rm max}$, as the only source of change in eccentricity in these systems is the K-L dynamics. We see that in this setup, the GR effects damp the K-L oscillations for the entire range of C for $a \lesssim 0.14R_{\rm p}$. At the same time, for $a \gtrsim 0.3R_{\rm p}$, the K-L dynamics is less affected; that is, the zero eccentric orbit is stable only for $C \gtrsim \sqrt{3/5}$, shown by the white dashed line in Fig. 3.

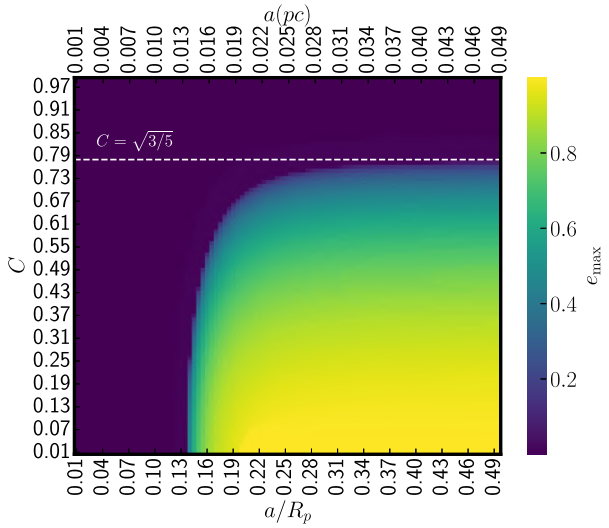

Figure 3. Heat map of largest variation in eccentricity for a 1 $M_\odot$ star initially on an orbit of eccentricity $e = 10^{-4}$ in the combined potential of a central dominant body ($M_\bullet = 4 \times 10^6$ $M_\odot$) and a distant perturber ($M_{\rm p} = 10^4$ $M_\odot$ and $R_{\rm p} = 0.1$ pc) on a circular orbit. The lower value of maximum eccentricity in a significant range of the parameter space shows that the relativistic corrections due to the SMBH partially or entirely dampen the K-L oscillations.

3.4 Interparticle potential

In order to describe the four-body setup, Haas et al. (2011b) evaluated the averaged interparticle potential for circular orbits,

$$\overline{\mathcal{R}}_{\rm i} = -\frac{Gmm'}{a}\Psi(\alpha, \boldsymbol{n}\cdot\boldsymbol{n}'), \tag{9}$$

where $\alpha \equiv a'/a$. $\boldsymbol{n}$ and $\boldsymbol{n}'$ are the unit vectors that are normal to the mean orbital plane for the two stars, which can be parametrized as $\boldsymbol{n} = [\sin i \sin\Omega, -\sin i \cos\Omega, \cos i]^T$ and $\boldsymbol{n}' = [\sin i' \sin\Omega', -\sin i' \cos\Omega', \cos i']^T$. We can define the function Ψ as

$$\Psi(\zeta, x) = \sum_{l\geqslant 2}[P_l(0)]^2\zeta^l P_l(x)\ , \tag{10}$$

where $P_l(x)$ are the Legendre polynomials.

We can express the potential energy due to the interaction of inner circular orbits and the outer perturber,

$$\overline{\mathcal{R}}_{\rm p,0} = -\frac{GmM_{\rm p}}{R_{\rm p}}\Psi(a/R_{\rm p}, \cos i), \tag{11}$$

$$\overline{\mathcal{R}}'_{\rm P,0} = -\frac{Gm'M_{\rm p}}{R_{\rm p}}\Psi(a'/R_{\rm p}, \cos i'). \tag{12}$$

3.5 VHS mechanism

The total averaged potential of the four-body setup described in Section 2 is:

$$\overline{\mathcal{R}} = \overline{\mathcal{R}}_i + \overline{\mathcal{R}}_{\mathrm{p},0} + \overline{\mathcal{R}}'_{\mathrm{p},0} \tag{13}$$

and the classical orbital elements are assumed to evolve according to the Lagrange equations (see e.g. Bertotti, Farinella & Vokrouhlický 2003):

$$\frac{\mathrm{d}\cos i}{\mathrm{d}t} = -\frac{1}{m\eta a^2}\frac{\partial\overline{\mathcal{R}}}{\partial\Omega}, \quad \frac{\mathrm{d}\Omega}{\mathrm{d}t} = -\frac{1}{m\eta a^2}\frac{\partial\overline{\mathcal{R}}}{\partial\cos i}, \tag{14}$$

$$\frac{\mathrm{d}\cos i'}{\mathrm{d}t} = -\frac{1}{m'\eta' a'^2}\frac{\partial\overline{\mathcal{R}}}{\partial\Omega'}, \quad \frac{\mathrm{d}\Omega'}{\mathrm{d}t} = -\frac{1}{m'\eta' a'^2}\frac{\partial\overline{\mathcal{R}}}{\partial\cos i'}, \tag{15}$$

here η and η' are the mean motion frequencies of the two bodies. Although the average potential due to either the extended mass or relativistic corrections plays an essential role in damping the K-L oscillations of the circular orbits, we may omit it here as it does not contribute to the target subset of Lagrange equations (14) and (15).

The set of equations (14) and (15) with mean perturbing Hamiltonian (equation 13) has been first studied by Haas et al. (2011b) and we refer to their solution in general as the VHS mechanism. These equations may be translated to equations for normal vectors, $\boldsymbol{n}$ and $\boldsymbol{n'}$, of the orbital planes (equations 21–26 of Haas et al. 2011b).

$$\begin{aligned}\frac{\mathrm{d}\boldsymbol{n'}}{\mathrm{d}t} &= \omega'_{\mathrm{I}}\,(\boldsymbol{n'}\times\boldsymbol{n}) + \omega'_{\mathrm{p}}\,(\boldsymbol{n'}\times\boldsymbol{e}_z),\\ \frac{\mathrm{d}\boldsymbol{n}}{\mathrm{d}t} &= \omega_{\mathrm{I}}\,(\boldsymbol{n}\times\boldsymbol{n'}) + \omega_{\mathrm{p}}\,(\boldsymbol{n}\times\boldsymbol{e}_z),\end{aligned} \tag{16}$$

where

$$\omega'_{\mathrm{I}} = -\eta'\alpha\left(\frac{m}{M_\bullet}\right)\Psi_x(\alpha, \boldsymbol{n}\cdot\boldsymbol{n'}), \quad \omega_{\mathrm{I}} = -\eta\left(\frac{m'}{M_\bullet}\right)\Psi_x(\alpha, \boldsymbol{n}\cdot\boldsymbol{n'}), \tag{17}$$

$$\omega'_{\mathrm{p}} = -\eta'\left(\frac{M_{\mathrm{p}}}{M_\bullet}\right)\Psi_x\left(\frac{a'}{R_{\mathrm{p}}}, \cos i'\right), \quad \omega_{\mathrm{p}} = -\eta\left(\frac{M_{\mathrm{p}}}{M_\bullet}\right)\Psi_x\left(\frac{a}{R_{\mathrm{p}}}, \cos i\right), \tag{18}$$

and

$$\Psi_x(\zeta, x) \equiv \frac{\mathrm{d}}{\mathrm{d}x}\Psi(\zeta, x). \tag{19}$$

The frequencies ω_{I}, ω'_{I} and ω_{p}, ω'_{p} correspond to the frequencies caused by the mutual interaction of the two bodies and the perturber, respectively.

Haas et al. (2011b) have shown both by means of analysis of the averaged Hamiltonian as well as direct integration of the Lagrange equations that there exist two qualitatively distinct classes of solutions. On a qualitative level, if the masses of the inner orbits are small enough, or their separation (in terms of semimajor axes) is sufficiently large or a combination of both, we call the regime of interaction weak. In the opposite case, we call the interaction strong. Explicit formula defining boundary between the two modes is not known, nevertheless, an estimate for particular setup can be obtained comparing the frequencies ω_{I} and ω'_{I} to ω_{p} and ω'_{p}. In the *strong* mode, ω_{I}, $\omega'_{\mathrm{I}} >> \omega_{\mathrm{p}}$, ω'_{p} which means that evolution of the orbital planes described by equation (16) is governed by the mutual interaction of the inner orbits. On the other hand, if ω_{I}, $\omega'_{\mathrm{I}} << \omega_{\mathrm{p}}$, ω'_{p}, the weak mode of the VHS mechanism takes place in which the two planes precess differentially due to the gravitational influence of the outer orbit. Note that none of the frequencies ω_{I}, ω'_{I}, ω_{p}, and ω'_{p} are constant over time. Hence, determination of which mode realizes cannot be reliably determined from their initial values.

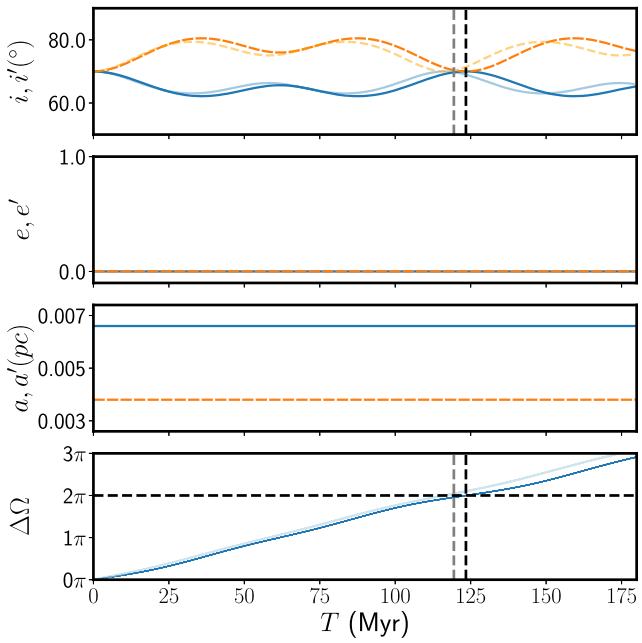

Figure 4. Evolution of model `M1` showing the weak mode of evolution in VHS mechanism. Weak mode of VHS mechanism results in different rate of change in evolution of $\Delta\Omega$ along with oscillations in inclination. The lighter version of the lines is the result of integration of secular equations, while the darker versions are the result of integration of equations of motion. The black dashed lines highlight that the mutual inclination becomes 0 when the value of $\Delta\Omega$ is a multiple of 2π in the integration of equations of motion. Similarly the grey line is for the integration of secular equations.

Table 1. Parameters of the two light bodies in the four-body setup. For all the models, the parameters of the central body and the perturber stay consistent. The central dominant body is at the origin and has mass $M_\bullet = 4 \times 10^6\,\mathrm{M}_\odot$. The perturber has a mass of $M_{\mathrm{p}} = 10^4\,\mathrm{M}_\odot$ in a circular orbit at radius $R_{\mathrm{p}} =$ 0.1 pc.

Model	m,m' ($\mathrm{M}_\odot$)	a' (pc)	a (pc)	e,e'	Figure
`M1`	1	0.0035	0.007	0.0	4
`M2`	1	0.0035	0.007	0.721	6
`M3`	10	0.0035	0.0045	0.0	5
`M4`	10	0.0035	0.0045	0.77	7
`M5`	10	0.0196	0.0215	0.01	8
`M6`	10	0.0151	0.0168	0.03	9

3.5.1 *Weak mode of the interparticle interaction*

In the weak mode of the VHS mechanism, the two orbits periodically interchange their angular momenta such that their magnitudes stay constant, but mutual inclination changes. The longitudes of their ascending nodes rotate at different rates while still being mutually influenced. This independent rotation of Ω disrupts the original co-planar configuration. At the moments when $\Delta\Omega \equiv \Omega' - \Omega$ reaches the value of a multiple of 2π, the relative inclination of the two orbits drops to zero, and the planar structure is re-established for the moment.

An example of this solution is shown in Fig. 4 with parameters of the system given in Table 1 under the label `M1`. Besides showing the orbital evolution according to the secular approximation, we also plot the evolution of the orbital elements coming from direct integration of the equations of motion. For the latter case, we utilize the ARWV

integrator (Chassonnery, Capuzzo-Dolcetta & Mikkola 2019) since it allows for integrations of a few-body system with up to 2.5 order post-Newtonian approximation. Both solutions share the same qualitative properties with slight differences in the amplitude and period of oscillations of the inclinations which indicate the quality of the secular approximation in this particular configuration.

Estimate of characteristic time-scale, $T_{\rm char}$, of the weak mode of the VHS mechanism comes from that (i) the precession of Ω is dominated by the distant perturber, that is, it is nearly constant but different for the two inner bodies and (ii) the period of oscillation of inclinations is determined by the time instances when $\Omega - \Omega' = 2\pi$. To find $T_{\rm char}$ for which $\Omega(T_{\rm char}) - \Omega'(T_{\rm char}) = 2\pi$, we can apply equation (6) independently to both the inner and outer orbits, approximating inclinations and eccentricities with their initial values ($I = I' = I_0$ and $e = e' = e_0$) which yields:

$$T_{\rm char} \approx \frac{16\pi\sqrt{1-e_0^2}}{3(3e_0^2+2)\cos I_0}\left[\frac{1}{T_{\rm K}} - \frac{1}{T'_{\rm K}}\right]^{-1}. \tag{20}$$

For the case of $e_0 = 0$, this simplifies to the formula given by Haas et al. (2011b, equation 34). Plugging the initial conditions of `M1` in equation (20) we get $T_{\rm char} \approx 192$ Myr which is same order of magnitude of $T_{\rm M1} = 123.42$ Myr.

3.5.2 *Strong mode of the interparticle interaction*

The *strong* mode of the VHS mechanism occurs when the masses of the inner orbits are large and/or their orbits are closer to each other. In this case, interparticle interaction surpasses the differential precession of Ω and Ω' induced by the distant perturber, and the orbits corotate. Similarly to the weak case, the two inner orbits keep the magnitude of total angular momenta constant, yet exchange angular momentum so that their inclinations undergo mirrored oscillations. The amplitude of these oscillations is typically smaller than in the weak mode and, therefore, the two orbits stay nearly coplanar during the whole course of the secular orbit evolution.

Fig. 5 shows a typical example of strong mode which occurs in the setup with initial conditions labelled as model `M3` in Table 1. Just like the weak case, we show results of the orbital evolution according to the secular approximation as well as direct integration of the equations of motion. The solutions are qualitatively the same which proves that the secular theory is suitable for understanding the nature of the VHS mechanism.

As the differential precession of Ω is suppressed in this mode of the VHS mechanism, it cannot be used to define any characteristic time-scale. Instead, the fact that $\omega_{\rm I}$ and $\omega'_{\rm I}$ dominate in equation (16) can be used to estimate period of the orbital evolution as $T_{\rm char} = 2/(\omega_{\rm I} + \omega'_{\rm I})$. For `M3`, we get $T_{\rm char} \approx 0.98$ Myr, while the numerical integrations give a period of 0.97 Myr.

4 NUMERICAL SOLUTIONS

The secular theory discussed above relies on the assumption of constant zero eccentricity of the two nearby orbits. This section aims to investigate the four-body dynamics that relax this strict constraint. Since no analytic theory is formulated for the non-zero eccentricity case (and is expected to be non-trivial as the dynamics of nearby eccentric orbits is susceptible to chaotic behaviour induced by close encounters), we study our desired setups with sufficient accuracy using direct numerical integrations.

The lack of analytic theory makes it difficult to define distinct classes of possible evolution. Our strategy is then to perform a set of integratons with different initial conditions and compare the results with the ideal cases (zero eccentricity) for which we have an analytic insight. Therefore, the set of examples presented below is likely to be incomplete in terms of all the possible outcomes but it still shows that the two basic modes of the VHS mechanism have identifiable effects in more general setups.

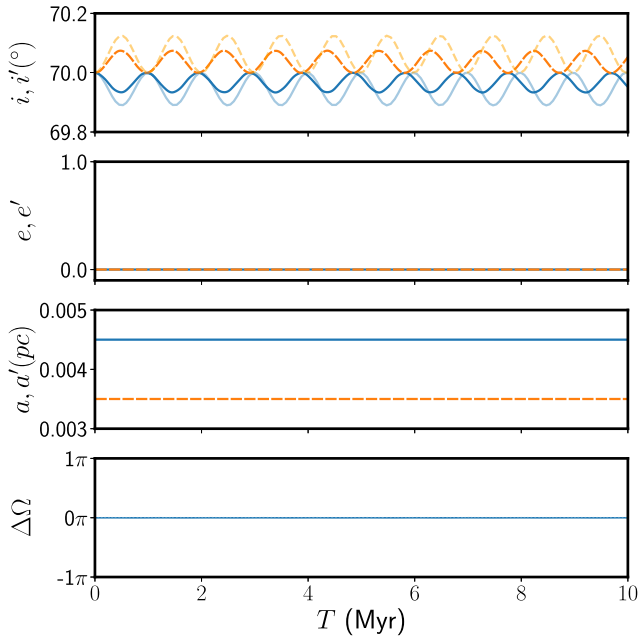

Figure 5. These graphs show the evolution of the orbital parameter of model `M3`. The stronger mutual interaction between the two stars results in strong mode of VHS mechanism, resulting in a constant $\Delta\Omega = 0^\circ$, which is a complete overlap for integration of both secular and equations of motion. There are tiny inclination oscillations for both integration of equations of motion (darker) and secular equations (lighter), which have slightly different amplitude and period.

Table 1 lists the initial conditions of the four setups we discuss in this section, along with the zero eccentricity cases discussed in the previous section. A large number of direct integrations with relativistic corrections using ARWV were conducted; We selected a subset of the runs to clearly demonstrate the strong and weak modes of the VHS mechanism when we relax certain requirements for secular theory. These individual cases are discussed separately in the following sections.

4.1 Weak mode with $e > 0$

Let us start by relaxing the condition of zero eccentricity of the two nearby orbits. The model `M2` is then straightforwardly derived from `M1` simply by changing the initial eccentricity values from zero to 0.721. Since the K-L oscillations are damped, the eccentricity of the orbits does not evolve. We can see this in the temporal evolution of selected orbital elements of the two particles for this setup in Fig. 6. When $\Omega - \Omega'$ reaches a multiple of 2π, the relative inclination of the two particles drops to zero. This directly agrees with the angular momentum exchange in the weak mode of VHS mechanism between the two bodies as described in Section 3.5.1.

Period of the secular evolution within the weak mode of the VHS mechanism for model `M2` is clearly shorter with respect to the circular case (`M1`). This is in accord with the dependence of equation (20) for characteristic time-scale on eccentricity. For model `M2`, it gives $T_{\rm char}$

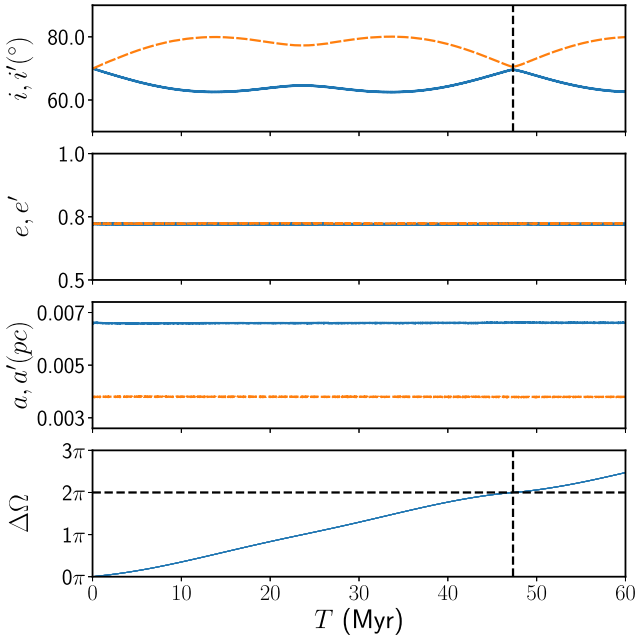

Figure 6. Example of weak mode of VHS mechanism with non-zero eccentricity. It shows the evolution of the model M2 which is similar to M1, but with non-zero eccentricity. The evolution is similar to Fig. 4 and we again see $\Delta i = 0$ when $\Delta\Omega = 2\pi$ as shown by the black dashed lines.

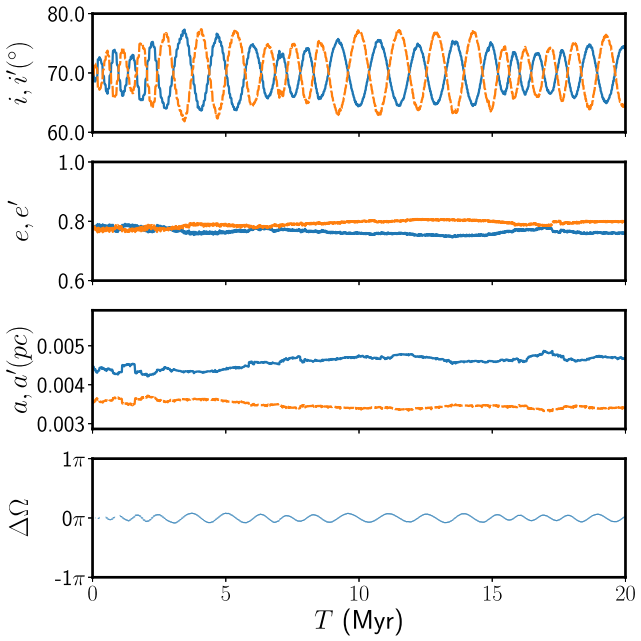

Figure 7. This figure exemplifies how the strong mode of VHS mechanism behaves with non-zero eccentricity. It show the evolution of model M4 which is similar to M3, but with orbits with eccentricity of $e = 0.77$.

≈ 75 Myr, while the period determined directly from the numerical integrations is $T_{\mathrm{M2}} \approx 47$ Myr.

4.2 Strong mode with $e > 0$

In another example, we consider a system based on M3, but with an initial eccentricity of 0.77 and we refer to this model as M4. Fig. 7 shows the evolution of the orbital elements of this model. We observe that the inclinations of the two bodies exhibit mirrored oscillations, while the value of $\Delta\Omega$ oscillates around zero. These two signatures suggest that the system is influenced by the strong mode of VHS mechanism, albeit with some qualitative differences compared to the zero eccentricity case.

Contrary to the previous cases (M1–M3), the orbits undergo non-periodic changes of their semimajor axes, which means that there is a stochastic energy exchange occurring between the two particles. We attribute this to particles on two nearby eccentric orbits occasionally getting so close to each other that the instantaneous two-body scattering noticeably affects their semimajor axes and eccentricities. These scattering events mean that we cannot treat the orbital evolution as secular.

A clear distinction between M3 and M4 is the evolution of the inclination of the two particles. In M3, the orbits evolve in accordance with the secular theory of Haas et al. (2011b), which implies that the inner of the two coplanar orbits is pushed to higher values of inclination, while the inclination of the outer orbit decreases. The evolution is more complex in M4 compared to M3. In M4, the value of $\Delta i \equiv i' - i$ periodically changes its sign (see Appendix A for further discussion). On the other hand, the (quasi)periodic mirrored oscillations of inclinations of the two orbits suggest that the angular momentum transfer between them is secular. The magnitude of the change in inclination is also higher in M4 compared to M3, but still smaller compared to the inclination oscillations present in weak mode of VHS mechanism (models M1 and M2).

Finally, let us focus on the evolution of the longitudes of the ascending nodes Ω and Ω' of the two particles. If these were test particles, that is, not interacting with each other, Ω and Ω' would evolve at different constant rates according to equation (6), which means that $\Delta\Omega$ would grow monotonically in time, reaching a value of $\approx 28^\circ$ on the time-scale of 20 Myr in the setup of model M4. However, in the bottom panel of Fig. 7, we see limited oscillations of $\Delta\Omega$ around zero with maximum amplitude $\approx 10^\circ$. Small $\Delta\Omega$ means that differential precession is suppressed, although not as ideal as in model M3 with zero eccentricity.

Considering the two necessary signatures in the evolution of the orbital elements, that is, small amplitude mirrored oscillations of inclinations and suppressed differential precession in terms of $\Delta\Omega$, we state that the system described in model M4 undergoes a generalized mode of the strong mode of VHS mechanism with non-zero eccentricity.

4.3 Strong mode on the top of Kozai–Lidov cycles

Now that we have seen examples of systems with nonzero eccentricity showing either the weak or strong mode of VHS mechanism, we now try to relax the requirement of having constant eccentricity by reducing the damping of K-L dynamics. We can do this by increasing the ratio of a/R_{p}, which strengthens the perturbing potential due to the outer body with respect to the damping potential due to the post-Newtonian corrections. We study model M5 (Table 1) to explore the VHS mechanism with variable eccentricity.

The left panels of Fig. 8 show the evolution of orbital elements for this system, with the eccentricity oscillations of the two particles now sharing a common period and amplitude. Their inclinations have a more complex evolution, but it is straightforward to identify short-term mirrored oscillations around the mean value. The mean value of the inclination oscillates due to K-L dynamics, which is on a much longer time scale than the strong mode of VHS mechanism. In this case, the inclinations evolve according to the secular theory of Haas et al. (2011b) in that the inclination of the inner body is

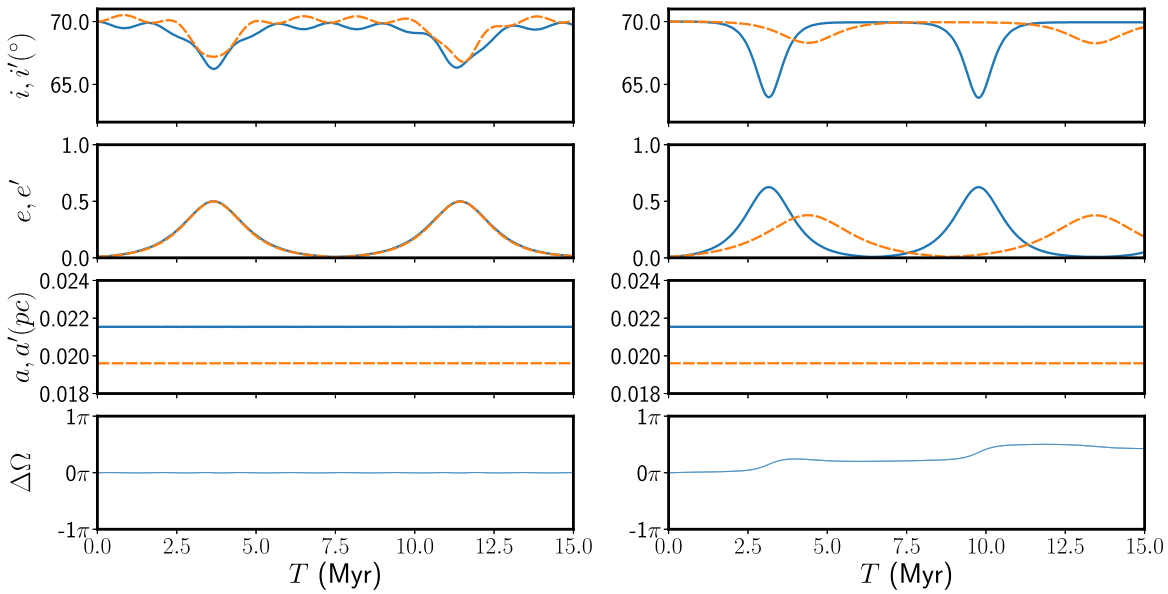

Figure 8. The left panel shows an example run of strong mode of VHS mechanism with dynamically evolving eccentricity due to K-L oscillations in model M5. The interaction between the two stars results in a combination of the strong mode of the VHS mechanism and K-L oscillations in both bodies. The strong modes constant $\Delta\Omega$ is still present and the characteristic oscillations in the inclination overlap with the K-L oscillations. However, the right panel shows the evolution of orbital elements when we remove the effects of VHS mechanism by decreasing masses of the two inner particles. The constant zero $\Delta\Omega$ changes to a systematic growth, while the two particles have independent K-L oscillations in inclination and eccentricity.

always greater than that of the outer one. Finally, it is the suppressed differential precession of Ω and Ω' which indicates that we see the two particles moving in the regime where strong mode of VHS mechanism is present, that is, with a mutually locked orientation of their orbital planes while undergoing typical long-term K-L cycles.

Since the particles undergo two independent types of secular evolution at once, we find it beneficial to demonstrate how the orbits will evolve without the VHS mechanism. We can achieve this in the test-particle regime, that is, when mutual interaction between the two inner bodies is suppressed, as shown in the right panels of Fig. 8. Both particles undergo independent K-L oscillations in the test-particle regime with different periods and amplitudes. Difference of the longitudes of the ascending nodes, $\Delta\Omega$, systematically (though not monotonically) grows over time. We can also see the period of the K-L oscillations are different between the left and right figures. This means that the VHS mechanism changes T_K of the two bodies so that the new T_K is between the T_K of the two bodies if they were evolving independently.

Let us also point out the apparent regular nature of this setup contrary to the above-discussed model M4 in Section 4.2. This property, however, is not generic as the system is chaotic; slightly modified initial parameters of the system may lead to dramatically different evolution of orbits.

4.4 Transition from the strong to weak mode

It has been demonstrated already in Section 4.2 (model M4) that the systems with non-zero eccentricity may be subject to slightly chaotic evolution due to stochastic close encounters between the two inner particles. Model M6 in Table 1 is another example of a system where such encounters play an essential role. One notable difference from M4 is that the initial eccentricity in the current setup is close to zero but not precisely zero. The left panels of Fig. 9 show the temporal evolution of the setup M6.

From the beginning, until $T \approx 56$ Myr, it shows an evolutionary pattern similar to that of model M4, that is, inclinations of the two inner particles undergo mirrored oscillations with Δi periodically changing its sign. At the same time, $\Delta\Omega$ oscillates around zero value, meaning the two orbits corotate and are almost coplanar, that is, the orbits undergo the strong mode of VHS mechanism. Also similar to model M4 is the stochastic (though rather subtle) evolution of semimajor axes and eccentricities.

At $T \approx 56$ Myr, another close encounter of the two inner particles leads to a more substantial perturbation of their orbits in semimajor axes and eccentricities. Subsequent evolution shows that this event led to the transition from the weak to the strong mode: the inclinations of the two particles exhibit larger amplitude mirrored oscillations. At the same time, longitudes of the ascending nodes precess differentially. At the moments when $\Delta\Omega$ reaches a natural multiple of 2π, both orbits share the same value of inclination, that is, they are coplanar for that short period.

Another remarkable feature during the phase of weak mode is short-periodic oscillations of eccentricity and inclination of the outer particle. These are K-L oscillations induced by the outer perturbing body that now become less damped because of a suitable angular momentum and energy change. To confirm the nature of these oscillations, we show the evolution of a system of two test particles in the external potential with initial conditions taken from the state of M6 shortly after the two-body scattering event at $T = 55.5$ Myr in the right panels of Fig. 9. These lighter bodies then have the following orbital parameters: $a = 0.0183\,\mathrm{pc}, a' = 0.0146\,\mathrm{pc}, e = 0.21, e' = 0.11$, and $\Delta i = 0.202°$. The outer particle, which is more influenced by the distant perturber, undergoes coupled regular oscillations of eccentricity and inclination. In contrast, the oscillations of the inner particle are strongly damped due to the stronger effect of the relativistic precession.

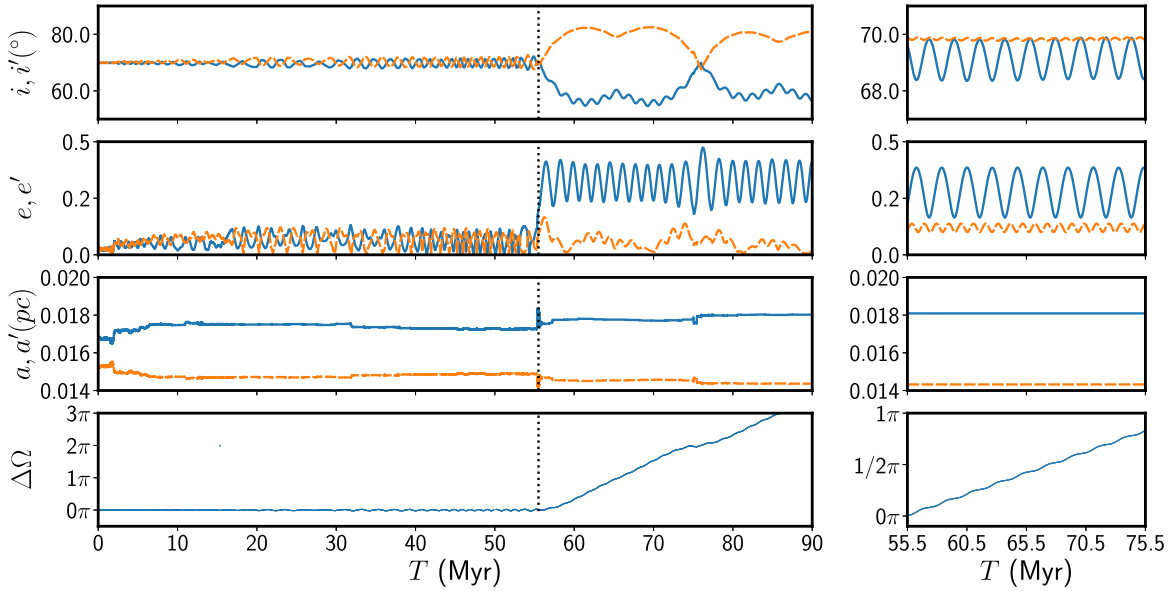

Figure 9. The left panel shows an example run of weak mode of VHS mechanism with dynamically evolving eccentricity (model `M6`). The initial strong mode of VHS mechanism between the two stars is changed due to stochastic effects and results in the stars separating. This leads to a combination of weak mode of VHS mechanism and the K-L oscillations in the blue body (solid line). The characteristic oscillations in the inclination are present but overlap the K-L oscillations in the blue body (solid line). In the right figure, we show how the system would have evolved after the time-step ($T = 55.5$ Myr) marked by the black dashed line if there had been no mutual interaction between the two particles, and thus no VHS mechanism. We see that the orbits have a consistent K-L oscillations without any extra oscillations in inclination.

4.5 Disc-like structures

Let us demonstrate the VHS mechanism in the evolution of an N-body system. We study a setup inspired by Haas et al. (2011a) but with two significant differences. First, the initial eccentricities of the orbits are uniformly distributed within the range [0,1), while Haas et al. (2011a) initially considered circular orbits. Second, the post-Newtonian corrections to the central body's gravity dampen the K-L oscillations instead of the extended mass distribution included in Haas et al. (2011a).

We consider a hypothetical disc of 50 stars orbiting around SgrA*, an SMBH of mass $M_\bullet = 4 \times 10^6\,\mathrm{M}_\odot$. The disc is perturbed by a massive perturber of mass $M_\mathrm{p} = 1 \times 10^4\,\mathrm{M}_\odot$ orbiting SgrA*on a circular orbit at $R_\mathrm{p} = 0.1$ pc. The masses of the stars in the disc are sampled from a Salpeter distribution function, $\xi(m) \propto m^{-2.35}$, in the mass range 1–15 $\mathrm{M}_\odot$.

For all orbits, the initial values of the argument of pericentre ω and the longitude of the ascending node Ω are set to zero. At the same time, other orbital elements are sampled uniformly with $a \in [0.0035, 0.02)\,\mathrm{pc}$, $e \in [0.0,\ 1.0)$, $i \in [65°,\ 75°)$, and the true anomaly $\nu \in [0,\ 2\pi)$. We integrate this setup with the same integration code, ARWV, which we used in the previous sections.

Fig. 10 illustrates the temporal evolution of the orbital elements of all 50 stellar orbits. Fig. 11 shows the projection of the normal vectors of the orbital planes of the same orbits at $T = 0, 2.5,$ and 20 Myr. We currently separate the stars whose Ω stays within 20° of the median of the whole sample throughout the course of evolution and mark them in red in both figures. We refer to this as the disc-like structure as the orbits are corotating with each other. The stars depicted in blue are objects whose orbits rotate independently and visually occupy a more spread out region in Fig. 11.

Although the current configuration differs from the model presented in Haas et al. (2011a), the main dynamical effects are qualitatively similar: approximately 2/3 of the orbits, predominantly from the inner region of the disc, maintain the disc-like configuration, characterized by similar values of both i and Ω, throughout the entire course of evolution. The remaining outer orbits precess differentially

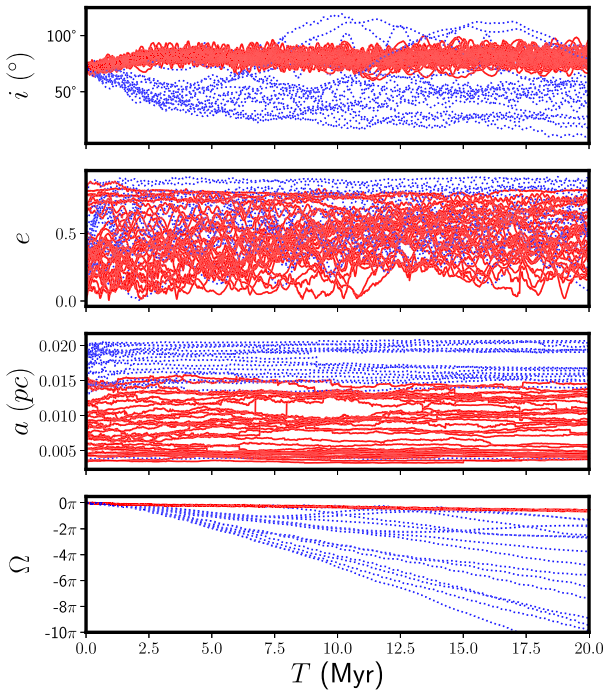

Figure 10. Evolution of orbital elements of individual stars within the model described in Section 4.5. Evolutionary tracks depicted with red solid lines correspond to orbits that are part of the coherent structure the whole integration time. Blue dotted lines correspond to orbits that get more separated from the coherent structure for at least some period of time.

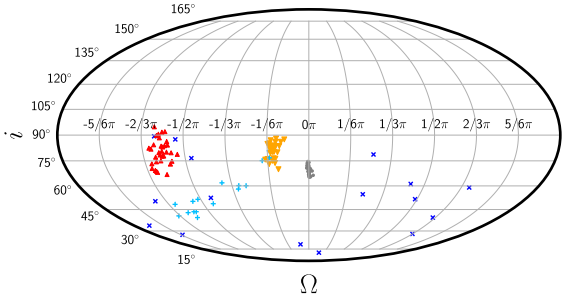

Figure 11. Projection of angular momentum vectors of individual orbits of the system discussed in Section 4.5. Red (triangle) and blue points (X) represent final states ($T = 20$ Myr) with the colour coding being the same as in Fig. 10. Orange (upside down triangle) and light blue points (+) represent the state of the red and blue orbits at $T = 2.5$ Myr, respectively. The grey points shows the initial state of the system.

in terms of Ω, resulting in a scattered structure. However, this structure still exhibits a specific feature, as the inclinations of these orbits are typically smaller than their initial values.

In contrast, the inclination of the coherent structure grows with respect to the initial value, becoming nearly perpendicular to the orbital plane of the outer perturbing body. We interpret this evolution similarly as was done in Haas et al. (2011b). Specifically, we suggest that the inner orbits mutually interact in the strong VHS mode. Furthermore, the inner and outer parts of the disc initially act as two bodies that mutually interact in the weak VHS mode. After some time, the outer body loses initial coherency due to the differential precession of the orbits of its individual members, which suppresses the weak mode of VHS mechanism between the inner and outer bodies of the disc.

It is worth noting that the model presented here is scaled so that the coherent structure has spatial dimensions similar to those of the system of S-stars observed in the Galactic Centre. While this paper cannot provide any insight into the role of the VHS mechanism in the dynamical evolution of stars in the Galactic Centre, recent research by Ali et al. (2020) suggests that coherent disc-like structures can be identified within the S-star cluster. This presents an opportunity to observe the potential effects of the VHS mechanism on the stars in the Galactic Centre.

5 CONCLUSIONS

In this work, we built on the previous study conducted by Haas et al. (2011b) that explored the dynamical evolution of two nearby, Keplerian, and initially co-planar orbits under the influence of a massive, distant perturber. The secular theory proposed in Haas et al. (2011b) assumes constant zero eccentricity of orbits of all bodies (the two inner objects close to the dominant body and the distant perturber). This assumption is only applicable to systems where an additional non-Keplerian spherically symmetric potential is not only present, but is also strong enough to damp K–L oscillations of the two inner bodies caused by the gravity of the distant perturber. The secular theory provides two qualitatively different solutions of orbital evolution of the inner bodies, which we refer to as the weak and strong modes of the VHS mechanism.

Generally, the weak mode applies when the masses of the bodies on the inner orbits are small, and/or their separation in semi-major axes is large. This mode results in independent rotations of the longitudes of the ascending nodes of the two orbits due to the influence of the distant perturber. Additionally, the two orbits periodically exchange their angular momentum, leading to periodic coupled oscillations of their inclinations. However, when $\Delta\Omega$ is an integer multiple of 2π, both inner orbits become coplanar again.

For systems with more massive bodies and/or minor separations between the two inner orbits, the strong mode applies. In this mode, the inner orbits have a common rotation rate of Ω, accompanied by oscillations of small-amplitude inclinations.

This paper demonstrates that the qualitative features of the two modes of VHS mechanism are identifiable in systems where some of the critical assumptions of the secular theory are relaxed. Instead of the external potential of some extended mass distribution, post-Newtonian corrections to the dominant body's gravity can dampen the K-L oscillations. This damping is well understood within the original secular theory of Haas et al. (2011b) with the first-order post-Newtonian approximation given by Rubincam (1977). By relaxing the need for the extended mass to dampen the K-L oscillations, VHS mechanism applies to a broader range of astrophysical systems, such as compact planetary systems or the innermost regions of galactic nuclei.

We have further studied systems with non-zero eccentricity of the inner orbits. We cannot use the secular theory of Haas et al. (2011b) to study such a setup. Nevertheless, by directly integrating the equations of motion, we have identified key features of both the weak and strong modes of the VHS mechanism. The main difference we found in these setups compared to the zero eccentricity case is within the strong mode. In this mode, the orbital inclinations of the inner particles may swap, meaning that in some setups, they oscillate around the common starting value. None the less, this does not change the general statement that the orbits corotate ($\Delta\Omega \approx 0$) within this evolutionary mode.

In order to achieve a more general setup, we have partially relaxed the assumption of constant eccentricity, which assumes complete damping of K-L oscillations of the inner orbits due to the gravity of the outer perturber. We have presented examples of systems where we observe only partially damped K-L oscillations of the inner orbits.[1] The typical features of the VHS mechanism's weak or strong modes are identifiable in these systems.

Finally, we have demonstrated, similarly to Haas et al. (2011a, b), that the VHS mechanism applies to more complex systems with a larger set of initially coplanar bodies in a relativistic potential. Recent research by Ali et al. (2020) suggests that coherent disc-like structures can be identified within the S-star cluster. This opens avenues for observing the possible effects of VHS mechanism in the stars in the Galactic Centre.

In summary, the analytical expression of VHS mechanism described in Haas et al. (2011b) appears to be a robust phenomenon that can even govern the evolution of systems that do not meet the assumptions of the analytic theory. We have demonstrated through several examples that the VHS mechanism patterns can be found even in systems where instantaneous close encounters significantly affect the orbital evolution. Specifically, the persistent near corotating configuration within the strong mode may have straightforward, observationally detectable consequences for a broad range of astrophysical systems, such as compact planetary systems or stellar structures in the innermost regions of galactic nuclei. However, it is essential to note that the strong mode of the VHS mechanism does not create coplanar and corotating structures within our current

[1]It is important to note that we considered post-Newtonian dynamics in all the examples, which means that some level of damping of K-L oscillations due to the relativistic pericentre advance was always present.

understanding; instead, it allows for the survival of existing such structures for extended periods. The weak mode may lead to a specific evolution of its orientation, as shown in Section 4.5, which was discussed for a particular setup in Haas et al. (2011a).

The result of a more general understanding of the VHS mechanism is a potential application in the Galactic Centre to orbits of the S-star cluster. A consequence of evolving eccentric orbits is the introduction of chaos in these systems, which needs to be understood better. Studying this in more detail can facilitate a deeper understanding of the evolution of disc-like structures with the VHS mechanism. These studies will lead to significant insights into the behaviour of astrophysical systems and contribute to a better understanding of the underlying mechanisms that govern their evolution.

FUNDING

MS is supported by the Grant Agency of Charles University under the grant no. 179123. LŠ and JH acknowledge support from the Grant Agency of the Czech Republic under the grant 20-21855S.

ACKNOWLEDGEMENTS

We thank Sai Sasank Chava and Yugantar Prakash for feedback on the manuscript. We thank David Vokrouhlický for his input on using the Rubincam approximation.

DATA AVAILABILITY STATEMENT

The data and tools used to produce the plots in this paper will be shared on reasonable request to the corresponding author.

REFERENCES

Ali B. et al., 2020, ApJ, 896, 100
Baltagiannis A. N., Papadakis K. E., 2011, Int. J. Bifurcation Chaos, 21, 2179
Bartko H. et al., 2009, ApJ, 697, 1741
Bartko H. et al., 2010, ApJ, 708, 834
Bertotti B., Farinella P., Vokrouhlický D., 2003, in Physics of the solar system: dynamics and evolution, space physics, and spacetime structure. Dordrecht: Kluwer Academic Publishers, 323ISBN 1-4020-1428-7
Blaes O., Lee M. H., Socrates A., 2002, ApJ, 578, 775
Chassonnery P., Capuzzo-Dolcetta R., Mikkola S., 2019, preprint (arXiv:1910.05202)
Eisenhauer F. et al., 2005, ApJ, 628, 246
Ghez A. M. et al., 2003, ApJ, 586, L127
Gillessen S., Eisenhauer F., Trippe S., Alexander T., Genzel R., Martins F., Ott T., 2009a, ApJ, 692, 1075
Gillessen S., Eisenhauer F., Fritz T. K., Bartko H., Dodds-Eden K., Pfuhl O., Ott T., Genzel R., 2009b, ApJ, 707, L114
Goicoechea J. R., Pety J., Chapillon E., Cernicharo J., Gerin M., Herrera C., Requena-Torres M. A., Santa-Maria M. G., 2018, A&A, 618, A35
Haas J., Šubr L., 2021, ApJ, 922, 74
Haas J., Šubr L., Kroupa P., 2011a, MNRAS, 412, 1905
Haas J., Subr L., Vokrouhlicky D., 2011b, MNRAS, 416, 1023
Holman M., Touma J., Tremaine S., 1997, Nature, 386, 254
Hsieh P.-Y., Koch P. M., Ho P. T. P., Kim W.-T., Tang Y.-W., Wang H.-H., Yen H.-W., Hwang C.-Y., 2017, ApJ, 847, 3
Hsieh P.-Y. et al., 2021, ApJ, 913, 94
Huang S.-S., 1960, AJ, 65, 347
Karas V., Šubr L., 2007, A&A, 470, 11
Kozai Y., 1962, AJ, 67, 591
Levin Y., Beloborodov A. M., 2003, ApJ, 590, L33
Lidov M. L., 1962, Planet. Space Sci., 9, 719
Lim H., Rodriguez C. L., 2020, Phys. Rev. D, 102, 064033
Lithwick Y., Naoz S., 2011, ApJ, 742, 94
Liu H. B., Hsieh P.-Y., Ho P. T. P., Su Y.-N., Wright M., Sun A.-L., Minh Y. C., 2012, ApJ, 756, 195
Lu J. R., Do T., Ghez A. M., Morris M. R., Yelda S., Matthews K., 2013, ApJ, 764, 155
Martín S., Martín-Pintado J., Montero-Castaño M., Ho P. T. P., Blundell R., 2012, A&A, 539, A29
Michaely E., Perets H. B., 2014, ApJ, 794, 122
Naoz S., Farr W. M., Lithwick Y., Rasio F. A., Teyssandier J., 2011, Nature, 473, 187
Naoz S., Kocsis B., Loeb A., Yunes N., 2013, ApJ, 773, 187
Paumard T. et al., 2006, ApJ, 643, 1011
Rubincam D. P., 1977, Celest. Mech., 15, 21
Scheeres D. J., 1998, Celest. Mech. Dyn. Astron., 70, 75
Simó C., 1978, Celest. Mech., 18, 165
Šubr L., Schovancová J., Kroupa P., 2009, A&A, 496, 695
Tsuboi M., Kitamura Y., Uehara K., Tsutsumi T., Miyawaki R., Miyoshi M., Miyazaki A., 2018, PASJ, 70, 85
von Fellenberg S. D. et al., 2022, ApJ, 932, L6
Yelda S., Ghez A. M., Lu J. R., Do T., Clarkson W., Matthews K., 2010, in Morris Mark R., Wang Q. Daniel, Yuan Feng, eds, The Galactic Center: a Window to the Nuclear Environment of Disk Galaxies. Astron. Soc. Pac., San Francisco, p. 167

APPENDIX A: INCLINATION CROSSING IN ECCENTRIC STRONG MODE

In Section 4.2, we describe qualitative difference of the strong mode of the VHS mechanism with eccentric orbits in comparison to the circular case. It has been argued in Haas et al. (2011b) that, starting from coplanar configuration, the inclination of the inner orbit always grows, while that of the outer one decreases. An important piece of their argument is that precession of the outer orbit due to the distant perturber is always faster which leads to positive value of $\sin(\Omega' - \Omega)$ which implicitly occurs in equations (14) and (15) through the dependence of $\overline{\mathcal{R}}_{\rm i}$ on $\boldsymbol{n}.\boldsymbol{n}'$.

We do not have secular equations for the VHS mechanism with eccentric orbits in hands, still, we may assume that dependence of $\mathrm{d}i/\mathrm{d}t$ and $\mathrm{d}i'/\mathrm{d}t$ on $\Delta\Omega \equiv \Omega' - \Omega$ is similar to the circular case. Fig. A1 shows zoomed-in evolution of model `M4` for a short period of time. Indeed, we see that, in contrary to the circular case, $\Delta\Omega$ reaches non-zero (both positive and negative) vales at the instances of $i = i'$. Depending on the sign of $\Delta\Omega$, inclination of the inner orbits either grows similarly to the circular case ($\Delta\Omega > 0$) or decreases. For comparison, we also show detailed view of evolution of orbital elements for setup similar to model `M4`, but now with small eccentricities of the two inner orbits, $e_0 = e_0' = 0.08$, in Fig. A2. The oscillatory pattern of $\Delta\Omega$ is preserved, but now with (i) several orders of magnitude smaller amplitude, (ii) near zero value at the instances of $i \approx i'$, and (iii) positive derivative at those instances. Evolution of i and i' is then in accord with the analytic argumentation for the zero eccentricity case.

Let us note that due to lack of analytic secular theory for the non-zero eccentricity case, it is hard to discriminate, whether evolution of $\Delta\Omega$ in the strong mode of the VHS mechanism is primarily due to non-uniform precession of the orbits in the field of the distant perturber, or whether it is mainly governed by their mutual torques.

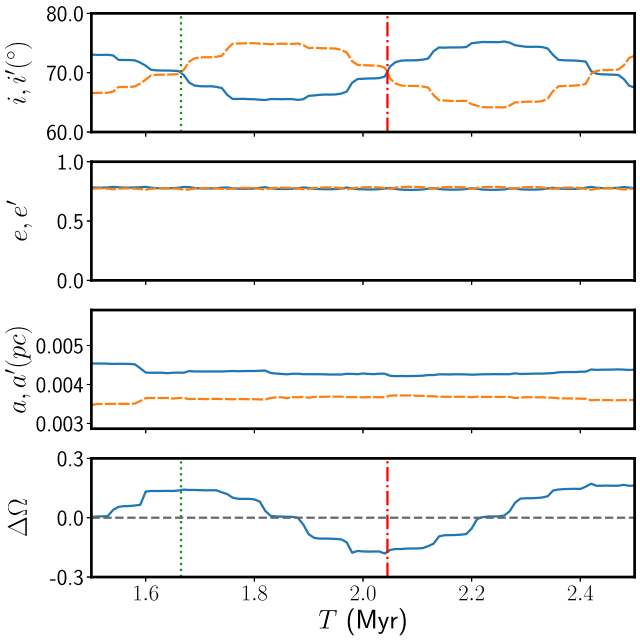

Figure A1. Evolution of the orbital elements within model `M4` for a short period of time. The two points where $\Delta i = 0$ are marked with green (dotted) and red (dashed–dotted) vertical lines, with appropriate markings in $\Delta\Omega$.

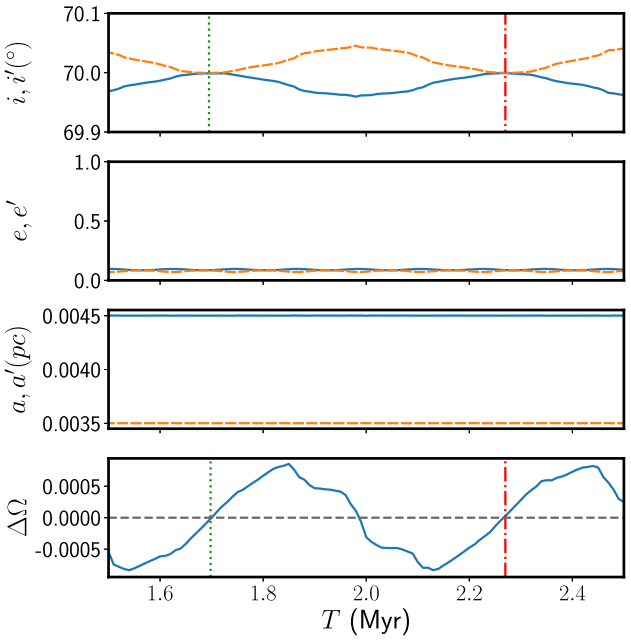

Figure A2. Evolution of the orbital elements within a model similar to model `M4` but low eccentricity, $e_0 = e'_0 = 0.08$. Green (dotted) and red (dashed-dotted) vertical lines indicate instances of $i = i'$.

This paper has been typeset from a TEX/LATEX file prepared by the author.

5 Production of Hypervelocity Stars from Tidal Disruptions of Stellar Binaries

Along with the orientation of stellar orbits in the S-cluster, we also want to explore the possible origin of S-stars. One of the hypotheses that aims to solve the "paradox of youth" for young stars in the S cluster is their origin in the young stellar disk. During close passages to Sgr A* , the binary system can undergo the Hills mechanism, which results in one of the stars from the binary system to be on a tightly bound orbit around Sgr A* while the other star gets kicked out of the system with high velocity. Usually the velocity of these stars are so high that they can escape the potential of the galaxy, and are called hypervelocity stars.

There are many hypervelocity stars observed in the galactic halo but often feature ambiguous trajectories, lower velocities, or alternative origins like galactic disk supernovae or ejections from the Large Magellanic Cloud (Brown, 2015) .The hypervelocity star of focus in this work is S5-HVS1 (Koposov et al., 2020). Unlike the halo hypervelocity stars, S5-HVS1 star is ~ 9 kpc away from the Sun with velocity in the Galactic frame of about 1800 km/s, which when integrated back in time results in a origin from the Galactic center $\approx$4.8 Myr ago (Koposov et al., 2020).

In this work, we follow up on work by Šubr and Haas (2016), to test compatibility of their model of origins of HVS as counterparts to S-stars with the observed HVS S5-HVS1. we perform direct N-body simulations using the `NBODY6` integrator to model an eccentric disk consisting of 2,000 stars (forming 1,000 binaries). The gravitational environment is dominated by the SMBH ($M_\bullet = 4 \times 10^6 M_\odot$), while the disk itself provides a non-axisymmetric perturbation to the potential. The binaries' center of mass follow a power-law distribution for their semi major axis between 0.04 and 0.4 pc. The binaries themselves follow an Öpik distribution for the semi-major axis separation between $0.05 - 100$ au. The system features an eccentricity gradient dependent on the binaries' center of mass semi-major axis.

We study the evolution of hypervelocity stars ejected from this system, and calculate where they would be present after 4.8 Myr after getting kicked out. We then compare these stars to the location of S5-HVS1 in the sky. We cover the parameter space of the different orientation of the disk to find orientations that provide high probability of finding S5-HVS1 at its current position. We find that the current orientation of the young stellar disk is compatible with producing a HVS which can be observed in the vicinity of S5-HVS1 in the night sky.

In the following proceeding paper (accepted), I re-analysed N-body simulations presented in Šubr and Haas (2016), and did all the comparisons along with production of the figures and writing. The text underwent improvements based on the suggestions of the other co-authors.

Compact Objects and Binaries in Dense Stellar Systems
Proceedings IAU Symposium No. 398, 2025
doi:10.1017/xxxxx

Investigating the Origins of Hypervelocity Stars in the Galactic Center

M. Singhal[1], **L. Šubr**[1], **J. Haas**[1]

[1] Charles University, Faculty of Mathematics and Physics, Astronomical Institute, V Holešovičkách 2, 18000 Prague, Czech Republic

Abstract. Understanding the origin of hypervelocity stars (HVSs) in the Galactic Center is a critical question, particularly regarding the dynamic processes that have shaped this region. In this study, we assert that HVSs likely formed as counterparts to S stars, specifically through the Hills mechanism originating in the young stellar disk. By employing N-body simulations, we thoroughly analyze the statistical likelihood of HVS production in our models and robustly compare these results with observational data of a recently detected HVS, S5-HVS1, with an origin in the Galactic Center. Our findings provide a consistent model that enables the production of HVSs like S5-HVS1 and captures the known dynamics of the Galactic Center.

Keywords. Star clusters, Hypervelocity stars, Stellar dynamics

1. Introduction

Hypervelocity stars (HVS) are rare stellar objects first identified by Brown et al. (2005) as young (B-type) stars travelling at velocities of several hundred to over one thousand km s^{-1}, exceeding the escape velocity of the Milky Way. A promising explanation is the *Hills mechanism* (Hills 1988), in which a binary star undergoes a close encounter with an SMBH: capturing one component while the other star gets ejected at high velocity. The required presence of an SMBH is in agreement with the current observations of the Galactic Center, which hosts a single SMBH, Sagittarius A* (Sgr A*), with a mass of $\sim 4 \times 10^6\, M_\odot$ (GRAVITY Collaboration 2022) and a population of young, massive stars on tight orbits—the so-called S-stars—has been detected within 0.01–0.1 pc of Sgr A* (Ghez et al. 2003; Gillessen et al. 2009).

At larger radii, a disk of young stars has been observed in the central region (Paumard et al. 2006; Bartko et al. 2009; von Fellenberg et al. 2022), which may represent the remnants of a molecular cloud infall and fragmentation event (Mapelli et al. 2012; Bonnell and Rice 2008). These structures provide natural initial conditions for studying the joint origin of HVS and S-stars. Previous work by Šubr and Haas (2016) has explored such a setup with N-body simulations and showed that HVS together with S stars could have originated in a disc-like stellar structure similar to the stellar disc we currently observe in the Galactic Center. However, the currently observed HVS in the Galactic Center halo cannot have originated from the current disc, but may have some counterparts in the S stars. This leaves an unanswered question: where are the HVSs originating from the current disc?

We expand on previous works by testing this model with a notable recent observation, the HVS, S5-HVS1 (Koposov et al. 2020). Its velocity vector points almost directly away from the Galactic Center, with an inferred flight time of ~ 4.8 Myr. In this work, we investigate whether a young stellar disk around the SMBH can account for the observed properties of S5-HVS1. Using direct N-body simulations of binaries embedded in an eccentric disk, we follow the dynamical evolution of stars over several Myr and track both ejected and bound populations. We demonstrate that the Kozai-Lidov mechanism (Kozai 1962; Lidov 1962) operating in a stellar disk, in conjunction with the Hills mechanism, can account for the observations of S5-HVS1, providing a unified framework for the stellar dynamics of the Galactic center.

2. Methods

In order to study the origins of HVS and S stars in the Galactic center, we perform numerical integrations of mutually gravitationally interacting point masses in a disk configuration orbiting around a supermassive black hole. We use values guided by observations of our Galactic center, starting with the central SMBH, mimicking Sgr A*, of mass $M_\bullet = 4 \times 10^6 M_\odot$. We sample 2000 stars from a power-law distribution function $n_m \propto m^{-1.5}$ with $1M_\odot < m < 150M_\odot$ which gives us a disk mass of $M_d = 24500M_\odot$. We pair all stars to form binaries with a mass ratio as close to unity as possible. The binaries are in circular orbits, with the orbital angular momentum aligned to be parallel to the angular momentum of the disk. We sample the binary's semimajor axis from the Öpik distribution function, $n_{a_b} \propto a_b^{-1}$ where a_b is in the range $0.05 - 100$ au (Kobulnicky and Fryer 2007; Ling et al. 2004).

The binary systems are orbiting the SMBH on Keplerian orbits with semimajor axis following a power law distribution $n_a \propto a^{-1}$ with $a_{\rm in} = 0.04$ pc $\leq a \leq a_{\rm out} = 0.4$ pc. These orbits are inclined following the distribution function $n_i \propto \sin i$ with $i \in \langle 0, 2.5^\circ \rangle$. The eccentricity of the orbits of the center of masses of the binaries follows a radial gradient according to $e = 0.9(a - a_{in})/(a_{out} - a_{in})$ from Šubr and Haas (2016). The eccentricity vectors of the orbits are parallel, which means the ellipses are mutually aligned and not randomly oriented. This is motivated by works of Mapelli et al. (2012) and Bonnell and Rice (2008), which model star formation in the vicinity of an SMBH from an infalling gas cloud.

This system does not include the spherical cluster of the old star due to computational constraints. We use NBODY 6 to perform the numerical integration of this system (Aarseth 2003). A thorough explanation of the simulation methodology and technical details is provided in Šubr and Haas (2016).

3. Results

Šubr and Haas (2016) demonstrated that hypervelocity stars can form as counterparts to the S-stars via the Hills mechanism. They also found that the ejected stars by the Hills mechanism are preferentially launched within the plane of the stellar disk and show a preferred azimuthal direction of escape. This anisotropy provides a potential diagnostic tool for tracking observed HVS back to their origin. The rate of ejections is not constant over time. We find that ejections peak at $T \approx 1.5$ Myr after disk formation, which corresponds to the timescale for Kozai–Lidov oscillations to drive binaries to high eccentricities (Šubr and Haas 2016). At this stage, close passages by the SMBH efficiently disrupt binaries, producing both unbound hypervelocity stars and tightly bound S-star counterparts.

To test the consistency of our model with the observation of S5-HVS1, we evolved the ejected stellar population forward in time within the compound potential of the SMBH and a spherical potential of the galaxy (Kenyon et al. 2008). We project the distribution of ejected stars onto the plane of the sky. The left panel of Fig. 1 shows that after 4.8 Myr of evolution, after the ejections peak at 1.5 Myr, the simulated HVS population shows a spatial distribution confined to a narrow band defined by the disk plane. The location of S5-HVS1 is denoted by a white star and the galactic plane with the red line. Since the spatial distribution is dependent on the disk orientation, we do a parameter search for all possible disk orientations. A heatmap of all disk orientations in the phase space of its longitude of ascending node (Ω) and inclination (i) with respect to the galactic plane is shown in the right panel of Fig. 1. The colour denotes the number of stars in a 5-degree window after projection around the observed S5-HVS1. The orientation of the currently observed clockwise disk is marked with a black dot.

However, in the galactic center, we also have the circumnuclear disk (CND), a massive torus of gas and dust at ~ 1.5 pc from Sag A* (Martín et al. 2012). The massive CND can perturb the young stellar disk over time, causing it to precess and evolve its orientation (Šubr et al.

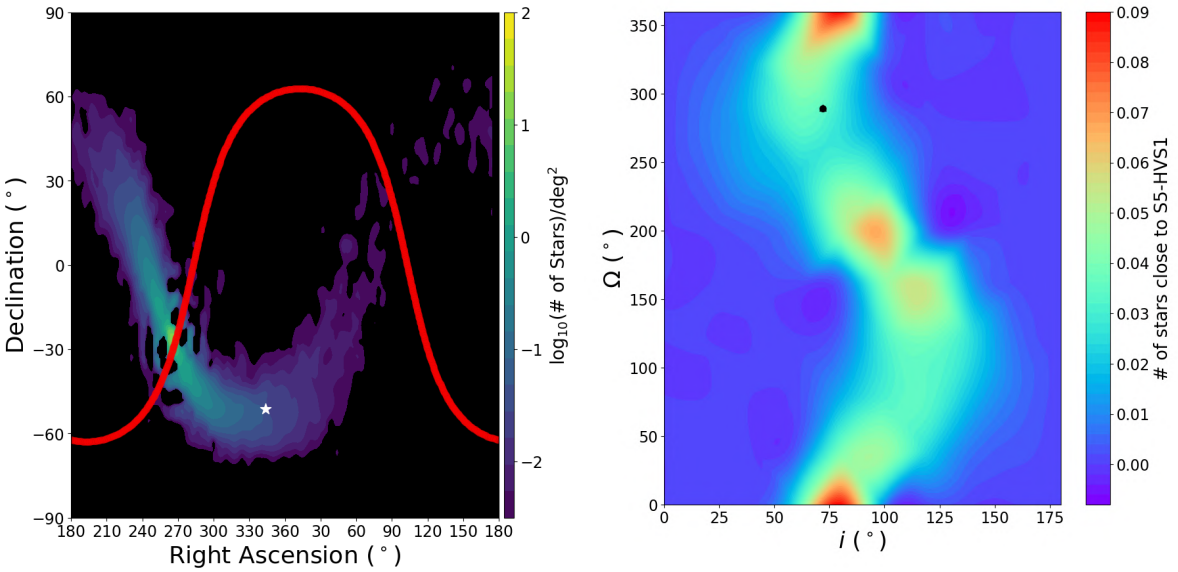

Figure 1. Left: Shows the heatmap of the number of HVS after projection of the 3D simulation onto our night sky. A disk orientation of $\Omega = 360°$ and $i = 72°$. The red line is the galactic plane, and the white star is the observed location of S5-HVS1. Right: A heatmap of the different disk orientations possible, with the colour representing the number of stars observed in a 5-degree window around S5-HVS1 in a projection shown like the left panel. The black dot represents the current location of the clockwise disk.

2009). Thus, our results indicate that both the timing and geometry of S5-HVS1 is compatible with an origin in the young stellar disk of the Galactic Center.

4. Conclusions

Our simulations in conjunction with results from Šubr and Haas (2016) show that the Hills mechanism and Kozai–Lidov mechanism acting on binaries in a young stellar disk can simultaneously produce hypervelocity stars and tightly bound S-stars near Sgr A* in the Galactic Center.

The observed properties of S5-HVS1, including its trajectory and ∼4.8 Myr flight time, are consistent with this scenario. The agreement could be affected when precession due to torques exerted by the circumnuclear disk onto the clockwise disk are taken into account.

These results support a common origin for both HVS and S-stars in the Galactic Center. Future work will extend the models by including stellar collisions, which should reduce the number of observed HVS originating from the Galactic Center, and provide an answer for the lack of observed HVS like S5-HVS1. We also want to study and compare our model with the growing sample of HVS identified by future surveys.

References

Aarseth, S. J. 2003,. *Gravitational N-Body Simulations: Tools and Algorithms*. Cambridge Monographs on Mathematical Physics. Cambridge University Press.

Bartko, H., Martins, F., Fritz, T. K., Genzel, R., Levin, Y., Perets, H. B., Paumard, T., Nayakshin, S., Gerhard, O., Alexander, T., Dodds-Eden, K., Eisenhauer, F., Gillessen, S., Mascetti, L., Ott, T., Perrin, G., Pfuhl, O., Reid, M. J., Rouan, D., Sternberg, A., & Trippe, S. 2009, Evidence for Warped Disks of Young Stars in the Galactic Center. *The Astrophysical Journal*, 697, 1741–1763. ADS Bibcode: 2009ApJ...697.1741B.

Bonnell, I. A. & Rice, W. K. M. 2008, Star Formation Around Supermassive Black Holes. *Science*, 321, 1060.

Brown, W. R., Geller, M. J., Kenyon, S. J., & Kurtz, M. J. 2005, Discovery of an Unbound Hypervelocity Star in the Milky Way Halo. *The Astrophysical Journal*, 622(1), L33.

Ghez, A. M., Duchêne, G., Matthews, K., Hornstein, S. D., Tanner, A., Larkin, J., Morris, M., Becklin, E. E., Salim, S., Kremenek, T., Thompson, D., Soifer, B. T., Neugebauer, G., & McLean, I. 2003, The First Measurement of Spectral Lines in a Short-Period Star Bound to the Galaxy's Central Black Hole: A Paradox of Youth. *The Astrophysical Journal*, 586, L127–L131. ADS Bibcode: 2003ApJ...586L.127G.

Gillessen, S., Eisenhauer, F., Trippe, S., Alexander, T., Genzel, R., Martins, F., & Ott, T. 2009, Monitoring Stellar Orbits Around the Massive Black Hole in the Galactic Center. *The Astrophysical Journal*, 692, 1075–1109. ADS Bibcode: 2009ApJ...692.1075G.

GRAVITY Collaboration 2022, Deep images of the Galactic center with GRAVITY. *Astronomy and Astrophysics*, 657, A82. Publisher: EDP ADS Bibcode: 2022A&A...657A..82G.

Hills, J. G. 1988, Hyper-velocity and tidal stars from binaries disrupted by a massive Galactic black hole. *Nature*, 331(6158), 687–689. Publisher: Nature Publishing Group.

Kenyon, S. J., Bromley, B. C., Geller, M. J., & Brown, W. R. 2008, Hypervelocity Stars: From the Galactic Center to the Halo. *The Astrophysical Journal*, 680(1), 312. Publisher: IOP Publishing.

Kobulnicky, H. A. & Fryer, C. L. 2007, A New Look at the Binary Characteristics of Massive Stars. *The Astrophysical Journal*, 670(1), 747.

Koposov, S. E., Boubert, D., Li, T. S., Erkal, D., Da Costa, G. S., Zucker, D. B., Ji, A. P., Kuehn, K., Lewis, G. F., Mackey, D., Simpson, J. D., Shipp, N., Wan, Z., Belokurov, V., Bland-Hawthorn, J., Martell, S. L., Nordlander, T., Pace, A. B., De Silva, G. M., Wang, M.-Y., & S5 Collaboration 2020, Discovery of a nearby 1700 km s-1 star ejected from the Milky Way by Sgr A*. *Monthly Notices of the Royal Astronomical Society*, 491, 2465–2480.

Kozai, Y. 1962, Secular perturbations of asteroids with high inclination and eccentricity. *AJ*, 67, 591–598.

Lidov, M. L. 1962, The evolution of orbits of artificial satellites of planets under the action of gravitational perturbations of external bodies. *Planetary and Space Science*, 9(10), 719–759.

Ling, J. F., Magdalena, P., & Prieto, C. 2004, The Distribution of Separations of DMSA Hipparcos Catalogue. *International Astronomical Union Colloquium*, 191, 77–78.

Mapelli, M., Hayfield, T., Mayer, L., & Wadsley, J. 2012, In Situ Formation of SgrA* Stars Via Disk Fragmentation: Parent Cloud Properties and Thermodynamics. *The Astrophysical Journal*, 749, 168.

Martín, S., Martín-Pintado, J., Montero-Castaño, M., Ho, P. T. P., & Blundell, R. 2012, Surviving the hole. I. Spatially resolved chemistry around Sagittarius A. *Astronomy and Astrophysics*, 539, A29. ADS Bibcode: 2012A&A...539A..29M.

Paumard, T., Genzel, R., Martins, F., Nayakshin, S., Beloborodov, A. M., Levin, Y., Trippe, S., Eisenhauer, F., Ott, T., Gillessen, S., Abuter, R., Cuadra, J., Alexander, T., & Sternberg, A. 2006, The Two Young Star Disks in the Central Parsec of the Galaxy: Properties, Dynamics, and Formation. *The Astrophysical Journal*, 643, 1011–1035. ADS Bibcode: 2006ApJ...643.1011P.

Šubr, L. & Haas, J. 2016, The Properties of Hypervelocity Stars and S-stars Originating from an Eccentric Disk around a Supermassive Black Hole. *The Astrophysical Journal*, 828, 1.

Šubr, L., Schovancová, J., & Kroupa, P. 2009, The warped young stellar disc in the Galactic centre. *Astronomy and Astrophysics*, 496, 695–699. ADS Bibcode: 2009A&A...496..695S.

von Fellenberg, S. D., Gillessen, S., Stadler, J., Bauböck, M., Genzel, R., de Zeeuw, T., Pfuhl, O., Amaro Seoane, P., Drescher, A., Eisenhauer, F., Habibi, M., Ott, T., Widmann, F., & Young, A. 2022, The Young Stars in the Galactic Center. *The Astrophysical Journal*, 932, L6.

6 Binary Star Mergers in a Stellar disk

This chapter presents the results of our N-body investigation of the dynamical evolution of a disk of stellar binaries and its role in the formation of dusty objects observed near Sgr A* . The primary motivation for this work is the long-standing puzzle regarding the origin of these infrared-excess sources, which remain stable against tidal forces despite their close proximity to the SMBH. While their nature is still debated, recent spectroscopic evidence identifying a binary star system within the dusty object D9 suggests that stellar binaries themselves, and potentially their mergers, could provide a self-consistent formation channel for the dusty objects. However, a comprehensive model that explains how these binaries are transported from their potential birthplaces in a stellar disk to the vicinity of the SMBH, while merging "on the run", has been largely absent from the literature.

We use a model similar to the one described in the previous chapter, however with physical collisions between stars enabled in `NBODY6`, and the semi-major axis of the binaries range from $0.1 - 100$ au. Our results indicate that the dynamical evolution of this system is primarily driven likely by the KL mechanism. In this framework, the "outer" orbits of the binaries' centers of mass experience increased eccentricity due to the disk's self-gravity, drawing them toward the SMBH. Simultaneously, the "inner" orbits of the individual stars within each binary undergo eccentricity oscillations driving the stars toward close passages and eventual mergers, or due to chaotic three body interactions between the binary and the SMVH. A key finding of our simulations is the identification of two distinct merger populations based on their radial distance from the SMBH (d). The majority of mergers occur within the main body of the parent stellar disk ($d \geq 10$ mpc). However, a specific subset of binaries is transported into the inner S-cluster ($d < 10$ mpc), where most of the dusty sources are currently observed. These binaries start to merge approximately 1-2 million years after the start of the simulation. This delay corresponds to the dynamical timescale required for KL oscillations and stochastic interactions to migrate the binaries' pericenter closer to Sgr A* .

Specifically, our simulations reveal that physical collisions between binaries and other disk stars are an important factor which was ignored in previous studies, and the overall result is that the mergers are three times less likely than binary disruptions. Furthermore, the results demonstrate that the binary fraction in the disk naturally evolves to increase with distance from SgrA*, a trend that aligns with current observational constraints.

Beyond the formation of dusty objects, our work suggests that the young stellar disk should also host other merger products that have settled back on to the main sequence and may be identified observationally as chemically peculiar or fast-rotating stars. By providing a self-consistent mechanism for the inward transport and merger of binaries, this research provides evidence that the dynamical evolution of the young stellar disk plays a crucial role in shaping the exotic stellar content of the Galactic Center.

In the following submitted paper, I did all the analytical calculations, numerical

simulations, production of the figures and writing. The initial conditions for the simulations were provided by a co-author. The text went through iterative improvements with the co-authors inputs through comments or direct rewrites.

Draft version June 26, 2026
Typeset using LaTeX **default** style in AASTeX7.0.1

Binary Dynamics and Mergers in a Stellar Disk and the Formation of Dusty Objects in the Galactic Center

Myank Singhal [1], Ladislav Šubr [1], Jaroslav Haas [1], Florian Peissker [2], and Michal Zajaček [3]

[1] *Astronomical Institute, Faculty of Mathematics and Physics,V. Holešovičkách 2,Prague,18000, Czech Republic*
[2] *I.Physikalisches Institut, Universität zu Köln, Zülpicher Str. 77,Köln, 50937, Germany*
[3] *Department of Theoretical Physics and Astrophysics, Faculty of Science, Masaryk University, Kotlářská 2, Brno, 61137, Czech Republic*

ABSTRACT

For more than a decade, observers have been tracking a population of enigmatic dusty objects orbiting the central supermassive black hole of the Milky Way, Sagittarius A* (SgrA*). In one interpretation, these objects are products of stellar mergers enshrouded in gaseous-dusty envelopes, which account for their infrared excess, emission lines, and stability against the tidal forces of SgrA*. Recent near-infrared observations of D9, one of the dusty objects, revealed that it embeds a spectroscopic stellar binary. In this work, we present full-fledged N-body simulations of an eccentric disk of binary stars similar to the young stellar disk observed around SgrA*. We find that some of the binaries in the disk are naturally drawn towards SgrA*and merge there due to Kozai-Lidov (KL) oscillations in their orbits. Together with the observed nature of D9, these findings represent a self-consistent picture of how the population of the observed dusty objects could have been brought into existence. The binary fraction in our N-body model evolves to increase with distance from SgrA*, which is also in agreement with the observational constraints. Our simulations also suggest that beside the dusty objects, stellar mergers are present within the young stellar disk, which could be identified as chemically peculiar or fast-rotating stars. Our results show that dynamical evolution of binary stars in the young stellar disk plays a crucial role in shaping the stellar content in the Galactic Center.

Keywords: Galactic centre (565) — Binary stars (154) — Celestial mechanics (211) — N-body simulations (1083)

1. INTRODUCTION

The center of our Galaxy harbors a supermassive black hole (SMBH) associated with the compact and variable radio source SgrA*with a mass of about $4.3 \times 10^6 M_\odot$ (GRAVITY Collaboration et al. 2022; Event Horizon Telescope Collaboration et al. 2022); see also A. Eckart et al. (2017), R. Genzel (2022), and A. Ciurlo & M. R. Morris (2025) for recent reviews. It is embedded in an old (nuclear) star cluster whose total mass is about six times higher than that of the SMBH and a characteristic (half-light) radius of roughly 4 pc (R. Schödel et al. 2014). The presence of such an old and massive cluster around SgrA*has always been expected (P. Young 1980; R. Genzel et al. 2003; D. Merritt 2006), but what came as a surprise was the discovery of very young stars closer than 0.5 pc from SgrA*(A. Eckart & R. Genzel 1996; A. M. Ghez et al. 1998; B. Ali et al. 2020; A. Ciurlo et al. 2020; F. Peißker et al. 2024b, 2025). Moreover, it turned out that a significant fraction (20-50%; S. Yelda et al. 2014) of these stars are orbiting SgrA*coherently in multiple well-defined disc-like structure, with the most prominent one spanning between 40 mpc $\lesssim r \lesssim$ 400 mpc and known as the clockwise disk (Y. Levin & A. M. Beloborodov 2003; T. Paumard et al. 2006; S. D. von Fellenberg et al. 2022). Quite in contrast, closer than 40 mpc from SgrA*(within the so-called S-cluster), the orbits of the young stars are more or less isotropically oriented (A. M. Ghez et al. 2003; F. Eisenhauer et al. 2005); however, see B. Ali et al. (2020) who suggests that the young stars form various disk like structures as well. The origin of the young stars in the innermost half-parsec of our Galaxy and the configuration of their orbits around SgrA*is still debated.

Email: myank.singhal@matfyz.cuni.cz

Recent observations of the immediate surroundings of SgrA* have revealed an even more mysterious population of dust-embedded objects (S. Gillessen et al. 2012; K. Phifer et al. 2013; A. Eckart et al. 2013; M. Valencia-S. et al. 2015; A. Ciurlo et al. 2020; F. Peißker et al. 2020; F. Peißker et al. 2024b, 2025). They are located mainly in the S-cluster, and their orbits around SgrA* are similar to those of the young stars. The nature and origin of these dusty objects is puzzling, with two prominent ideas discussed in the literature. One possibility is that these are pure gas clouds in orbit around SgrA*(S. Gillessen et al. 2012; S. Gillessen et al. 2025). Alternatively, other authors suggest that the dusty envelope contains a stellar core. Within this view, there are two main possibilities: in one, these dusty objects contain a forming star (R. A. Murray-Clay & A. Loeb 2012; N. Scoville & A. Burkert 2013; M. Zajaček et al. 2014). Interestingly, this hypothesis immediately raises another puzzling question: How can individual stars form so close to SgrA*(A. M. Ghez et al. 2003; M. Morris 1993)?

Another interpretation of the dusty objects is that they could result from stellar binary mergers which eject material that condenses into dusty envelopes. Notably, these various formation scenarios are not mutually exclusive. The recent discovery of a stellar binary behind the dusty curtain of the object D9 provides an example of stellar cores in dusty objects, while also demonstrating that dusty envelopes can develop in binary systems before merging (F. Peißker et al. 2024a).

A necessary prerequisite for the stellar binary merger formation scenario is a source of stellar binaries. A natural source for these stellar binaries can be the clockwise disk (D. S. Chu et al. 2023; A. K. Gautam et al. 2024). L. Šubr & J. Haas (2016) studied the evolution of binary systems made up of point masses in a disk-like system, where the binaries undergo KL oscillations due to the disk. KL oscillations lead to an increase in eccentricity of the outer orbits (the orbits of the binary system's center of mass around SgrA*), resulting in close passages near SgrA* and the production of hyper-velocity stars (HVS) and S-stars through the Hills mechanism (J. G. Hills 1988). At the same time, the inner orbit (orbit of the binary system around their own center of mass) of the binaries can undergo KL oscillations due to the influence of SgrA*. The KL oscillations increase the eccentricity of the inner orbit, resulting in close passages of the two stars that can drive the individual binaries towards mergers (S. Naoz 2016; A. P. Stephan et al. 2016, 2019; A. Ciurlo et al. 2020).

Until now, however, a self-consistent model for the transport of binaries from their possible birthplaces in the clockwise disk to the S-cluster—with mergers occurring "on the run"—has been missing. While previous studies have explored the dynamical fate of binaries near the Galactic Center, they often operate under different parameter spaces or environmental assumptions. For instance, B. Bradnick et al. (2017) focused primarily on tight binaries with separations up to 0.3 au. In contrast, our work considers a broader range of 0.1–100 au. This distinction is critical: the wider separation range significantly alters the ratio of stars that merge versus those that separate. Furthermore, whereas B. Bradnick et al. (2017) and B. Sersante et al. (2025) largely focus on individual binary evolution or the Hills mechanism in isolation, we demonstrate that interactions between binaries and other stars within the disk/cluster environment are a dominant factor. Our findings indicate that mergers are three times less likely than separations; this is largely due to these disk-star interactions, which reduce the number of binaries undergoing the classic Hills mechanism by disrupting them prematurely.

In this work, we use direct N-body modeling to show that the evolution of a disk of binary stars—driven by the eccentric Kozai-Lidov (KL) mechanism within its own potential—naturally transports binaries into the S-cluster. We emphasize that in our current simulations, stars are modeled as rigid spheres and tidal effects are not yet incorporated. Tidal effects can dissipate energy, leading to orbital decay and circularization of an eccentric orbit generated by KL oscillations. Previous studies have linked this orbital shrinkage as a potential way of forming tighter binaries and even mergers (D. Fabrycky & S. Tremaine 2007; S. Naoz & D. C. Fabrycky 2014). Studies with a hierarchical setup in the Galactic Center where the binary system orbits SgrA*also provide similar results (F. Antonini & H. B. Perets 2012; S. Prodan et al. 2015). Some recent work suggests that tidal dissipation can occur rapidly over a few orbital periods, effectively circularizing the binary in a short time without merging M. Dodici et al. (2025); H. Hao-Tse Huang & W. Lu (2025). Although a direct comparison is difficult due to the differing setups, H. Hao-Tse Huang & W. Lu (2025) suggests that these chaotic tides are most pronounced for binaries with initial inner separations of ~ 1 au, while being significantly lower at 0.1 au.

The inclusion of such tides would likely affect our simulation outcomes; however, the degree of this impact remains an open question. Notably, their work considers outer orbital evolution governed by relaxational effects over gigayear timescales, whereas we demonstrate that the KL mechanism drives the evolution of outer orbits on much shorter dynamical timescales. We show in our work that during close passages to SgrA*, the stellar binary can undergo

chaotic interactions that change its orbital elements. Although we currently cannot quantify how this rapid dynamics affects the likelihood of chaotic tides, they present a compelling avenue for future study.

The production of S-stars via the Hills mechanism within this framework is also subject to ongoing simulations and will be addressed in a subsequent paper. Here, we focus on the spatial distribution and binary fraction as a function of distance from SgrA*. We compare these merger products with observed dust-embedded objects in the Galactic Center, demonstrating that this transport and merger channel is a promising explanation for the population currently observed.

The structure of this paper is as follows. In Section 2 we introduce the model setup including initial conditions, numerical methods, the treatment of stellar mergers, and information about KL oscillations and relativistic damping. In Section 3 we present the main results concerning the stellar-merger temporal, mass, and orbital distributions, including their comparison with the observed dusty objects. We conclude with Section 4.

2. MODEL & METHODS

2.1. *Setup*

We simulate the evolution of a disk of binary stars in the Galactic Center in orbit around SgrA*. The setup consists of a disk of 2000 stars orbiting a massive central SMBH, mimicking SgrA*, of mass $M_\bullet = 4 \times 10^6 M_\odot$ (A. M. Ghez et al. 2003; F. Eisenhauer et al. 2005; S. Gillessen et al. 2009b,a; S. Yelda et al. 2010). The stellar masses for disk stars are sampled from a power-law distribution function $n_m \propto m^{-1.5}$ and $1M_\odot < m < 150M_\odot$ motivated by the analysis of young stars in the Galactic Center and star formation in molecular clouds (J. R. Lu et al. 2013; G.-Y. Zhang et al. 2024). The total mass of the disk is $M_{\rm disk} \approx 24500 M_\odot$.

In the disk, all stars are paired to form binaries with a mass ratio close to unity, motivated by the observed binaries in the near vicinity of the SMBH, GCIRS 16SW and IRS 16NE having mass ratio close to unity (F. Martins et al. 2006; O. Pfuhl et al. 2014). This is in accordance with H. A. Kobulnicky & C. L. Fryer (2007) who find that massive stars tend to form binaries with similar masses. For simplicity, we have also assembled the low-mass binaries to be of similar masses [4]. The binaries are in circular orbits (the "inner" orbits henceforth), and their orbital angular momentum is parallel to the disk's angular momentum. The semi-major axis of the inner orbits ($a_{\rm inner}$) is sampled from the Öpik distribution function, $n_{a_{\rm inner}} \propto a_{\rm inner}^{-1}$(H. A. Kobulnicky & C. L. Fryer 2007; J. F. Ling et al. 2004). The range of $a_{\rm inner}$ is $0.1 - 100$ au, which gives us a mixture of tight and wide binaries, with a preference for tighter ones. Also, the binaries are paired so that they do not merge at the start of the simulation.

These binaries are placed in the disk with their center of masses orbiting the SMBH (the "outer" orbits henceforth). The semi-major axes of the outer orbits ($a_{\rm outer}$) follow a power-law distribution $n_{a_{\rm outer}} \propto a_{\rm outer}^{-1}$. The disk's inner edge is at $a_{\rm min} = 0.02$pc while its outer edge is at $a_{\rm max} = 0.4$pc. The eccentricity of the outer orbits follows a radial gradient according to $e = 0.9(a_{\rm outer} - a_{min})/(a_{max} - a_{min})$, motivated by simulations that model the formation of the young stellar disk observed in the Galactic Center by an infalling molecular gas cloud in the vicinity of an SMBH (I. A. Bonnell & W. K. M. Rice 2008; M. Mapelli et al. 2012; A. Generozov et al. 2022). The binaries are also verified to be stable against the tidal potential of SgrA*at the start of the simulation. The eccentricity vectors of the orbits are parallel, which means that they are mutually aligned and are not randomly oriented. Hence, binaries form a disk which provides a non-axisymmetric perturbation to the gravitational potential of SgrA*. These binaries are placed on orbits with an inclination that follows the distribution function $n_i \propto \sin i$ with $i \in \langle 0, 2.5^\circ \rangle$. The impact of the binary separation ($a_{\rm inner}$) and the inner edge of the disk ($a_{\rm min}$) are not critical, and the overall physics remains the same, which is discussed in Appendix A

To save computational resources, we omit the nuclear stellar cluster. Previous work shows its effect on KL damping is negligible unless the cluster mass significantly exceeds $M_{\rm disk}$ with the cluster enclosed within a radius of $a_{\rm max}$(L. Šubr & J. Haas 2016). The stellar mass estimated to be enclosed in the galactic center up to 1 pc away from SgrA*is $0.8 - 1.2 \times 10^6 M_\odot$ based on various different normalization factors (R. Schödel et al. 2018). This could mean that the mass enclosed within $a_{\rm max}$ can be up to an order of magnitude higher than $M_{\rm disk}$, which, however, will still not completely dampen KL oscillations but might reduce stars that go extremely close to SgrA*and undergo the Hills mechanism (L. Šubr & J. Haas 2016). It also depends on the radial distribution of the stars, which can affect how

[4] Since the binary pairs are not exact twins, we do not exclude the effects of the eccentric KL mechanism, which can go to zero for systems with the same masses (S. Naoz 2016).

much the KL oscillations are damped (J. Haas & L. Šubr 2021). Other limitations of the numerical setup are discussed in Appendix B.

2.2. *Integrator*

We perform NBODY integrations using NBODY6 (S. J. Aarseth 2003). This code integrates the equations of motion for each body within the mutual interaction of other bodies. We use a modified version of the code which increases logging frequency and uses a weighted decision criterion (weighted by mass of the bodies) for adding stars to the neighbor list (L. Šubr & J. Haas 2016).

We allow stellar collisions throughout the integration of the equations of motion. The stars merge into a single object if their separation gets smaller than the collisional radius,

$$R_{\rm coll} = 1.7 \left(\frac{m_1 + m_2}{2m_1} \right)^{1/3} r_1^*, \tag{1}$$

where, m_1 and m_2 are the stellar masses and r_1^* is the larger of the stellar radii (Eq. 9.21; S. J. Aarseth 2003). We further assume that the merger product retains all of the mass of the parent stars. This is done for simplicity, as the goal of the work is to understand the dynamical evolution of binaries.

Using this integrator, we run 200 independent simulations with initial conditions sampled from the parameters described above. However, some of the simulations could not be used due to large accumulated errors during their integration. So we use a reduced sample of 182 simulations, which is sufficient to characterize the system's general evolution.

2.3. *Kozai-Lidov oscillations*

Due to the overall geometry of the investigated system, one of the driving dynamical processes is the KL oscillations of the individual stellar (or binary star) orbits around SgrA*induced by the gravitational influence of the disk itself. In addition to this, however, the inner orbits of the components of individual binary stars will undergo such oscillations due to the gravitational pull of SgrA*.

In their simplest (quadrupole) mode, KL oscillations occur on the characteristic KL timescale, $T_{\rm KL}$. The quadrupole approximation corresponds to the configuration in which the orbit of the subject particle around the dominant body (SgrA*or binary center of mass in our case) is perturbed by a distant perturber whose orbit around the dominant body is circular. The KL timescale is given by (Y. Kozai 1962; M. L. Lidov 1962):

$$T_{\rm KL} \equiv \frac{M_{\rm cent}}{M_{\rm pert}} \frac{a_{\rm pert}^3}{a\sqrt{GM_{\rm cent}a}} (1 - e_{\rm pert}^2)^{3/2}, \tag{2}$$

where $a_{\rm pert}$ denotes the semi-major axis of the orbit of the perturber,$e_{\rm pert}$ is the eccentricity of the perturber, a is the semi-major axis of the subject particle (both quantities are measured with respect to the dominant body), $M_{\rm cent}$ and $M_{\rm pert}$ stand for the mass of the dominant body and the perturber, respectively, and G is the gravitational constant. If the orbit of the perturber around the dominant body is eccentric, the quadrupole KL oscillations are typically modulated on a longer timescale and octupole order effects need to be included (see S. Naoz (2016) for further information).

The parameters given above in our model can be used to estimate characteristic timescales of the KL oscillations, $T_{\rm KL}$ (Equation 2). In the case of the KL oscillations of the outer binary in our model, the dominant body is represented by SgrA*, $M_{\rm cent} = M_\bullet$, and the disk serves as the perturber $M_{\rm pert} = M_{\rm disk}$, as well as the reservoir of the subject orbits (mostly from its inner parts). For $a_{\rm pert} \approx 0.12$pc and $e_{\rm pert} \approx 0.45$ (roughly corresponding to the center of mass of the stellar disk), and $a \approx 20$mpc (initial inner edge of the disk), $T_{\rm KL}$ is about 0.52 Myrs, which decreases for $a \approx 40$mpc to about 0.18 Myrs. This KL timescale calculated here is just an approximate one for the disk as a single perturber, while the realistic KL timescale due to the disk configuration cannot be estimated here. The KL timescale of the inner binary, $T_{\rm KL}$, in our model depends sensitively on the distance of the binary from SgrA*and can therefore vary by orders of magnitude between systems. As an illustrative example, consider a binary with component masses of $1.5\,M_\odot$ and $0.5\,M_\odot$, an inner semi-major axis $a_{\rm inner} = 1\,$au, and initially circular inner and outer orbits. If binary orbits SgrA*with $a_{\rm outer} = 20\,$mpc, the inner KL time scale is $\sim 0.004\,$Myr, corresponding to a ratio $T_{\rm outer}/T_{\rm inner} \sim 134$. For a wider orbit with $a_{\rm outer} = 90\,$mpc, this ratio changes dramatically to $T_{\rm outer}/T_{\rm inner} \sim 0.15$.

This strong variation demonstrates that the hierarchy of timescales can change substantially as the outer orbit evolves, implying that the inner KL evolution may proceed in a non-adiabatic regime. In particular, during phases of high outer eccentricity, $T_{\rm KL}$ for the inner binary can decrease rapidly, further enhancing this effect.

We are omitting relativistic effects due to SgrA*in our simulations, for a decreased computational cost. This removes damping of KL oscillations due to the relativistic precession of orbits. Since KL oscillations arise from coherent secular torques exerted by a distant perturber on an inclined inner orbit. In the double-averaged approximation, these torques vary slowly and enable a resonant exchange between eccentricity and inclination. However, when relativistic apsidal precession becomes sufficiently rapid, the argument of periapsis circulates on a time scale shorter than the KL timescale. This rapid precession disrupts the phase coherence required for eccentricity growth, thereby suppressing KL oscillations.

However, relativistic precession strongly affects stars with small a or high e, as shown in V. Karas & L. Šubr (2007), which studied the effects of damping of KL oscillations due to relativistic precession and precession due to an extended spherical cluster. They showed a reduction in stars with close flybys to the central massive black hole. However, since in our work we are not focusing on extremely close fly-bys, we address the question in Appendix C with an overall conclusion that the relativistic corrections do modify the KL dynamics, which could lead to a slight reduction in merger and ejection rates but it does not qualitatively alter the dynamical behavior of the system.

The inner KL oscillations may also be affected by relativistic precession; however, we also want to briefly comment on the possible role of tidal dissipation within the stellar binaries as a way of modifying the inner orbit. Previous studies of hierarchical triple systems have shown that tidal dissipation can convert high–eccentricity KL cycles into orbital shrinkage rather than prompt stellar mergers (A. P. Stephan et al. 2016, 2019; M. Dodici et al. 2025; H. Hao-Tse Huang & W. Lu 2025). These studies typically consider systems in which the outer orbit evolves slowly compared to the inner KL cycle. In our simulations, however, the binaries orbit the supermassive black hole SgrA*and their outer orbits themselves can undergo KL oscillations driven by the stellar disk or evolution from close encounters with other stars in the disk. As a result, the timescale of the inner KL oscillations can change rapidly as the outer orbit evolves, particularly when the binary reaches highly eccentric phases of the outer orbit. This produces non–adiabatic variations in the inner secular evolution and can lead to rapid eccentricity excitation during close passages near SgrA*. Examples of this can be seen in Sec. C.2. In such cases, the binary may reach the collision condition on timescales shorter than those required for efficient tidal circularization, which can be estimated to be on the order of Myr (when using the model of P. Hut (1981) and estimates by G. Fragione & F. Antonini (2019)). However, we need to re-emphasize that circularization due to tides could happen over a few orbits for highly eccentric orbits (M. Dodici et al. 2025; H. Hao-Tse Huang & W. Lu 2025). Tidal dissipation may therefore circularize a subset of binaries that experience prolonged high–eccentricity phases, but it is unlikely to suppress all mergers found in our simulations. The impact of tidal dissipation on mergers in our model will require further studies as the dynamics introduced by the KL oscillations induced by disk could affect the rates of mergers.

3. RESULTS AND DISCUSSION

3.1. *Stellar Mergers*

In the simulations, we first examine the locations and other properties of the mergers. Figure 1 illustrates the radial distance, d, from SgrA*at which each binary merged, along with the time and mass of the resulting product, $M_{\rm mp}$. Two distinct populations emerge: most coalescences occur within the main body of the parent stellar disk, at radial distances $d \gtrsim 10\,$mpc from SgrA*. Those taking place well below the inner edge of the stellar disk form a separate group. They start to appear at $T \approx 1\,$Myr after the beginning of integration with the peak of their production at $T \approx 2\,$Myr. This delay is comparable to the time required for eccentric (octupole) KL oscillations to increase the outer orbits eccentricity due to the parent disk, while also undergoing stochastic interactions with other stars in the disk that change both the inner and outer orbital elements (J. Haas & L. Šubr 2016; A. P. Stephan et al. 2016; L. Šubr & J. Haas 2016; A. P. Stephan et al. 2019).

We now discuss the properties of the two groups of mergers distinguished by d at the time of merging.

3.1.1. *Collisions in the main body of the stellar disc ($d \gtrsim 10$mpc)*

Binaries within the disk begin to merge shortly after the integration starts since they mutually perturb each other in a relatively dense environment. These perturbations during close encounters can result in sudden and large changes of the inner orbital elements. This results in binary disruptions and mergers, whose rate decays in time in accordance with

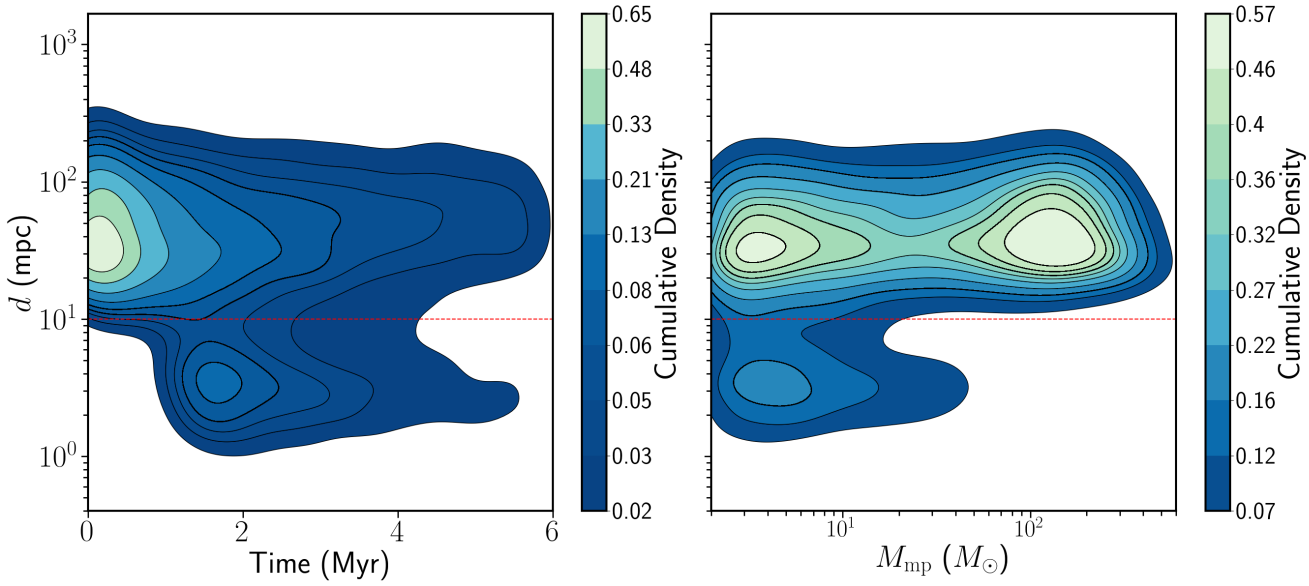

Figure 1. Properties of stellar mergers. Left and right panels show the cumulative density distribution of radial distance from SgrA* (d) at which collisions occurred as a function of time and mass of the merger product, $M_{\rm mp}$, respectively. The colours represent the area outside of which a certain percentage of the population resides.The red dotted line at $d = 10$ mpc is an arbitrarily selected dividing line based on the properties of the mergers, where the region of $d > 10$ mpc is the disk body and the region of $d \leq 10$ mpc is the innermost region of the Galactic Center, within the S cluster.

slow disintegration of the stellar disk, which leads to a decrease in stellar density. Beside that, there are mergers that occur due to the gradual growth of inner eccentricity—most likely driven by KL oscillations due to SgrA*—ultimately leading to stellar collision. In Figure 2 (a), we show an example of a merger that takes place at $d = 225.2$mpc due to oscillations of eccentricity. The same example also shows instantaneous changes of semi-major axis caused by close interactions with other stars at various time points, with some example at $T \approx 0.7$Myr and $T \approx 4.3$Myr.

Mergers within the disk involve stars from the whole mass range with two prominent peaks in mass distribution of the merger products (right panel of Figure 1). We attribute this shape of the distribution function to the fact that low-mass stars are more abundant in the system, hence, the number of their mergers is also higher. The high-mass peak of the distribution function comes from the fact that the most massive stars have larger radii, i.e. they are closer to the merger limit (Equation 1). As the initial setup just verifies that the binaries were not below the merger limit before the start of the simulation, even small perturbations in the orbital elements can cause a large number of high mass binaries to merge at the start of the simulation.

3.1.2. *Collisions below the inner edge of disk ($d < 10$mpc)*

The less prominent group of mergers that occur below the inner edge of the stellar disk are driven towards the coalescence by a similar binary evolution. In some aspects, however, the evolution is quantitatively different because now the binary undergoes evolution of the outer orbit, likely due to KL oscillations induced by the disk (J. Haas & L. Šubr 2016; L. Šubr & J. Haas 2016). When the outer orbit enters a phase with a very large eccentricity, the binary suffers from close encounters with SgrA* in contrast to stellar-mass perturbers in the disk.

During the orbit around SgrA*, the inner binary is subject to perturbations from SgrA*, which can result in KL oscillations or chaotic changes in orbital elements. This can lead to a merger that retains the outer orbital properties of the parent binary around SgrA*. In Figure 2, panel (b), we show a merger during a close pericenter passage near SgrA*($d = 4.4$mpc), marked by rapid oscillation in the inner eccentricity. If we assume that these eccentricity oscillations are caused by KL oscillations, the proximity to SgrA* shortens $T_{\rm KL}$ for the inner binary, resulting in rapid KL oscillations that can trigger a prompt merger.

During close pericenter passages, the binary gets perturbed by SgrA*. This could result in the separation of the two stars with one of them being accelerated to a high velocity, leaving the other on an orbit more tightly bound to SgrA*, than was the progenitor binary (the Hills mechanism; J. G. Hills 1988; F. Antonini et al. 2011; L. Šubr & J.

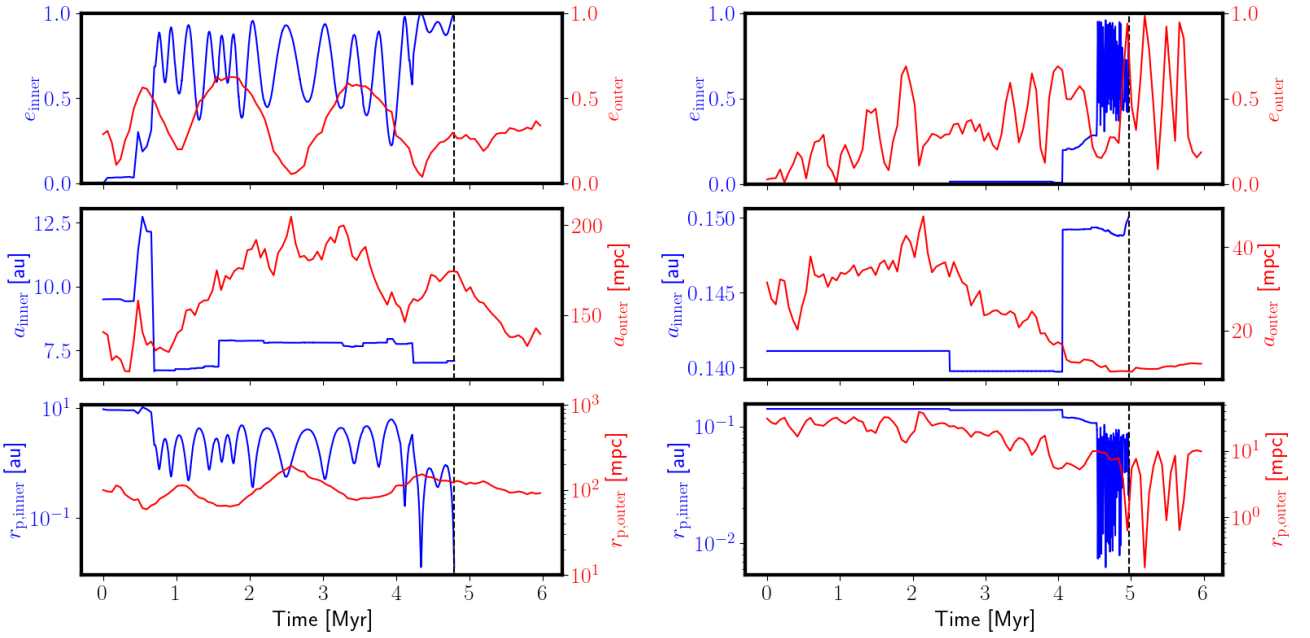

(a) (b)

Figure 2. Example of the orbital evolution of two different binary systems that merge. The blue lines show the orbital parameters of the inner orbit with the scale given on the left, and the red lines represent the outer orbital parameters and the scale is given on the right. The top panel shows the eccentricity evolution, middle panel represents the semi-major axis, and the bottom panel depicts the temporal evolution of the pericenter distance. The merger time is depicted with vertical dashed lines. In panel (a), the inner binary undergoes eccentricity oscillations before the merger occurs at $T = 4.79$ Myr, $d = 225.2$ mpc, while in panel (b) we see a binary merging due to rapid eccentricity oscillations induced by evolution of the outer orbit around SgrA*at $T = 4.97$ Myr, $d = 4.40$ mpc.

Haas 2016). Our simulations indicate that mergers are roughly three times less likely than separations occurring near SgrA*. Strong perturbation to the inner orbit may also result in chaotic interactions, in which the binary may become regular again once it travels farther from SgrA*, but with different inner orbital elements.

The mergers that occur below the inner edge of the disk are preferably from the low-mass end of the mass spectrum (right panel of Figure 1). This is mainly a selection effect – most of the massive binaries that were susceptible to collisions due to minor perturbations from other stars have merged already within $\lesssim 0.5$ Myr in the main body of the stellar disk. Only the more abundant lower-mass binaries have survived in a sufficiently large amount to later times when KL oscillations push a (relatively small) subset of them to highly eccentric orbits.

3.2. *Orbital elements of Merger products*

Locations of the merger events as displayed in Figure 1 serve as an effective tool to distinguish the effect of the KL oscillations on the inner and outer orbits before merging. However, the merger products continue orbiting SgrA* and due to relaxational processes the orbits lose memory of their origin on a time-scale of the order of few Myr and will be observed with different orbital elements and different location with respect to the merger event. We therefore evaluate separately the end states of three types of objects in our simulations which may also be distinguished observationally: (1) surviving primordial binary stars (note that the number of dynamically formed binaries is negligible in our setup), (2) single stars/separated binaries (formerly binaries whose companion was stripped away), and (3) merger products .

The surviving binaries are located predominantly farther away from the SMBH than the other two groups of objects, with the maximum number count at $a \gtrsim 200$ mpc (see the top panel of Figure 3). Still some of them have semi-major axes below the original inner edge of the stellar disk due to the disk radial dispersion (L. Šubr & J. Haas 2014) . The presence of single stars on tightly bound orbits is a consequence of the Hills mechanism, which has been suggested as a source of S stars in a similar setup by L. Šubr & J. Haas (2016) along with other works that study the eccentric disk

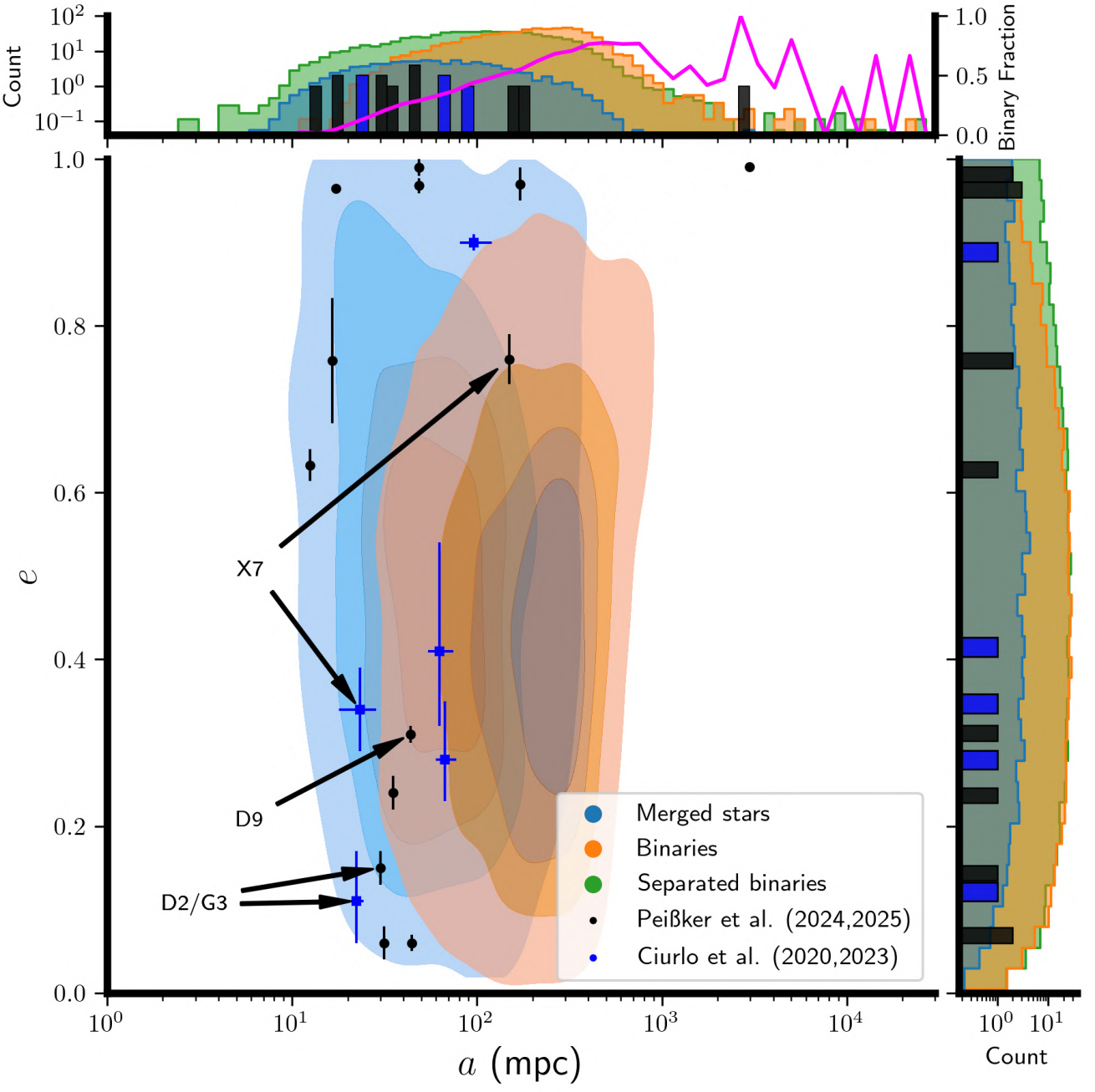

Figure 3. In the central density plot, we showcase the final eccentricity and semi-major axis of observed and simulated objects of total mass less than $20 M_{\odot}$. The density plot shows the surviving binaries and the merged stars, with each increasing colour bin corresponding to an additional 20% population outside the colour boundary. The blue dots in the figure show the orbital elements of dust enshrouded objects as given by A. Ciurlo et al. (2020, 2023) and the black dots are orbital elements for dust enshrouded objects given by F. Peißker et al. (2024b,a, 2025). Out of these, we highlight certain objects for some particular information. We highlight D9 since it has been confirmed to be a binary (F. Peißker et al. 2024a). The highlighted X7 is in disagreement in orbital elements calculated by different works for the same object, which is why they are compared to our results separately. The highlighted D2/G3 is a potential binary merger that created X7 (A. Ciurlo et al. 2023). The histograms on the sides show in addition the number count averaged over all the simulations. In the histograms we also include the distribution of separated binaries in our simulation. In the top panel, the pink line indicates an increasing binary fraction as radial distance increases, a phenomenon observed in the Galactic Center. The right panel shows the number count of all different objects over eccentricity. Both histograms confidently demonstrate compatibility with the observed objects, aligning seamlessly with our simulations.

instability and the Hills mechanism as a source of HVS (A. Generozov & A.-M. Madigan 2020; A. Generozov et al. 2022; T. Akiba et al. 2025).

The merged objects have a histogram with a maximum close to the initial inner edge of the disk, with a rather flat histogram within the range of 10 mpc $\lesssim a \lesssim$ 200 mpc. We find 47.8 ± 7.0 merger products (34.4 ± 6.2 for $M_{\rm mp} < 20 M_\odot$) with $a < 40$mpc, that is, within the S cluster. The number of dusty sources currently observed in the S cluster is smaller, which could be due to observational restrictions, but also after a certain period, the merged stars are supposed to settle back on the main sequence and lose the dusty envelope. Some examples of these merger products have been observed in the Galaxy (R. Tylenda et al. 2005; R. Tylenda & T. Kamiński 2016). As shown in recent work by P. Vynatheya et al. (2026), merger products are "puffed up," extended, and fast-rotating. Thus, after the merged stars settle back in the main sequence, they may still be identified among the other young stars that have higher rotation velocities and/or peculiar chemical composition (F. R. N. Schneider et al. 2019; F. R. Ferraro et al. 2023).

An estimate for a dust embedded star of luminosity $L \sim 10 L_\odot$, photosphere radius of $R \sim 1$ au and a mass of $M_{\rm mp} \sim 4 M_\odot$ we get a thermal time estimate for the star to contract back to main sequence of $\approx 2.3 \times 10^5$years; however, the lifetime of these dusty objects is up to debate as it can both increase and decrease by various effects, which are discussed more in Appendix D. If we generously approximate the estimated lifetime of a dusty object to be 1Myr, then we would have $\sim 4.2 \pm 2.3$ ($\sim 3.3 \pm 2.1$ for $M_{\rm mp} \leq 20 M_\odot$)[5] dusty sources within the inner S-cluster, while the rest of the merger products, $\sim 46.5 \pm 6.6$ ($\sim 33.2 \pm 6.1$ for $M_{\rm mp} \leq 20 M_\odot$) would have settled back onto the main sequence, out of which a small subset could result in fast rotating stars in the inner S-cluster.

We compare orbital properties of the merger products to the observed dust-embedded objects in our Galactic Center. Since there are currently only a few dusty sources identified with measured orbital elements, we cannot perform thorough statistical analysis. F. Peißker et al. (2024b) reports orbital elements of 12 dusty sources, of which 6 have $a_{\rm outer} \leq 40$mpc, and similarly A. Ciurlo et al. (2020, 2023) list 5 dusty objects, of which 2 have $a_{\rm outer} \leq 40$mpc. Unfortunately, orbital elements attributed to the sources also suffer from large uncertainties as is shown in Figure 3. As an extreme example, orbital solution for the source identified as X7 differs by nearly one order of magnitude in terms of semi-major axis between the recent works of different groups of observers (A. Ciurlo et al. 2023; F. Peißker et al. 2024b, 2025). This is due to the debated nature of X7, which could be a dust embedded star (F. Peißker et al. 2024b) or a collection of dust and gas inspiraling into SgrA*(A. Ciurlo et al. 2023). A potentially related dusty object is D2/G3. which is suggested to be a stellar merger that created X7, a collection of gas and dust ejected during the collision process (A. Ciurlo et al. 2023). The position of D2/G3 also coincides with the region where we expect merger products.

Somewhat unique among the dusty sources is D9, which has recently been confirmed to be a binary system (F. Peißker et al. 2024a). It is located close to the maximum of the 2D density plot of semi-major axes and eccentricities (main panel of Fig. 3) of the merged objects. At the same time, the region of the $a - e$ space where D9 is located is occupied with surviving binaries with an abundance similar to that of the merged objects. This is compatible with D9 being a binary and as suggested by F. Peißker et al. (2024a) is likely to undergo coalescence in the near future. We note that several other dusty sources are located in the region where, according to our model, surviving binaries and merged objects have similar abundances. This suggests a possibility of them being either recent mergers or surviving binaries. Still, Figure 3 shows that the overall shape of the histogram of the merged objects from the model coincides very well with observations of dusty objects, regardless of their origin.

A direct implication of the above described histogram of number counts over semi-major axes is a lower abundance of binaries orbiting SgrA*with smaller semi-major axis. Figure 3 shows that our model predicts that the binary fraction among young stars originating in a disk in the Galactic Center will grow from zero value at $a \lesssim 20$mpc to more than 50% above ≈ 0.5pc[6]. This behavior is broadly consistent with observations that report an increasing binary fraction with distance from SgrA*in the young nuclear cluster (D. S. Chu et al. 2023; A. K. Gautam et al. 2024). However, we note that these observational studies are not restricted to binaries formed or present within the stellar disk. The observed population may therefore include additional binaries that formed outside the disk and would contribute to the measured binary fraction. Our results should thus be interpreted as describing the evolution of the disk-born binary population, which likely constitutes only a subset of the observed systems.

[5] This number assumes merger products produced within the last 1 Myr from the simulation end at $\sim$ 6Myr, but the numbers will increase if we end the simulation earlier and look at merger products from there.

[6] Let us note that the maximum value of the binary fraction can change depending on the initial value (100% in our model), the overall trend should remain unchanged, however.

The distribution of eccentricities of all three classes of objects is broad, covering the whole range from zero to unity. We find the best fit for eccentricity distribution for each population is a Beta function. The initial disk-born state fits well to Beta($\alpha = 0.68, \beta = 2.31$), which is characterized by a circular-dominated "cold" profile, where $\alpha < 1$ represents the primordial spike at $e \approx 0$. Following dynamical evolution, all three classes of objects shift toward a "thermal" distribution ($f(e) = 2e$), which represents the statistical equilibrium limit where Beta($\alpha = 2$ $\beta = 1$). The surviving binaries remain the most ordered or "sub-thermal" population Beta($\alpha \approx 2.37, \beta \approx 3.16$), maintaining a mode near $e \approx 0.4$. In contrast, single-star populations show advanced signs of dynamical heating; the separated binaries Beta($\alpha \approx 2.06, \beta \approx 2.27$) have reached the thermal α-threshold, while merger products are the most randomized ($\alpha \approx 1.85, \beta \approx 1.70$). With the lowest value of β among the three groups, the merger products sit closest to the thermal limit, indicating that the collision process effectively erases the initial disk-like orbital memory. Similarly to the case of semi-major axes, we state that eccentricities of the observed dusty sources are in agreement with the properties of merged stars in our model.

We also compare the inclination distribution of our simulated systems with that of the young stellar population in the Galactic Center. Observations indicate that the innermost region is characterized by a more isotropic distribution of stellar orbits, while at larger radii a coherent clockwise disk is present, albeit with a significant fraction of stars dispersed out of the disk plane (H. Bartko et al. 2009; J. R. Lu et al. 2013; S. Yelda et al. 2014; S. D. von Fellenberg et al. 2022). Figure 4 shows the inclination distribution of the outer orbits after 6 Myr along with the initial binary distribution. In the inner region ($a_{\rm outer} \leq 40$ mpc), the inclination distribution is significantly broadened and approaches an isotropic configuration (inclinations in that region are supposed to be altered by vector resonant relaxation, as suggested by C. Hopman & T. Alexander (2006) and demonstrated by L. Šubr & J. Haas (2014).). This is consistent with observations of the innermost Galactic Center, where the stellar population does not exhibit a strong preference for a common orbital plane.

At larger radii ($a_{\rm outer} > 40$ mpc), the distribution remains broad but retains a clear excess at low inclinations. This indicates that, while a substantial fraction of systems are dynamically excited out of the initial disk, a non-negligible population still preserves memory of the original thin disk configuration. This behavior qualitatively resembles the observed structure of the clockwise disk, where a coherent disk component coexists with a population of stars on more inclined orbits.

The emergence of an isotropic component in the inner region and a partially coherent disk at larger radii suggests that dynamical evolution alone can reproduce key qualitative features of the Galactic Center stellar distribution, even when starting from an initially thin disk ($i \in [0, 2.5°]$). However, additional sources of perturbations, such as the gaseous circum-nuclear disk, may counter the redistribution of orbital inclinations(S. Martín et al. 2012; H. B. Liu et al. 2012; P.-Y. Hsieh et al. 2017; M. Tsuboi et al. 2018; J. R. Goicoechea et al. 2018; P.-Y. Hsieh et al. 2021) . The works of J. Haas et al. (2011) and M. Singhal et al. (2024) present the VHS mechanism, which shows that perturbations can preserve disk-like structures closer to the central dominant body, while regions farther away are more affected. The magnitude of the effect of the VHS mechanism on our simulations is currently unknown and will be explored in future studies

Overall, currently our results indicate that an initially thin stellar disk can evolve into a configuration that qualitatively matches the observed Galactic Center structure: an isotropic inner population and a partially coherent outer disk.

4. CONCLUSIONS

In this work, we investigated the dynamical evolution of a disk of binary stars orbiting the supermassive black hole SgrA*using direct N-body simulations. By modeling the interplay between the disk's self-gravity and the graviational field of the SMBH, we explored the formation of dusty objects via stellar mergers. Our main conclusions are as follows.

- **Mechanisms of Merger:** The simulations reveal two distinct populations of stellar mergers. The first group, which represents the majority of mergers, consists of early mergers (which may be partly unrealistic due to initial conditions) occurring within the main stellar disk due to random mutual perturbations and KL oscillations of the binaries' inner orbits. The second distinct group occurs within the innermost S-cluster ($d \leq 10$ mpc) and is driven by the eccentric KL mechanism, which first excites outer orbital eccentricities and drives binary systems towards SgrA*after which the eccentric KL mechanism of the binaries' inner orbits or chaotic three body dynamics involving SgrA*(or both) causes coalescence.

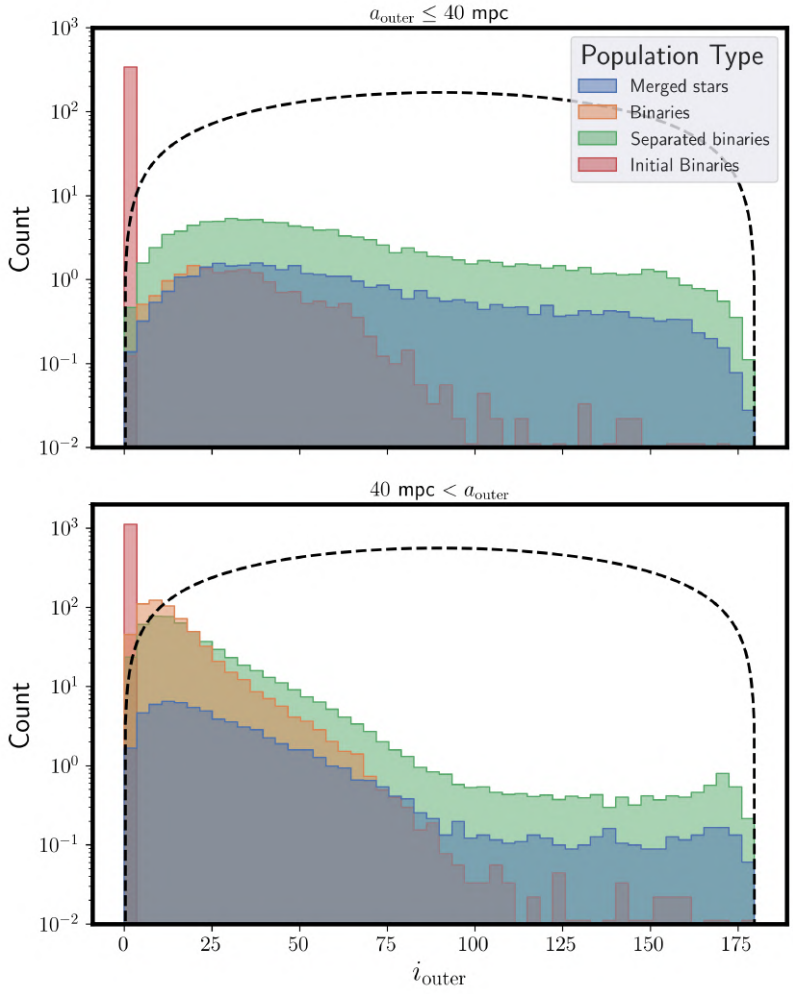

Figure 4. Distribution of outer orbital inclinations for stellar systems after 6 Myr, shown separately for systems with $a_{\rm outer} \leq 40$ mpc (top panel) and $a_{\rm outer} > 40$ mpc (bottom panel). The distributions are divided into initial binaries (red), merged stars (blue), surviving binaries (orange), and separated binaries (green). The black dashed lines shows an isotropic distribution normalized to the number of stars as in the initial binaries. At small radii (top panel), the inclination distribution is significantly broad and approaches isotropic distribution. At larger radii (bottom panel), the distribution becomes significantly broader, but retains a preference for lower inclinations, reflecting partial memory of the initially thin disk configuration

- **Consistency with Observations:** The orbital elements (semi-major axes and eccentricities) of the simulated merger products exhibit an agreement with the population of dust-embedded objects currently observed in the Galactic Center. Specifically, the model with our initial conditions, predicts the existence of approximately 47.8 ± 7.0 merger products (34.4 ± 6.2 for $M_{\rm mp} < 20 M_\odot$) within the inner S-cluster ($a < 40$ mpc) for the duration of the simulation. However, only a subset of those are possibly observed as dusty sources because of their lifetimes, which is not well known. For an estimated lifetime of 1 Myr, we would expect $\sim 4.2 \pm 2.3$ ($\sim 3.3 \pm 2.1$ for $M_{\rm mp} \leq 20 M_\odot$) merger products within the inner S-cluster.

- **Another way of detection:** Some stellar merger products could have settled back on the main sequence and lost their dusty envelope. A fraction of those may be detectable as fast rotators and/or have a specific chemical composition. Based on rough estimates of lifetimes presented in the previous point, we can expect around $\sim 46.5 \pm 6.6$ ($\sim 33.2 \pm 6.1$ for $M_{\rm mp} \leq 20 M_\odot$) stars that could have settled back on to the main sequence within the inner S-cluster ($a < 40$mpc).

- **Binary Fraction Gradient:** The simulations naturally reproduce the observed radial dependence of the binary fraction around Sgr A*. We find that the binary fraction drops to zero in the immediate vicinity of the SMBH ($a \leq 20$ mpc) due to the Hills mechanism and mergers, while rising to over 50% at distances beyond 0.5 pc.

These results suggest that stellar mergers induced by secular dynamical evolution are a robust and statistically consistent formation channel for the puzzling dusty objects observed in the Galactic Center. Binary mergers thus play an important role in shaping the stellar content in the Galactic Center.

ACKNOWLEDGMENTS

MS is supported by the Grant Agency of Charles University under the grant number 179123. MZ acknowledges the financial support of the Czech Science Foundation Junior Star grant no. GM24-10599M. LS, JH and MS acknowledge the support of Czech Science Foundation grant no. 26-21774S. FP gratefully acknowledge the Collaborative Research Center 1601 funded by the Deutsche Forschungsgemeinschaft (DFG, German Research Foundation) – SFB 1601 [sub-project A3] – 500700252.

AUTHOR CONTRIBUTIONS

M.S. ran all the simulations, did the analysis, and led the writing of the manuscript. L.S. and J.H. contributed codes and tools to perform the simulations along with discussions to analyze the results. M.Z. contributed for the discussion of lifetime of dust-embedded objects. F.P. contributed to the interpretation of observations of dusty objects. All authors contributed to the writing of the manuscript.

Software: NBODY6 (S. J. Aarseth 2003), Astropy (Astropy Collaboration et al. 2013, 2018, 2022), NumPy (C. R. Harris et al. 2020), Matplotlib (J. D. Hunter 2007), ARWV (P. Chassonnery et al. 2019), REBOUND (H. Rein & S.-F. Liu 2012), REBOUNDx (D. Tamayo et al. 2020)

APPENDIX

A. IMPACT OF INITIAL CONDITIONS

Table 1 summarizes the initial conditions adopted for the model investigated in this study (M1) together with two additional ones with different parameters (M2 & M3). The models differ in their choices of minimum and maximum outer semi-major axes ($a_{\rm min}$, $a_{\rm max}$) and the ranges for the inner binary semi-major axes ($a_{\rm inner,low}$, $a_{\rm inner,high}$). Model M1, which is the primary focus in the main text, utilizes the smallest $a_{\rm min}$ value, while M2 and M3 employ moderately larger values. Notably, M2 allows for tighter inner binaries compared to the other models. These differences are intended to test the sensitivity of the binary evolution outcomes to variations in the initial configuration. Let us also note that the model M3 has the same initial conditions as in L. Šubr & J. Haas (2016).

Figure 5 presents a comparison of the final spread of semi-major axes for merged stars, binary stars, and separated binaries across the three models at 6 Myr. The histograms indicate that a lower value of $a_{\rm min}$ in M1 results in a modest excess of objects with smaller semi-major axes. For separated binaries, M1 exhibits a minor bump near $a_{\rm min}$, reflecting the imposed initial boundary. In contrast, the histograms for M2 and M3 show that the range of $a_{\rm inner}$ has a minimal effect on the populations of merged and binary stars. The lower limit of $a_{\rm inner}$ in M2 results in a slight increase in the number of separated binaries with $a < 10$ mpc. Overall, these comparisons demonstrate that while initial conditions introduce some variation in the final histogram, the general evolutionary trends and population outcomes remain consistent among the models.

B. LIMITATIONS OF SIMULATIONS

The simulations use various simplifications to allow us to have a large statistical sample for the analysis. One main limitation is that our simulations do not include stellar evolution and mass loss. This mass loss and evolution would be crucial for massive stars, but in this work, we are primarily interested in lower-mass stellar mergers, which spend a much longer time on the main sequence and have lower mass-loss rates.

Name	$a_{\rm min}$	$a_{\rm max}$	$a_{\rm inner,min}$	$a_{\rm inner,max}$
M1	0.02pc	0.4pc	0.1au	100au
M2	0.04pc	0.4pc	0.05au	100au
M3	0.04pc	0.4pc	0.1au	100au

Table 1. Initial conditions of different models, with M1 being the model we presented in the main text. M2 and M3 have a higher value of $a_{\rm min}$ with M2 also having tighter binaries.

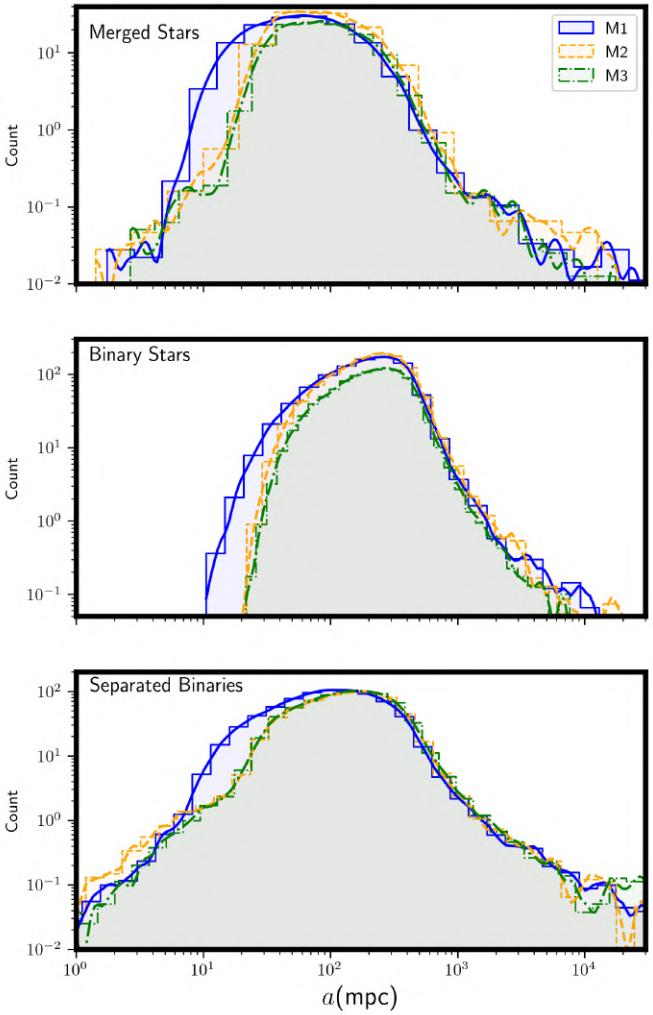

Figure 5. Impact of initial conditions on the final semi-major axis. In the histograms, we show the final semi-major axis histogram of merged stars, binary stars, and separated binaries (from top to bottom) for three different models with varying initial conditions as described in Table 1. The merged stars and binary stars show that for M1, the lower value of $a_{\rm min}$ results in a slight increase in the counts of these objects at lower semi-major axes. The distributions for M2 and M3 suggest that the final states of merged and binary stars are largely insensitive to the specific initial distribution of $a_{\rm inner}$ within the tested range. However, in the last panel, the smaller $a_{\rm inner}$ of M2 results in tighter orbits around SgrA*. Distribution of separated binaries in M1 shows a bump near $a_{\rm min}$, reflecting the initial setup. Overall, while the initial conditions exert a measurable influence on the specific orbital parameters, the qualitative evolutionary outcomes of the system remain consistent across the models.

Additionally, our simulations have a 100% efficient merger process, which is unrealistic. For instance, S. C. Rose et al. (2026) used a suite of SPH simulations to develop a framework for predicting mass loss and trajectory changes in stellar collisions within galactic nuclei. Similarly, P. Vynatheya et al. (2026) utilized the AREPO code to demonstrate that while both collisions and mergers produce massive, rapidly rotating stars, they differ significantly in their core hydrogen fractions and magnetic field structures. Due to the high computational cost and the different physical regimes involved, the detailed outcomes of these hydrodynamic works cannot currently be implemented directly into our N-body model. Integrating such realistic merger prescriptions—including non-isotropic mass loss and post-collision velocity kicks—remains a complex challenge that should be explored in future work. The final results should not vary much since we are comparing the orbital elements of the final merger products to the observed dusty objects, which, if the mass loss is minimal and isotropic, would not change substantially.

We also set up our simulations to have all stars on the main sequence at $T = 0$. However, star formation does not happen all at once, especially for lower-mass stars, which can result in a delayed formation of lower-mass binaries that are the progenitors of the dusty objects. This could delay the mergers and spread out the merger peaks at $T = 0$ and $T \approx 1.5$ Myrs. The same effect would be observed in case the disk is enriched by an inflow of more material, leading to another, more recent star formation event.

C. IMPACT OF GR

In our setup, relativistic apsidal precession induced by SgrA*can affect both the orbit of the binary center of mass around SgrA*and the internal orbit of the binary itself, particularly when the system approaches small pericenter distances. KL oscillations may be suppressed when relativistic precession becomes sufficiently rapid. Therefore, we explore the impact of relativistic precession on both the outer orbit of the binary center of mass and the inner orbit of the binary during close passages to SgrA*. We find that while relativistic precession can suppress KL oscillations in parts of parameter space, it does not fully eliminate them in more realistic disk environments.

C.1. *Outer Orbit*

Relativistic precession induced by SgrA*can affect our simulation results, as KL oscillations may be suppressed for systems with small semi-major axes and high eccentricities. To estimate which systems are most affected, we compare the relativistic apsidal precession rate to the characteristic timescale of KL oscillations. KL oscillations require slow and coherent evolution of the argument of periapsis, whereas relativistic effects introduce rapid precession that can break this resonance.

The relativistic precession rate is given by

$$\dot{\omega}_{\rm GR} = \frac{3GM_\bullet}{ac^2(1-e^2)}\sqrt{\frac{GM_\bullet}{a^3}} \tag{C1}$$

where $M_\bullet$ is the mass of SgrA*, a and e are the semi-major axis and eccentricity of the orbit, and c is the speed of light. This expression shows that relativistic precession becomes stronger for smaller semi-major axes and higher eccentricities.

We approximate the KL precession rate as

$$\dot{\omega}_{KL} \sim 1/T_{\rm KL} \tag{C2}$$

where $T_{\rm KL}$ is the characteristic KL timescale. When $\dot{\omega}_{\rm GR} \gtrsim \dot{\omega}_{\rm KL}$ relativistic precession dominates, and KL oscillations are expected to be suppressed.

In this estimate, we approximate the stellar disk as a single effective perturber located at the center of mass of the disk i.e., we consider a perturber of mass $M_{\rm pert} = 24500 M_\odot$ and orbital parameters $a_{\rm pert} = 0.12$pc and $e_{\rm pert} = 0.44$. In Figure 6 we show the ratio of $\dot{\omega}_{\rm GR}/\dot{\omega}_{KL}$ for a parameter space of $a_{\rm outer}$ and $e_{\rm outer}$. Regions where $\dot{\omega}_{\rm GR}/\dot{\omega}_{\rm KL} \gtrsim 1$ correspond to parameter combinations where relativistic precession occurs on a time scale comparable to or shorter than KL oscillations. In this regime KL oscillations are expected to be strongly suppressed. The black dots in Figure 6 show the orbital elements of binary systems with $M_c \leq 20 M_\odot$ around SgrA*at the time of merging, and the green dashed line marks $r_{\rm p,outer} = 10$mpc. As we see, a small fraction of the merging binaries are in the region where our approximation suggests KL oscillations should be damped, and for mergers that happen with orbits with a pericenter of less than 10 mpc, it is more evenly spread between the region where we expect damping of KL oscillations and where we do not. However, this approximation neglects the distributed nature of the disk potential and therefore provides only an order-of-magnitude estimate.

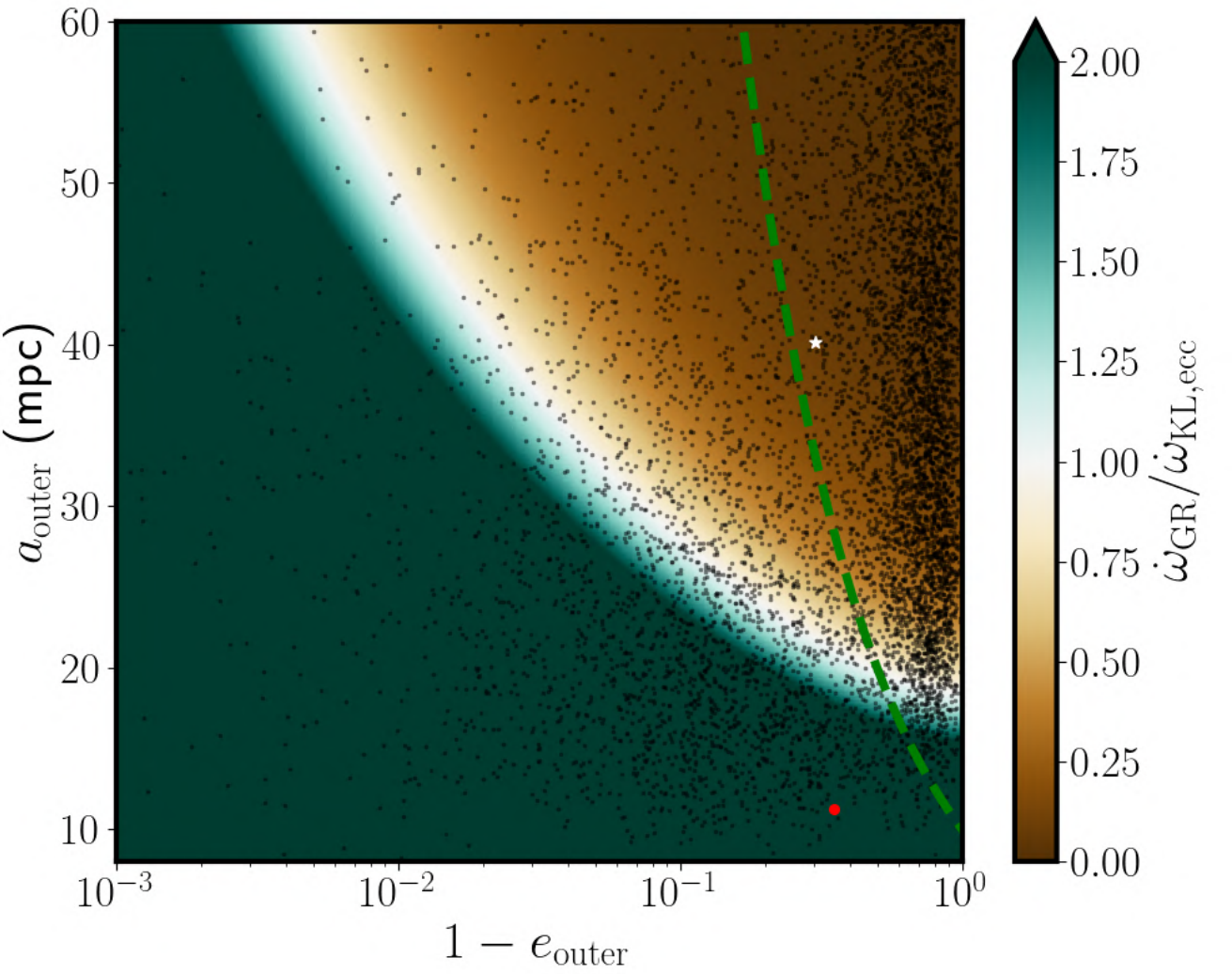

Figure 6. In the heatmap we show the ratio of $\dot{\omega}_{\rm GR}/\dot{\omega}_{KL}$ for the outer orbit of the binary system around SgrA*at $a_{\rm outer}$ with an eccentricity of $e_{\rm outer}$. The perturber is a single particle mimicing the center of mass of the disk $M_{\rm pert} = 24500 M_\odot$ orbitting at $a_{pert} = 0.12$pc with an eccentricity of $e_{pert} = 0.44$. The region where $\dot{\omega}_{\rm GR}/\dot{\omega}_{KL} \gtrsim 1$ is where we expect KL oscillations to be completely damped while for the rest of the parameter space we expect KL oscillations to be undamped. Black dots mark the orbital parameters of merging binaries with $M_c \leq 20 M_\odot$. Red dot marks the orbital parameter of a star that undegoes KL oscillations with GR in a numerical simulation as showed in Figure 7. The green dashed line represents where $r_{\rm p,outer} = 10$mpc. The white star marks the starting location of the binary shown in Figure 10.

To test the validity of this approximation, we perform numerical experiments that include relativistic effects in a more realistic stellar disk configuration. Without running accurate simulations of the entire disk of 2000 stars in a relativistic setup, we can study smaller setups with added relativistic effects to estimate effects of relativistic precession on KL oscillations. To do so, we use REBOUND which is a Nbody integrator with the additional REBOUNDX addon which allows us to implement an additional force that mimics the relativistic effects on our orbits (we use the "gr_potential" as it was computationally stable)(H. Rein & S.-F. Liu 2012; D. Tamayo et al. 2020). We simulate a disk of 490 stars of mass $50 M_\odot$ each, giving a total mass of the disk of 24500 $M_\odot$, same as the original setup. These stars were placed in the same orbits as the center of masses of the binaries in the original setup. In Figure 7 we see the evolution of a single body in the simplified setup with 50 $M_\odot$ bodies. The evolution initially reflects strong interactions with nearby disk stars. Later, the orbit settled into KL-like oscillations.

The orbital elements of this body right before it started undergoing KL oscillations is shown by the red dot in Figure 6, demonstrating that even though the approximation suggests the KL oscillations should be damped, they are

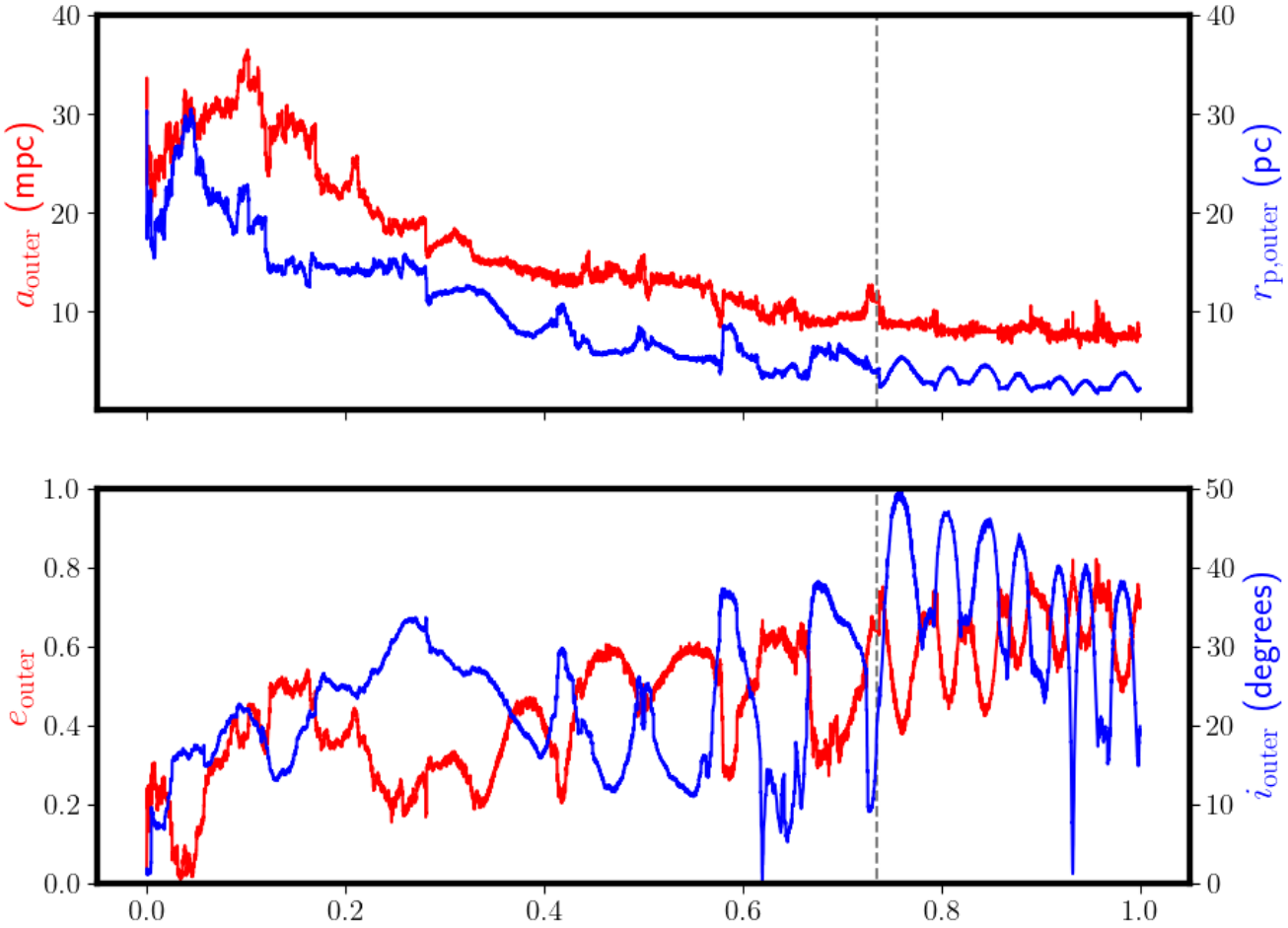

Figure 7. Time evolution of the orbital elements of a representative star in a simplified disk simulation including relativistic corrections using REBOUNDX. The disk consists of 490 stars of $50M_\odot$ each. After an initial phase dominated by local stellar interactions, the orbit exhibits KL-like oscillations despite lying in a region where analytic estimates predict suppression, highlighting the limitations of the single-perturber approximation. The dashed line is represents the time we use for the marker in Figure 6.

present and thus for a selection of mergers in our simulation, we can still expect KL oscillations to be present in their outer orbits.

C.2. *Inner Orbit*

The inner orbit of the binary system also undergoes KL oscillations with SgrA*as the perturber. We perform some 4 body integrations of a binary in orbit around SgrA*with a distant perturber mimicking the disk of stars. As discussed previously, the single particle approximation is not completely correct but it does allow an estimate on what undergoes at those scales. We use ARWV, a few body integrator which uses the AR-Chain algorithm to integrate a few bodies accurately with upto 2.5 order post-Newtonian corrections (P. Chassonnery et al. 2019).

We tested a binary system of $m_1 = 1.5M_\odot$ and $m_2 = 1M_\odot$ orbiting each other at a separation of $a_{\rm inner} = 1$ AU, with an initial eccentricity of $e_{\rm inner} = 0.01$ and an initial inclination of $i_{\rm inner} = 0°$ (with respect to the plane of the outer orbit). The binary system is placed on an eccentric orbit around SgrA*with $a_{\rm outer} = 40$ mpc and $e_{\rm outer} = 0.7$, since it is quite common for the eccentricity of the systems to increase as they undergo outer KL oscillations. The inclination of the outer orbit can vary widely, and can result in various different observed effects. We ran various tests to demonstrate the effects of GR on inner KL oscillations, and as mentioned before, since the binary itself is on an eccentric orbit around SgrA*, the KL timescale of the inner binary changes over time. There are systems that do not undergo inner KL oscillations before mergers but merge due to only the outer KL oscillations and the close flyby to

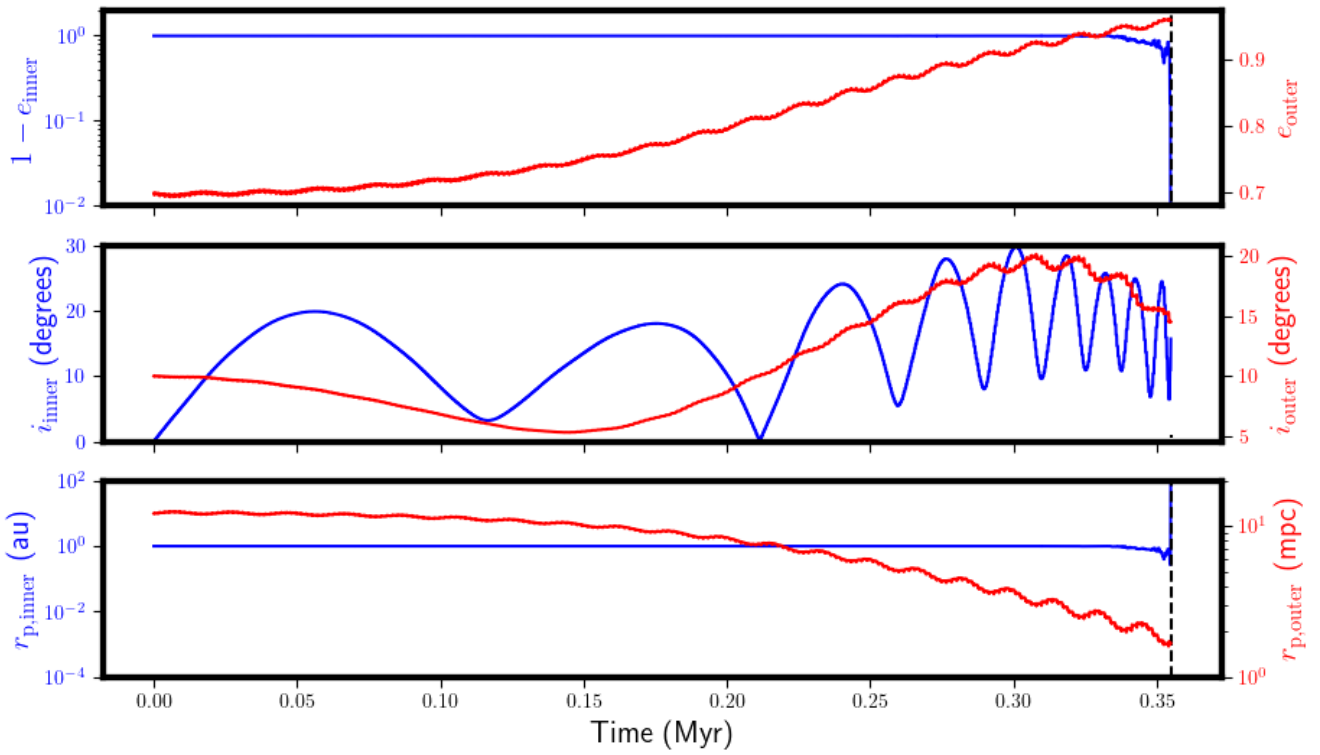

Figure 8. Evolution of the inner and outer orbital elements of a binary system orbiting Sgr A* with initial outer inclination $i_{\rm outer} = 10°$, including post-Newtonian corrections. The inner binary ($a_{\rm inner} = 1, {\rm AU}$, initially nearly circular) undergoes inclination oscillations as the outer eccentricity grows, reducing the pericenter distance. Eventually, the system reaches a regime of chaotic interactions near Sgr A*.

SgrA*. In Figure 8 we show the evolution of a binary with the orbital elements described above and with an initial $i_{\rm outer} = 10°$ with respect to a distant perturber. The perturber is modeled as a single massive particle with the same as the center of mass of the disk as described in the subsection C.1. In the top panel, we see the eccentricity of both the inner and outer binary, and in the second panel, we see the inclination of the inner and outer binary around SgrA*. We see that as the system evolves, the outer eccentricity is increasing slowly, which results in the pericenter of the outer orbit $r_{\rm p,outer}$ decreasing as seen in the third panel of Figure 8. The result of this is faster and faster oscillations of inclination of the inner orbit. These oscillations are likely not due to KL oscillations as there are no corresponding changes in eccentricity. As the system has close flybys with SgrA*, the inner eccentricity starts to rapidly increase, still not coupled with the oscillations in inclination. When the binary is so close to SgrA*, the system undergoes strong chaotic interaction as the code does not use stellar collisions, the binary system gets disrupted and the stars are no longer bound to each other. We do not know what would happen if the stars had physical radii and collisions were implemented; however, from the statistical rate of mergers, we suspect there is a probability of it resulting in a merger.

In Figure 9 we show the evolution of a similar setup, but the binary system is orbiting SgrA*with $i_{\rm outer} = 90°$ and we see clear example of KL oscillations, with large changes in eccentricity of the inner binary, whose timescale also changes as $e_{\rm outer}$ increases, resulting in $a_{\rm p,outer}$ decreasing. During the KL oscillations $r_{\rm p,inner}$ decreases significantly and in the original simulation would have merged already before the system pericenter was close to SgrA*and resulted in the system getting dissociated.

The damping due to relativity could affect the KL oscillations for tight binaries as suggested by Equation C1, so we have performed an analysis of $\dot{\omega}_{\rm GR}/\dot{\omega}_{\rm KL}$ for the same setup as described earlier, but with $a_{\rm inner} = 0.1$ AU. Figure 10 shows the heatmap of $\dot{\omega}_{\rm GR}/\dot{\omega}_{\rm KL}$ for the binary, with the value of $\dot{\omega}_{\rm GR}/\dot{\omega}_{\rm KL} \gtrsim 1$ are the regions where the inner KL oscillations are damped due to GR according to the analytical approximates. However, as we showed earlier, along with in subsection C.1, the outer orbit undergoes KL oscillations which change where the binary is located in this plot. The red dotted line in Figure 10 shows the orbital evolution of a binary with $a_{\rm inner} = 0.1$ AU as described earlier, while

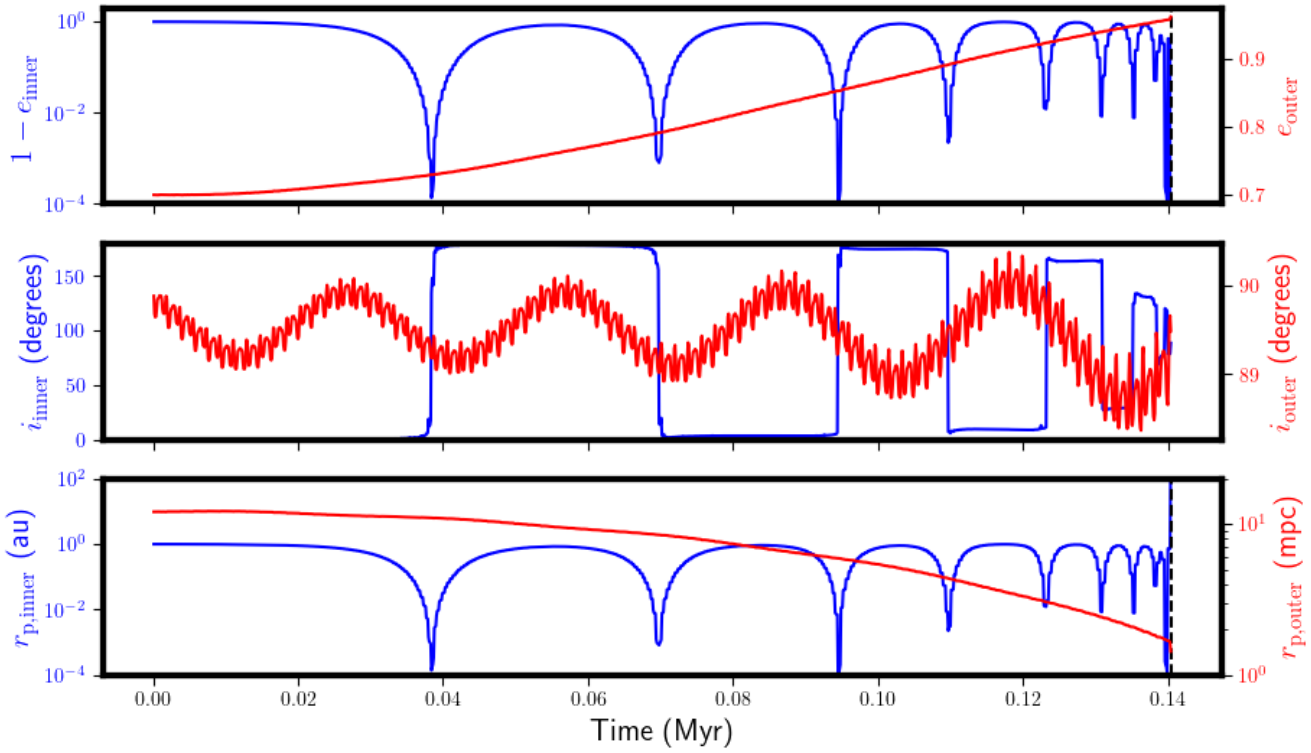

Figure 9. Same setup as in Figure 8, but with an initial outer inclination of $i_{\rm outer} = 90°$. Strong KL oscillations are evident, driving large eccentricity excursions in the inner binary. As the outer orbit becomes more eccentric and its pericenter decreases, the KL timescale shortens, leading to extreme inner eccentricities that would likely result in a merger before disruption in a more complete physical model.

its initial condition is shown by the white star. The binary starts in the region where the inner KL oscillations should be damped; however, as it undergoes outer KL oscillations, it passes through regions where we can expect inner KL oscillations. The evolution of the orbit is shown in detail in Figure 11, and we can see when the outer orbit reaches high eccentricity due to outer KL oscillations, the inner orbit undergoes rapid eccentricity oscillations, which could result in close flybys and mergers.

Overall, relativistic corrections can modify the KL dynamics and modestly reduce merger and ejection rates, but do not qualitatively alter the dynamical behavior of the system in our simulations.

D. MERGER LIFETIMES

We suggest that the stellar mergers that are produced in our numerical model are counterparts of the dusty sources observed in the Galactic Center. The match between the model and observations, however, does not need to be accurate. One important source of discrepancy can be caused by not considering internal evolution of stars, including the mergers, in the model. The merger products discussed in section 3 were analyzed over the entire duration of the simulation. However, the stellar objects that form via the collision of binary components do evolve in time. Hydrodynamic simulations showed that stellar merger remnants are initially far from hydrostatic and thermal equilibrium, often possessing inflated envelopes that also contain dust beyond the sublimation radius. The excess internal and mechanical energy deposited during the collision is subsequently radiated away as the remnant contracts on the Kelvin–Helmholtz (thermal) timescale (R. Kippenhahn & A. Weigert 1990; T. K. Suzuki et al. 2007; E. Glebbeek et al. 2009; S. C. Rose et al. 2023; F. R. N. Schneider 2025). On that time-scale, we assume that its dusty envelope tends to disappear. Hence, only the recent mergers should be interpreted as dusty sources. Considering the typical properties of dust-embedded stars with the luminosity of $L_{\rm c} \sim 10\,L_\odot$ and the photosphere radius of $R_{\rm c} \sim 1\,{\rm AU}$ (F. Peißker et al. 2020) and taking into account the mean merger product mass of $M_{\rm mp} \sim 4\,M_\odot$ (S cluster region; see Figure 1), the typical thermal

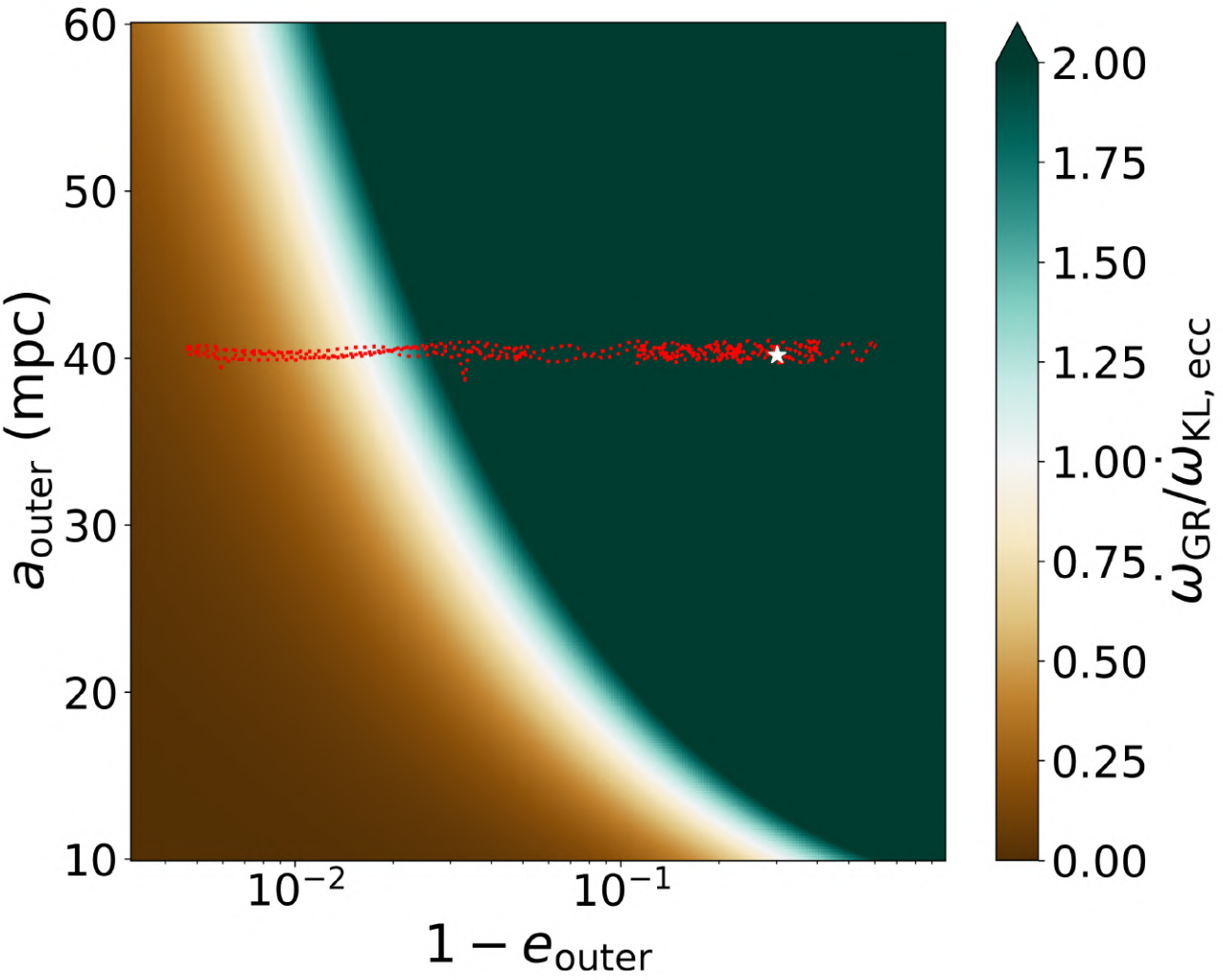

Figure 10. A heatmap showing the ratio of $\dot{\omega}_{\rm GR}/\dot{\omega}_{\rm KL}$ for the inner binary system orbiting SgrA*for the same setup as shown in Figure 6, with the inner binary having $a_{\rm inner} = 0.1$ AU. Similar to Figure 6, $\dot{\omega}_{\rm GR}/\dot{\omega}_{\rm KL} \gtrsim 1$ is where we expect KL oscillations of the inner binary to be completely damped. However due to outer KL oscillations, we expect the binary to migrate from region with damped KL oscillations to undamped KL oscillations as shown by an example evolution of a binary system which started at the location shown by the white star. The evolution of this system in $a - e$ space is marked by the red dotted line, and shown in detail in Figure 11.

timescale for the whole volume of the dusty object can be estimated as,

$$t_{\rm th} \sim \frac{GM_{\rm mp}^2}{R_{\rm c}L_{\rm c}}$$
$$\sim 2.3 \times 10^5 \left(\frac{M_{\rm mp}}{4\,M_\odot}\right)^2 \left(\frac{R_{\rm c}}{1\,{\rm AU}}\right)^{-1} \left(\frac{L_{\rm c}}{10\,L_\odot}\right)^{-1} {\rm years}. \tag{D3}$$

In our simulations, mergers are completely efficient, meaning that all the mass of the merging stars is retained in the resulting merger product. In this regard, Eq. (D3) rather provides an upper limit for the relaxation (thermal) timescale (for a given size and luminosity of the merger product) since stellar collisions typically lead to mass loss, which decreases the remnant mass and hence also the estimated Kelvin-Helmholtz timescale. This is in accordance with the fact that the observed dusty sources have a mass typically lower than the typical young stars in the Galactic Center (M. Habibi et al. 2017; F. Peißker et al. 2020, 2024b,a, 2025).

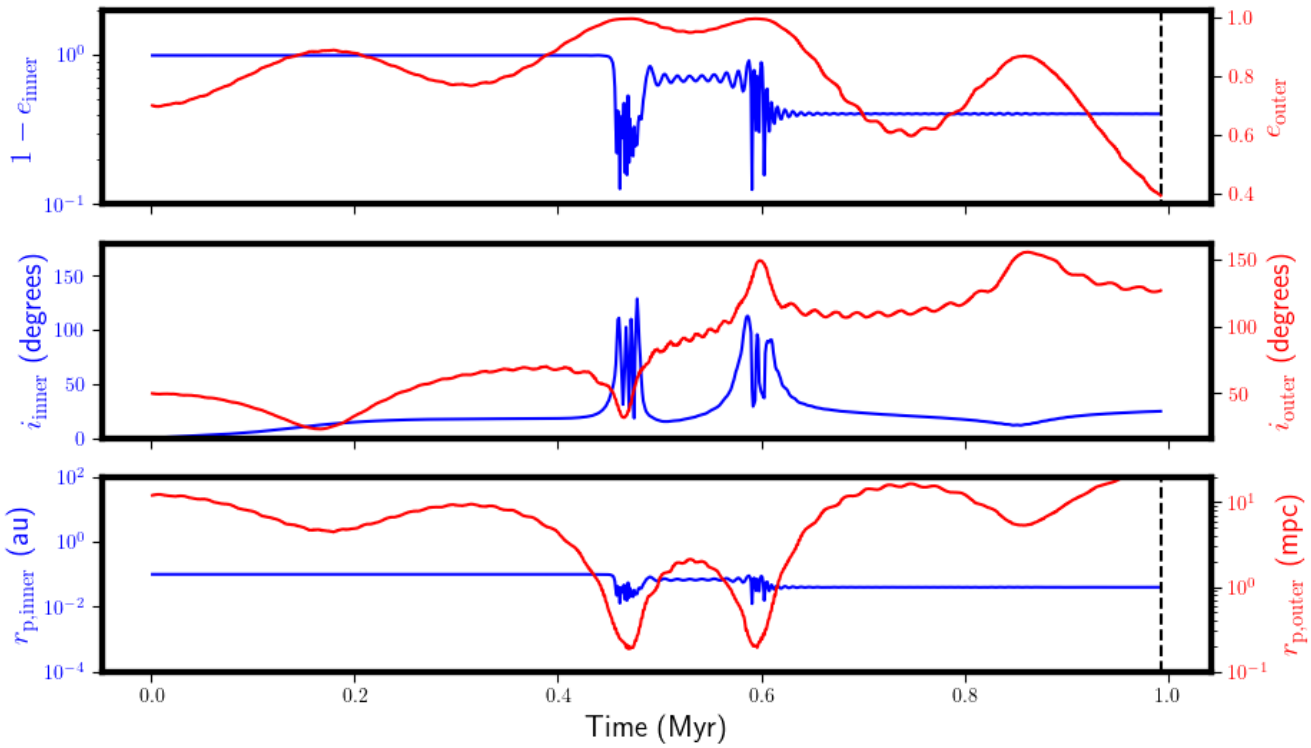

Figure 11. Similar setup as in Figure 8 , but with an initial semi-major axis $a_{\rm inner} = 0.1$ AU and outer inclination of $i_{\rm outer} = 50°$. Strong inner eccentricity oscillations are evident when the outer orbit becomes more eccentric and its pericenter decreases, leading to inner eccentricities that could result in a merger before disruption in a more complete physical model.

However, other factors can further affect the dusty envelope lifetime, both decreasing it and prolonging it, specifically the detailed dynamics of the outflows as well as accretion onto the merger product. Contributing effects include tidal stripping of the dusty envelope by the SMBH on the orbital (tidal) timescale (M. Zajaček et al. 2014), photoevaporation by the ambient UV field, dust-driven wind due to radiation from the embedded star, and the ram pressure stripping due to mildly supersonic motion through the circumnuclear medium (M. Zajaček et al. 2016; M. Zajaček et al. 2017).

The observation of D9, a dusty object confirmed to be a binary system, further suggests the possibility of formation of the dusty envelope during close, yet non-destructive encounters between the binary components. This may prolong the period of the appearance of the object as a dusty source with infrared excess for a long period of time. Recent hydrodynamic modeling by Y. Badoux et al. (2026) suggests that a circumbinary disk around D9 can remain stable for several million years with periodic outflows with repeated close encounters during the inner KL oscillations.

REFERENCES

Aarseth, S. J. 2003, Gravitational N-Body Simulations: Tools and Algorithms, Cambridge Monographs on Mathematical Physics (Cambridge University Press)

Akiba, T., Naoz, S., & Madigan, A.-M. 2025, The Astrophysical Journal Letters, 987, L27, doi: 10.3847/2041-8213/addc5d

Ali, B., Paul, D., Eckart, A., et al. 2020, The Astrophysical Journal, 896, 100, doi: 10.3847/1538-4357/ab93ae

Antonini, F., Lombardi, J. C., & Merritt, D. 2011, The Astrophysical Journal, 731, 128, doi: 10.1088/0004-637X/731/2/128

Antonini, F., & Perets, H. B. 2012, The Astrophysical Journal, 757, 27, doi: 10.1088/0004-637X/757/1/27

Astropy Collaboration, Robitaille, T. P., Tollerud, E. J., et al. 2013, A&A, 558, A33, doi: 10.1051/0004-6361/201322068

Astropy Collaboration, Price-Whelan, A. M., Sipőcz, B. M., et al. 2018, AJ, 156, 123, doi: 10.3847/1538-3881/aabc4f

Astropy Collaboration, Price-Whelan, A. M., Lim, P. L., et al. 2022, ApJ, 935, 167, doi: 10.3847/1538-4357/ac7c74

Badoux, Y., Pouw, L., van der Vuurst, T., & Portegies Zwart, S. 2026, Kozai-driven mass loss of the circumbinary disk in D9 in orbit around the supermassive black hole Sgr A*, arXiv, doi: 10.48550/arXiv.2604.09856

Bartko, H., Martins, F., Fritz, T. K., et al. 2009, The Astrophysical Journal, 697, 1741, doi: 10.1088/0004-637X/697/2/1741

Bonnell, I. A., & Rice, W. K. M. 2008, Science, 321, 1060, doi: 10.1126/science.1160653

Bradnick, B., Mandel, I., & Levin, Y. 2017, Monthly Notices of the Royal Astronomical Society, 469, 2042, doi: 10.1093/mnras/stx1007

Chassonnery, P., Capuzzo-Dolcetta, R., & Mikkola, S. 2019, ARWV Code User Manual, Tech. rep. https://ui.adsabs.harvard.edu/abs/2019arXiv191005202C

Chu, D. S., Do, T., Ghez, A., et al. 2023, The Astrophysical Journal, 948, 94, doi: 10.3847/1538-4357/acc93e

Ciurlo, A., & Morris, M. R. 2025, Sagittarius A* – The Milky Way Supermassive Black Hole, arXiv, doi: 10.48550/arXiv.2503.20081

Ciurlo, A., Campbell, R. D., Morris, M. R., et al. 2020, Nature, 577, 337, doi: 10.1038/s41586-019-1883-y

Ciurlo, A., Campbell, R. D., Morris, M. R., et al. 2023, The Astrophysical Journal, 944, 136, doi: 10.3847/1538-4357/acb344

Dodici, M., Tremaine, S., & Wu, Y. 2025, Dynamical evolution of stellar binaries in galactic centers, arXiv, doi: 10.48550/arXiv.2511.02905

Eckart, A., & Genzel, R. 1996, Nature, 383, 415, doi: 10.1038/383415a0

Eckart, A., Mužić, K., Yazici, S., et al. 2013, A&A, 551, A18, doi: 10.1051/0004-6361/201219994

Eckart, A., Hüttemann, A., Kiefer, C., et al. 2017, Foundations of Physics, 47, 553, doi: 10.1007/s10701-017-0079-2

Eisenhauer, F., Genzel, R., Alexander, T., et al. 2005, The Astrophysical Journal, 628, 246, doi: 10.1086/430667

Event Horizon Telescope Collaboration, Akiyama, K., Alberdi, A., et al. 2022, ApJL, 930, L12, doi: 10.3847/2041-8213/ac6674

Fabrycky, D., & Tremaine, S. 2007, The Astrophysical Journal, 669, 1298, doi: 10.1086/521702

Ferraro, F. R., Mucciarelli, A., Lanzoni, B., et al. 2023, Nature Communications, 14, 2584, doi: 10.1038/s41467-023-38153-w

Fragione, G., & Antonini, F. 2019, Monthly Notices of the Royal Astronomical Society, 488, 728, doi: 10.1093/mnras/stz1723

Gautam, A. K., Do, T., Ghez, A. M., et al. 2024, The Astrophysical Journal, 964, 164, doi: 10.3847/1538-4357/ad26e6

Generozov, A., & Madigan, A.-M. 2020, The Astrophysical Journal, 896, 137, doi: 10.3847/1538-4357/ab94bc

Generozov, A., Nayakshin, S., & Madigan, A. M. 2022, Monthly Notices of the Royal Astronomical Society, 512, 4100, doi: 10.1093/mnras/stac419

Genzel, R. 2022, Reviews of Modern Physics, 94, 020501, doi: 10.1103/RevModPhys.94.020501

Genzel, R., Schödel, R., Ott, T., et al. 2003, The Astrophysical Journal, 594, 812, doi: 10.1086/377127

Ghez, A. M., Klein, B. L., Morris, M., & Becklin, E. E. 1998, The Astrophysical Journal, 509, 678, doi: 10.1086/306528

Ghez, A. M., Duchêne, G., Matthews, K., et al. 2003, The Astrophysical Journal, 586, L127, doi: 10.1086/374804

Gillessen, S., Eisenhauer, F., Fritz, T. K., et al. 2009a, The Astrophysical Journal, 707, L114, doi: 10.1088/0004-637X/707/2/L114

Gillessen, S., Eisenhauer, F., Trippe, S., et al. 2009b, The Astrophysical Journal, 692, 1075, doi: 10.1088/0004-637X/692/2/1075

Gillessen, S., Genzel, R., Fritz, T. K., et al. 2012, Nature, 481, 51, doi: 10.1038/nature10652

Gillessen, S., Eisenhauer, F., Cuadra, J., et al. 2025, arXiv e-prints, arXiv:2510.00897, doi: 10.48550/arXiv.2510.00897

Glebbeek, E., Gaburov, E., de Mink, S. E., Pols, O. R., & Portegies Zwart, S. F. 2009, A&A, 497, 255, doi: 10.1051/0004-6361/200810425

Goicoechea, J. R., Pety, J., Chapillon, E., et al. 2018, Astronomy and Astrophysics, 618, A35, doi: 10.1051/0004-6361/201833558

GRAVITY Collaboration, Abuter, R., Aimar, N., et al. 2022, Astronomy and Astrophysics, 657, A82, doi: 10.1051/0004-6361/202142459

Haas, J., & Šubr, L. 2016, The Astrophysical Journal, 822, 25, doi: 10.3847/0004-637X/822/1/25

Haas, J., & Šubr, L. 2021, The Astrophysical Journal, 922, 74, doi: 10.3847/1538-4357/ac18c6

Haas, J., Šubr, L., & Kroupa, P. 2011, Monthly Notices of the Royal Astronomical Society, 412, 1905, doi: 10.1111/j.1365-2966.2010.18025.x

Habibi, M., Gillessen, S., Martins, F., et al. 2017, The Astrophysical Journal, 847, 120, doi: 10.3847/1538-4357/aa876f

Hao-Tse Huang, H., & Lu, W. 2025, Formation of Close Binaries through Massive Black Hole Perturbations and Chaotic Tides, arXiv, doi: 10.48550/arXiv.2511.11965

Harris, C. R., Millman, K. J., van der Walt, S. J., et al. 2020, Nature, 585, 357, doi: 10.1038/s41586-020-2649-2

Hills, J. G. 1988, Nature, 331, 687, doi: 10.1038/331687a0

Hopman, C., & Alexander, T. 2006, The Astrophysical Journal, 645, 1152, doi: 10.1086/504400

Hsieh, P.-Y., Koch, P. M., Ho, P. T. P., et al. 2017, The Astrophysical Journal, 847, 3, doi: 10.3847/1538-4357/aa8329

Hsieh, P.-Y., Koch, P. M., Kim, W.-T., et al. 2021, The Astrophysical Journal, 913, 94, doi: 10.3847/1538-4357/abf4cd

Hunter, J. D. 2007, Computing in Science & Engineering, 9, 90, doi: 10.1109/MCSE.2007.55

Hut, P. 1981, Astronomy and Astrophysics, 99, 126. https://ui.adsabs.harvard.edu/abs/1981A&A....99..126H

Karas, V., & Šubr, L. 2007, Astronomy and Astrophysics, 470, 11, doi: 10.1051/0004-6361:20066068

Kippenhahn, R., & Weigert, A. 1990, Stellar Structure and Evolution (Springer-Verlag: Berlin, Heidelberg, New York)

Kobulnicky, H. A., & Fryer, C. L. 2007, The Astrophysical Journal, 670, 747, doi: 10.1086/522073

Kozai, Y. 1962, AJ, 67, 591, doi: 10.1086/108790

Levin, Y., & Beloborodov, A. M. 2003, The Astrophysical Journal, 590, L33, doi: 10.1086/376675

Lidov, M. L. 1962, Planet. Space Sci., 9, 719, doi: 10.1016/0032-0633(62)90129-0

Ling, J. F., Magdalena, P., & Prieto, C. 2004, International Astronomical Union Colloquium, 191, 77, doi: 10.1017/S0252921100008526

Liu, H. B., Hsieh, P.-Y., Ho, P. T. P., et al. 2012, The Astrophysical Journal, 756, 195, doi: 10.1088/0004-637X/756/2/195

Lu, J. R., Do, T., Ghez, A. M., et al. 2013, The Astrophysical Journal, 764, 155, doi: 10.1088/0004-637X/764/2/155

Mapelli, M., Hayfield, T., Mayer, L., & Wadsley, J. 2012, The Astrophysical Journal, 749, 168, doi: 10.1088/0004-637X/749/2/168

Martins, F., Trippe, S., Paumard, T., et al. 2006, The Astrophysical Journal, 649, L103, doi: 10.1086/508328

Martín, S., Martín-Pintado, J., Montero-Castaño, M., Ho, P. T. P., & Blundell, R. 2012, Astronomy and Astrophysics, 539, A29, doi: 10.1051/0004-6361/201117268

Merritt, D. 2006, Reports on Progress in Physics, 69, R01, doi: 10.1088/0034-4885/69/9/R01

Morris, M. 1993, Astrophysical Journal v.408, p.496, 408, 496, doi: 10.1086/172607

Murray-Clay, R. A., & Loeb, A. 2012, Nature Communications, 3, 1049, doi: 10.1038/ncomms2044

Naoz, S. 2016, Annual Review of Astronomy and Astrophysics, 54, 441, doi: 10.1146/annurev-astro-081915-023315

Naoz, S., & Fabrycky, D. C. 2014, The Astrophysical Journal, 793, 137, doi: 10.1088/0004-637X/793/2/137

Paumard, T., Genzel, R., Martins, F., et al. 2006, The Astrophysical Journal, 643, 1011, doi: 10.1086/503273

Peißker, F., Eckart, A., & Parsa, M. 2020, The Astrophysical Journal, 889, 61, doi: 10.3847/1538-4357/ab5afd

Peißker, F., Hosseini, S. E., Zajaček, M., et al. 2020, A&A, 634, A35, doi: 10.1051/0004-6361/201935953

Peißker, F., Zajaček, M., Labadie, L., et al. 2024a, Nature Communications, 15, 10608, doi: 10.1038/s41467-024-54748-3

Peißker, F., Zajaček, M., Melamed, M., et al. 2024b, A&A, 686, A235, doi: 10.1051/0004-6361/202449729

Peißker, F., Zajaček, M., Karas, V., et al. 2025, Astronomy & Astrophysics, 704, A7, doi: 10.1051/0004-6361/202556229

Pfuhl, O., Alexander, T., Gillessen, S., et al. 2014, The Astrophysical Journal, 782, 101, doi: 10.1088/0004-637X/782/2/101

Phifer, K., Do, T., Meyer, L., et al. 2013, The Astrophysical Journal Letters, 773, L13, doi: 10.1088/2041-8205/773/1/L13

Prodan, S., Antonini, F., & Perets, H. B. 2015, The Astrophysical Journal, 799, 118, doi: 10.1088/0004-637X/799/2/118

Rein, H., & Liu, S.-F. 2012, Astronomy and Astrophysics, 537, A128, doi: 10.1051/0004-6361/201118085

Rose, S. C., Lombardi, Jr., J. C., González Prieto, E., Kıroğlu, F., & Rasio, F. A. 2026, The Astrophysical Journal, 1000, 162, doi: 10.3847/1538-4357/ae459b

Rose, S. C., Naoz, S., Sari, R., & Linial, I. 2023, ApJ, 955, 30, doi: 10.3847/1538-4357/acee75

Schneider, F. R. N. 2025, arXiv e-prints, arXiv:2509.18421, doi: 10.48550/arXiv.2509.18421

Schneider, F. R. N., Ohlmann, S. T., Podsiadlowski, P., et al. 2019, Nature, 574, 211, doi: 10.1038/s41586-019-1621-5

Schödel, R., Feldmeier, A., Kunneriath, D., et al. 2014, Astronomy and Astrophysics, 566, A47, doi: 10.1051/0004-6361/201423481

Schödel, R., Gallego-Cano, E., Dong, H., et al. 2018, Astronomy and Astrophysics, 609, A27, doi: 10.1051/0004-6361/201730452

Scoville, N., & Burkert, A. 2013, The Astrophysical Journal, 768, 108, doi: 10.1088/0004-637X/768/2/108

Sersante, B., Penoyre, Z., & Rossi, E. M. 2025, Monthly Notices of the Royal Astronomical Society, 544, 1688, doi: 10.1093/mnras/staf1766

Singhal, M., Šubr, L., & Haas, J. 2024, Monthly Notices of the Royal Astronomical Society, 531, 2028, doi: 10.1093/mnras/stae1276

Stephan, A. P., Naoz, S., Ghez, A. M., et al. 2016, Monthly Notices of the Royal Astronomical Society, 460, 3494, doi: 10.1093/mnras/stw1220

Stephan, A. P., Naoz, S., Ghez, A. M., et al. 2019, The Astrophysical Journal, 878, 58, doi: 10.3847/1538-4357/ab1e4d

Šubr, L., & Haas, J. 2016, The Astrophysical Journal, 828, 1, doi: 10.3847/0004-637X/828/1/1

Suzuki, T. K., Nakasato, N., Baumgardt, H., et al. 2007, ApJ, 668, 435, doi: 10.1086/521214

Tamayo, D., Rein, H., Shi, P., & Hernandez, D. M. 2020, Monthly Notices of the Royal Astronomical Society, 491, 2885, doi: 10.1093/mnras/stz2870

Tsuboi, M., Kitamura, Y., Uehara, K., et al. 2018, Publications of the Astronomical Society of Japan, 70, 85, doi: 10.1093/pasj/psy080

Tylenda, R., & Kamiński, T. 2016, Astronomy and Astrophysics, 592, A134, doi: 10.1051/0004-6361/201527700

Tylenda, R., Soker, N., & Szczerba, R. 2005, Astronomy and Astrophysics, 441, 1099, doi: 10.1051/0004-6361:20042485

Valencia-S., M., Eckart, A., Zajaček, M., et al. 2015, ApJ, 800, 125, doi: 10.1088/0004-637X/800/2/125

von Fellenberg, S. D., Gillessen, S., Stadler, J., et al. 2022, The Astrophysical Journal, 932, L6, doi: 10.3847/2041-8213/ac68ef

Vynatheya, P., Ryu, T., Wang, C., Sills, A., & Pakmor, R. 2026, The Astrophysical Journal, 999, 64, doi: 10.3847/1538-4357/ae40ba

Yelda, S., Ghez, A. M., Lu, J. R., et al. 2010, Increasing the Scientific Return of Stellar Orbits at the Galactic Center,, https://arxiv.org/abs/1002.1729v1

Yelda, S., Ghez, A. M., Lu, J. R., et al. 2014, The Astrophysical Journal, 783, 131, doi: 10.1088/0004-637X/783/2/131

Young, P. 1980, The Astrophysical Journal, 242, 1232, doi: 10.1086/158553

Zajaček, M., Eckart, A., Karas, V., et al. 2016, MNRAS, 455, 1257, doi: 10.1093/mnras/stv2357

Zajaček, M., Karas, V., & Eckart, A. 2014, Astronomy & Astrophysics, 565, A17, doi: 10.1051/0004-6361/201322713

Zajaček, M., Britzen, S., Eckart, A., et al. 2017, Astronomy and Astrophysics, 602, A121, doi: 10.1051/0004-6361/201730532

Zhang, G.-Y., André, P., Men'shchikov, A., & Li, J.-Z. 2024, Astronomy & Astrophysics, 689, A3, doi: 10.1051/0004-6361/202449853

Šubr, L., & Haas, J. 2014, The Astrophysical Journal, 786, 121, doi: 10.1088/0004-637X/786/2/121

Conclusion

In this work, I have explored the role of stellar dynamics near an SMBH. I focused on comparing these dynamics with those near the closest known SMBH, Sgr A* . Our Galactic Center provides direct observational access to stellar and gaseous systems. These systems are influenced by the tidal forces of Sgr A* and high stellar densities nearby. I used direct N-body simulations and high-precision few-body integrations with post-Newtonian corrections. I studied stellar dynamics, focusing especially on binaries and their role in shaping stellar populations near Sgr A* .

The core results of the Thesis are based on a series of papers that aim to provide insight into the dynamics that shape our Galactic Center and, in turn, could be useful for studying other galactic centers.

In Chapter 4 I present new results on the evolution of a four-body system. Two light bodies orbit a central massive body, with a distant perturber also orbiting the central body. Previous studies by (Haas et al., 2011a,b) explored these dynamics, which we refer to as the VHS mechanism. In this Thesis, I extend the VHS mechanism to include relativistic corrections. I also show how the non-zero eccentricity of the light bodies affects VHS by means of numerical integration. This includes results on the co-existence of the VHS mechanism with KL oscillations. Finally, I discuss how the VHS mechanism creates a disk of stars near the SMBH, leading to a coherent structure nearly perpendicular to the perturber's orbit.

In Chapter 5 and Chapter 6, we present simulations of a disk of binary stars around an SMBH. The binary systems' eccentricities around the SMBH correlate with their semi-major axes. The disk creates a non-axisymmetric perturbation. This causes binaries to undergo KL oscillations, bringing them close to the SMBH. Chapter 5 focuses on the production of HVS through the Hill's mechanism. We performed a probabilistic assessment across various parent disk geometries and demonstrated that the observed spatial trajectory and velocity vector of S5-HVS1 —an HVS ejected about 4.8 Myr ago from the Galactic Center— are remarkably compatible with an origin within the young stellar disk, validating our binary-disk disruption framework.

Following this, in Chapter 6 we incorporate physical mergers into our simulations to more accurately study the dynamics of binary evolution, and we find that mergers are three times less likely than binary disruptions. On top of that, these mergers tend to occur near the SMBH, which can provide a pathway for the origin of the dust-embedded objects (G-objects), which are hypothesized to be dust-enshrouded binary merger remnants. Furthermore, our simulations demonstrate that the dynamics of this setup result in a strong radial dependence of the binary fraction, which increases with increasing distance from the SMBH, a trend observed in the Galactic Center as well.

In conclusion, the models and simulations presented in this Thesis provide greater insight into the role of stellar dynamics in shaping the stellar population near an SMBH. The Thesis demonstrates how various interactions between stars can result in the production of HVS, dust-enshrouded mergers, and coherent structures observed within our Galactic Center. Due to limitations of computa-

tional resources and time, all these studies only include stellar dynamics without any consideration for hydrodynamical effects due to the surrounding gas in a galactic center, which is something we hope can eventually be addressed with better computational resources in the future, hopefully along with studies that can incorporate perturbations from the various massive structures within the Galactic Center, which are currently ignored in most studies.

Bibliography

Aarseth, S. J. 2003,. *Gravitational N-Body Simulations: Tools and Algorithms*. Cambridge Monographs on Mathematical Physics. Cambridge University Press.

Ali, B., Paul, D., Eckart, A., Parsa, M., Zajacek, M., Peißker, F., Subroweit, M., Valencia-S., M., Thomkins, L., & Witzel, G. 2020, Kinematic Structure of the Galactic Center S Cluster. *The Astrophysical Journal*, 896, 100. ADS Bibcode: 2020ApJ...896..100A.

Antonini, F., Lombardi, J. C., & Merritt, D. 2011, TIDAL BREAKUP OF BINARY STARS AT THE GALACTIC CENTER. II. HYDRODYNAMIC SIMULATIONS. *The Astrophysical Journal*, 731(2), 128. Publisher: The American Astronomical Society.

Baltagiannis, A. N. & Papadakis, K. E. 2011, Equilibrium points and their stability in the restricted four-body problem. *International Journal of Bifurcation and Chaos*, 21(08), 2179–2193.

Bar-Or, B. & Fouvry, J.-B. 2018, Scalar Resonant Relaxation of Stars around a Massive Black Hole. *The Astrophysical Journal*, 860, L23. ADS Bibcode: 2018ApJ...860L..23B.

Binney, J. & Tremaine, S. 2008,. *Galactic Dynamics: Second Edition*. Princeton University Press, rev - revised, 2 edition.

Bonnell, I. A. & Rice, W. K. M. 2008, Star Formation Around Supermassive Black Holes. *Science*, 321, 1060.

Brown, W. R. 2015, Hypervelocity Stars*. *Annual Review of Astronomy and Astrophysics*, 53(Volume 53, 2015), 15–49.

Chassonnery, P., Capuzzo-Dolcetta, R., & Mikkola, S. 2019,. ARWV Code User Manual. Technical report. Publication Title: arXiv e-prints ADS Bibcode: 2019arXiv191005202C Type: article.

Christopher, M. H., Scoville, N. Z., Stolovy, S. R., & Yun, M. S. 2005, HCN and HCO+ Observations of the Galactic Circumnuclear Disk. *The Astrophysical Journal*, 622(1), 346.

Dinh, C. K., Salas, J. M., Morris, M. R., & Naoz, S. 2021, Effects of Turbulence in the Circumnuclear Disk. *The Astrophysical Journal*, 920, 79. ADS Bibcode: 2021ApJ...920...79D.

Eckart, A. & Genzel, R. 1996, Observations of stellar proper motions near the Galactic Centre. *Nature*, 383(6599), 415–417.

Event Horizon Telescope Collaboration (Akiyama, K. et al.) 2022, First Sagittarius A* Event Horizon Telescope Results. I. The Shadow of the Supermassive Black Hole in the Center of the Milky Way. , 930(2), L12.

Ghez, A. M., Klein, B. L., Morris, M., & Becklin, E. E. 1998, High Proper-Motion Stars in the Vicinity of Sagittarius A*: Evidence for a Supermassive Black Hole at the Center of Our Galaxy. *The Astrophysical Journal*, 509(2), 678.

Ghez, A. M., Salim, S., Weinberg, N. N., Lu, J. R., Do, T., Dunn, J. K., Matthews, K., Morris, M. R., Yelda, S., Becklin, E. E., Kremenek, T., Milosavljevic, M., & Naiman, J. 2008, Measuring Distance and Properties of the Milky Way's Central Supermassive Black Hole with Stellar Orbits. *The Astrophysical Journal*, 689(2), 1044.

Gillessen, S., Eisenhauer, F., Fritz, T. K., Bartko, H., Dodds-Eden, K., Pfuhl, O., Ott, T., & Genzel, R. 2009, The Orbit of the Star S2 Around SGR A* from Very Large Telescope and Keck Data. *The Astrophysical Journal*, 707, L114–L117. ADS Bibcode: 2009ApJ...707L.114G.

Goicoechea, J. R., Pety, J., Chapillon, E., Cernicharo, J., Gerin, M., Herrera, C., Requena-Torres, M. A., & Santa-Maria, M. G. 2018, High-speed molecular cloudlets around the Galactic center's supermassive black hole. *Astronomy and Astrophysics*, 618, A35. ADS Bibcode: 2018A&A...618A..35G.

Gould, A. & Quillen, A. C. 2003, Sagittarius A* Companion S0-2: A Probe of Very High Mass Star Formation. *The Astrophysical Journal*, 592, 935–940. ADS Bibcode: 2003ApJ...592..935G.

GRAVITY Collaboration (Abuter, R. et al.) 2020, Detection of the Schwarzschild precession in the orbit of the star S2 near the Galactic centre massive black hole. *Astronomy & Astrophysics*, 636, L5.

Haas, J., Šubr, L., & Kroupa, P. 2011,a The coupling of a young stellar disc with the molecular torus in the Galactic Centre. *Monthly Notices of the Royal Astronomical Society*, 412a, 1905–1912. ADS Bibcode: 2011MNRAS.412.1905H.

Haas, J., Šubr, L., & Vokrouhlicky, D. 2011,b Secular theory of the orbital evolution of the young stellar disc in the Galactic Centre. *Monthly Notices of the Royal Astronomical Society*, 416b(2), 1023–1032. arXiv: 1105.4608.

Hills, J. G. 1988, Hyper-velocity and tidal stars from binaries disrupted by a massive Galactic black hole. *Nature*, 331(6158), 687–689.

Hopman, C. & Alexander, T. 2006, Resonant Relaxation near a Massive Black Hole: The Stellar Distribution and Gravitational Wave Sources. *The Astrophysical Journal*, 645, 1152–1163. ADS Bibcode: 2006ApJ...645.1152H.

Hsieh, P.-Y., Koch, P. M., Ho, P. T. P., Kim, W.-T., Tang, Y.-W., Wang, H.-H., Yen, H.-W., & Hwang, C.-Y. 2017, Molecular Gas Feeding the Circumnuclear Disk of the Galactic Center. *The Astrophysical Journal*, 847, 3. ADS Bibcode: 2017ApJ...847....3H.

Hsieh, P.-Y., Koch, P. M., Kim, W.-T., Martín, S., Yen, H.-W., Carpenter, J. M., Harada, N., Turner, J. L., Ho, P. T. P., Tang, Y.-W., & Beck, S. 2021, The Circumnuclear Disk Revealed by ALMA. I. Dense Clouds and Tides in the Galactic Center. *The Astrophysical Journal*, 913(2), 94.

Huang, S.-S. 1960, Very Restricted Four-Body Problem. *The Astronomical Journal*, 65, 347. ADS Bibcode: 1960AJ.....65S.347H.

Koposov, S. E., Boubert, D., Li, T. S., Erkal, D., Da Costa, G. S., Zucker, D. B., Ji, A. P., Kuehn, K., Lewis, G. F., Mackey, D., Simpson, J. D., Shipp, N., Wan, Z., Belokurov, V., Bland-Hawthorn, J., Martell, S. L., Nordlander, T., Pace, A. B., De Silva, G. M., Wang, M.-Y., & S5 Collaboration 2020, Discovery of a nearby 1700 km s-1 star ejected from the Milky Way by Sgr A*. *Monthly Notices of the Royal Astronomical Society*, 491, 2465–2480. ADS Bibcode: 2020MNRAS.491.2465K.

Kozai, Y. 1962, Secular perturbations of asteroids with high inclination and eccentricity. *The Astronomical Journal*, 67, 591–598. ADS Bibcode: 1962AJ.....67..591K.

Krabbe, A., Genzel, R., Eckart, A., Najarro, F., Lutz, D., Cameron, M., Kroker, H., Tacconi-Garman, L. E., Thatte, N., Weitzel, L., Drapatz, S., Geballe, T., Sternberg, A., & Kudritzki, R. 1995, The Nuclear Cluster of the Milky Way: Star Formation and Velocity Dispersion in the Central 0.5 Parsec. *The Astrophysical Journal*, 447, L95. ADS Bibcode: 1995ApJ...447L..95K.

Levin, Y. & Beloborodov, A. M. 2003, Stellar Disk in the Galactic Center: A Remnant of a Dense Accretion Disk? *The Astrophysical Journal*, 590(1), L33. Publisher: IOP Publishing.

Lidov, M. L. 1962, The evolution of orbits of artificial satellites of planets under the action of gravitational perturbations of external bodies. *Planetary and Space Science*, 9(10), 719–759.

Liu, H. B., Hsieh, P.-Y., Ho, P. T. P., Su, Y.-N., Wright, M., Sun, A.-L., & Minh, Y. C. 2012, MILKY WAY SUPERMASSIVE BLACK HOLE: DYNAMICAL FEEDING FROM THE CIRCUMNUCLEAR ENVIRONMENT. *The Astrophysical Journal*, 756(2), 195.

Lu, J. R., Do, T., Ghez, A. M., Morris, M. R., Yelda, S., & Matthews, K. 2013, StelLAR POPULATIONS IN THE CENTRAL 0.5 pc OF THE GALAXY. II. THE INITIAL MASS FUNCTION. *The Astrophysical Journal*, 764(2), 155.

Maoz, E. Dynamical constraints on alternatives to massive black holes in galactic nuclei 1998,, volume 184, 447. ADS Bibcode: 1998IAUS..184..447M.

Mapelli, M., Hayfield, T., Mayer, L., & Wadsley, J. 2012, In Situ Formation of SgrA* Stars Via Disk Fragmentation: Parent Cloud Properties and Thermodynamics. *The Astrophysical Journal*, 749, 168.

Martins, F., Trippe, S., Paumard, T., Ott, T., Genzel, R., Rauw, G., Eisenhauer, F., Gillessen, S., Maness, H., & Abuter, R. 2006, GCIRS 16SW: A Massive Eclipsing Binary in the Galactic Center*. *The Astrophysical Journal*, 649(2), L103.

Merritt, D. 2013,. *Dynamics and Evolution of Galactic Nuclei*. Publication Title: Dynamics and Evolution of Galactic Nuclei ADS Bibcode: 2013degn.book.....M.

Mikkola, S. & Merritt, D. 2006, Algorithmic regularization with velocity-dependent forces. *Monthly Notices of the Royal Astronomical Society*, 372, 219–223. ADS Bibcode: 2006MNRAS.372..219M.

Naoz, S. 2016, The Eccentric Kozai-Lidov Effect and Its Applications. *Annual Review of Astronomy and Astrophysics*, 54(1), 441–489. _eprint: https://-doi.org/10.1146/annurev-astro-081915-023315.

Paumard, T., Genzel, R., Martins, F., Nayakshin, S., Beloborodov, A. M., Levin, Y., Trippe, S., Eisenhauer, F., Ott, T., Gillessen, S., Abuter, R., Cuadra, J., Alexander, T., & Sternberg, A. 2006, The Two Young Star Disks in the Central Parsec of the Galaxy: Properties, Dynamics, and Formation. *The Astrophysical Journal*, 643, 1011–1035. ADS Bibcode: 2006ApJ...643.1011P.

Peißker, F., Zajaček, M., Karas, V., Pavlík, V., Bordier, E., Šubr, L., Haas, J., Melamed, M., Großekathöfer, L., Schmökel, N., & Singhal, M. 2025, Closing the gap: Follow-up observations of peculiar dusty objects close to Sgr A* using ERIS. *Astronomy & Astrophysics*, 704, A7.

Peißker, F., Zajaček, M., Labaj, M., Thomkins, L., Elbe, A., Eckart, A., Labadie, L., Karas, V., Sabha, N. B., Steiniger, L., & Melamed, M. 2024,a The Evaporating Massive Embedded Stellar Cluster IRS 13 Close to Sgr A*. II. Kinematic Structure. *The Astrophysical Journal*, 970a, 74. ADS Bibcode: 2024ApJ...970...74P.

Peißker, F., Zajaček, M., Melamed, M., Ali, B., Singhal, M., Dassel, T., Eckart, A., & Karas, V. 2024,b Candidate young stellar objects in the S-cluster: Kinematic analysis of a subpopulation of the low-mass G objects close to Sgr A*. *Astronomy & Astrophysics*, 686b, A235.

Perets, H. B., Gualandris, A., Kupi, G., Merritt, D., & Alexander, T. 2009, Dynamical Evolution of the Young Stars in the Galactic Center: N-body Simulations of the S-Stars. *The Astrophysical Journal*, 702, 884–889. ADS Bibcode: 2009ApJ...702..884P.

Rauch, K. P. & Tremaine, S. 1996, Resonant relaxation in stellar systems. *New Astronomy*, 1, 149–170. ADS Bibcode: 1996NewA....1..149R.

Requena-Torres, M. A., Güsten, R., Weiß, A., Harris, A. I., Martín-Pintado, J., Stutzki, J., Klein, B., Heyminck, S., & Risacher, C. 2012, GREAT confirms transient nature of the circum-nuclear disk. *Astronomy & Astrophysics*, 542, L21.

Rubincam, D. P. 1977, General relativity and satellite orbits: The motion of a test particle in the Schwarzschild metric. *Celestial mechanics*, 15(1), 21–33.

Sanders, R. H. 1992, The case against a massive black hole at the Galactic Centre. *Nature*, 359(6391), 131–132.

Scheeres, D. J. 1998, The Restricted Hill Four-Body Problem with Applications to the Earth–Moon–Sun System. *Celestial Mechanics and Dynamical Astronomy*, 70(2), 75–98.

Simó, C. 1978, Relative equilibrium solutions in the four body problem. *Celestial mechanics*, 18(2), 165–184.

Singhal, M., Šubr, L., & Haas, J. 2024, Dynamical coupling of Keplerian orbits in a hierarchical four-body system: from the Galactic Centre to compact planetary systems. *Monthly Notices of the Royal Astronomical Society*, 531(1), 2028–2039.

Tsuboi, M., Kitamura, Y., Uehara, K., Tsutsumi, T., Miyawaki, R., Miyoshi, M., & Miyazaki, A. 2018, ALMA view of the circumnuclear disk of the Galactic Center: tidally disrupted molecular clouds falling to the Galactic Center. *Publications of the Astronomical Society of Japan*, 70, 85. ADS Bibcode: 2018PASJ...70...85T.

von Fellenberg, S. D., Gillessen, S., Stadler, J., Bauböck, M., Genzel, R., de Zeeuw, T., Pfuhl, O., Amaro Seoane, P., Drescher, A., Eisenhauer, F., Habibi, M., Ott, T., Widmann, F., & Young, A. 2022, The Young Stars in the Galactic Center. *The Astrophysical Journal*, 932, L6.

von Fellenberg, S. D., Gillessen, S., Stadler, J., Bauböck, M., Genzel, R., de Zeeuw, T., Pfuhl, O., Amaro Seoane, P., Drescher, A., Eisenhauer, F., Habibi, M., Ott, T., Widmann, F., & Young, A. 2022, The Young Stars in the Galactic Center. *The Astrophysical Journal*, 932, L6. ADS Bibcode: 2022ApJ...932L...6V.

von Zeipel, H. 1910, Sur l'application des séries de M. Lindstedt à l'étude du mouvement des comètes périodiques. *Astronomische Nachrichten*, 183, 345. ADS Bibcode: 1910AN....183..345V.

Weinberg, S. 1972,. *Gravitation and Cosmology: Principles and Applications of the General Theory of Relativity*. John Wiley and Sons, New York.

Yelda, S., Ghez, A. M., Lu, J. R., Do, T., Meyer, L., Morris, M. R., & Matthews, K. 2014, PROPERTIES OF THE REMNANT CLOCKWISE DISK OF YOUNG STARS IN THE GALACTIC CENTER. *The Astrophysical Journal*, 783(2), 131. Publisher: American Astronomical Society.

Šubr, L. & Haas, J. 2014, TWO-BODY RELAXATION DRIVEN EVOLUTION OF THE YOUNG S LAR DISK IN THE GALACTIC CENTER. *The Astrophysical Journal*, 786(2), 121.

Šubr, L. & Haas, J. 2016, The Properties of Hypervelocity Stars and S-stars Originating from an Eccentric Disk around a Supermassive Black Hole. *The Astrophysical Journal*, 828, 1. ADS Bibcode: 2016ApJ...828....1S.

List of Figures

List of Abbreviations

CND	Circumnuclear Disk
CWS	Clockwise Stellar Disk
EHT	Event Horizon Telescope / Event Horizon Telescope Collaboration
EKL	Eccentric Kozai-Lidov
EMRI	Extreme Mass Ratio Inspiral
HVS	Hypervelocity Star
IMBH	Intermediate-Mass Black Hole
KL	Kozai-Lidov
PN	Post-Newtonian
RR	Resonant Relaxation
Sgr A*	Sagittarius A*
SMBH	Supermassive Black Hole
VHS	Vokrouhlický-Haas-Šubr
VLBI	Very-Long-Baseline Interferometry
YNC	Young Nuclear Cluster
YSO	Young Stellar Object

List of Publications

First Author Publications

Myank Singhal, Ladislav Subr, Jaroslav Haas, Florian Peißker, Michal Zajaček (Submitted to ApJ) **Origin of dust-embedded objects in the Galactic Center**

Myank Singhal, Ladislav Subr, Jaroslav Haas (Accepted in IAU398 proceedings) **Investigating the Origins of Hypervelocity Stars in the Galactic Center**

Myank Singhal, Ladislav Subr, Jaroslav Haas (2024) **Dynamical coupling of Keplerian orbits in a hierarchical four-body system: from the Galactic Centre to compact planetary systems**, Monthly Notices of the Royal Astronomical Society, Volume 531, Issue 1, June 2024, Pages 2028–2039

Other Publications

Florian Peißker, Michal Zajaček ... Myank Singhal et. al. (2025),**Closing the gap: Follow-up observations of peculiar dusty objects close to Sgr A* utilizing ERIS**, Astronomy & Astrophysics, 704 (2025) A7

Jaroslav Haas, Pavel Kroupa, Ladislav Šubr and Myank Singhal (2025),**The star grinder in the Galactic centre - Uncovering the highly compact central stellar-mass black hole cluster**, Astronomy & Astrophysics, 695 (2025) L19

Florian Peißker, Michal Zajaček ... Myank Singhal et. al. (2024),**Candidate young stellar objects in the S-cluster: Kinematic analysis of a subpopulation of the low-mass G objects close to Sgr A***, Astronomy & Astrophysics, 686 (2024) A235